



Universidade do Minho
Escola de Engenharia

Ivo Henrique Baltazar Colmiais

**Base station with wireless powering and
communication for small rodents monitoring**

Dissertação de Mestrado

Mestrado Integrado em Engenharia Biomédica

Ramo de Eletrónica Médica

Trabalho efetuado sob a orientação do

Professor Doutor Paulo Mateus Mendes

Outubro de 2017

DECLARAÇÃO

Nome: Ivo Henrique Baltazar Colmiais

Endereço eletrónico: i_colmiais@hotmail.com Telefone: 969639290

Bilhete de Identidade/Cartão do Cidadão: 14497218

Título da dissertação: Base station with wireless powering and communication for small rodents monitoring.

Orientador/a/es:

Professor Doutor Paulo Mateus Mendes

Ano de conclusão: 2017

Mestrado Integrado em Engenharia Biomédica

É AUTORIZADA A REPRODUÇÃO INTEGRAL DESTA DISSERTAÇÃO APENAS PARA EFEITOS DE INVESTIGAÇÃO, MEDIANTE DECLARAÇÃO ESCRITA DO INTERESSADO, QUE A TAL SE COMPROMETE.

Universidade do Minho, ____/____/____

Assinatura:

AGRADECIMENTOS

Quero agradecer, em primeiro lugar, ao meu orientador, o Professor Doutor Paulo Mateus Mendes, pelo trabalho, desafios propostos, disponibilidade e constante intervenção ao longo deste ano. Para além disso, também pelos ensinamentos, experiência, frontalidade e pela oportunidade de me integrar no projeto de investigação PTDC/EEI-TEL/5250/2014, suportado por fundos FEDER POCI-01-145-FEDER-16695.

Aos meus pais, Francisco e Alzira, o meu mais sincero obrigado pelo constante apoio, amor, carinho e dedicação que me deram ao longo de toda a minha vida. O meu percurso até aqui não poderia ter sido feito sem vocês.

Aos meus amigos e colegas de laboratório de Gualtar, tenho a agradecer o excelente ambiente de trabalho, os conselhos, as discussões e a entreaajuda. Agradeço também o auxílio e as discussões no âmbito desta dissertação, bem como a permanente boa disposição. Em particular, ao Hugo, tenho de agradecer o constante e incansável apoio, entreaajuda, presença e luta durante o desenvolvimento deste trabalho. Ao Vitor, fico também grato pelo apoio, discussões, motivação e o companheirismo ao longo destes últimos anos.

Aos meus colegas de curso, de todos os anos, que me acompanharam e apoiaram ao longo deste caminho e com quem todas as dificuldades foram superadas, um obrigado. Em especial aos meus colegas de casa, sem vocês esta longa etapa não teria sido possível.

RESUMO

O tratamento de complicações médicas, tais como a arritmia, diabetes, surdez e doenças neurológicas, é um desafio árduo que é, tipicamente, resolvido recorrendo a medicamentos. No entanto, algumas doenças são resistentes a este tipo de tratamento, o que leva a uma procura por soluções alternativas. Uma destas reside na utilização de dispositivos implantáveis, que são parte fundamental da monitorização e tratamento de doenças na medicina moderna. Contudo, previamente à sua aplicação em humanos, extensos e rigorosos testes em modelos animais devem ser realizados por forma a avaliar a segurança e eficácia do dispositivo.

Numa primeira fase, estes testes são feitos em animais de laboratório, normalmente roedores. Para que seja possível testar um dispositivo médico implantável neste tipo de animais, este deve ser o mais pequeno e leve possível e não ter ligações para o exterior. Isto é desejável para minimizar o seu impacto no comportamento natural do roedor, o que pode influenciar os resultados obtidos nas experiências. Para tal, é necessária a utilização de módulos de comunicação e carregamento sem fios no implante. Isto permite evitar problemas relacionados com o seu tamanho, forma, peso e biocompatibilidade. Adicionalmente, o carregamento sem fios da bateria permite maximizar o tempo de vida do implante e elimina a necessidade de procedimentos cirúrgicos para trocar baterias, reduzindo assim o choque para o animal e o risco de infeções.

Um dispositivo implantável para o tratamento da epilepsia, desenvolvido no âmbito de um projeto de investigação, necessita ser implantado em roedores para ser testado. Para tal, é necessário utilizar uma estação base que permita solucionar os problemas previamente mencionados. Devido à inexistência de sistemas de comunicação e carregamento sem fios adequados ao problema em mãos, estes foram propostos, desenvolvidos e testados no âmbito da presente dissertação.

O sistema de comunicação desenvolvido permite o envio e receção de dados com modulação OOK a uma frequência de 1 GHz, permitindo uma distância de comunicação de até 1.5 m, que pode ser aumentada recorrendo a amplificadores. Este sistema é regulado por um microcontrolador e composto por diversos blocos, o que facilita a sua adaptabilidade para as mais diversas aplicações.

O sistema de transferência de energia sem fios baseia-se num *array* de antenas com dois elementos que permite focar o máximo da potência no implante através de um mecanismo de seguimento, maximizando assim a transferência de energia. Este sistema de seguimento recorre a um mecanismo de *feedback* que recebe informação do implante sobre a quantidade de potência que este

está a receber num dado instante. Com esta informação, um algoritmo controla a diferença de fase dos sinais de excitação do *array* de antenas e faz com que o máximo de potência seja transmitida para o implante. O sistema adquire esta informação a uma taxa de 1 kHz, sendo que a transferência de potência sem fios ocorre a uma frequência de 2 GHz e com uma velocidade teórica máxima de seguimento de 3.41 m/s.

Uma vez que também é necessário fornecer energia e recarregar baterias de implantes colocados a uma certa profundidade, torna-se necessário estudar a distribuição de potência no interior de tecidos biológicos. Para tal, foi desenvolvido um sistema que permite fazer o mapeamento de níveis de potência no interior de um fantoma líquido. Sabendo-se que os tecidos biológicos interagem com a radiação eletromagnética e absorvem-na, foi necessário o estudo da sua dosagem. Consequentemente, foi desenvolvido um sistema que permite avaliar os níveis de SAR em fantasmas líquidos de tecido biológico, permitindo concluir se os limites de segurança destes níveis são ultrapassados. Este sistema foi posteriormente validado com recursos a ferramentas de simulação eletromagnética.

ABSTRACT

Dealing with medical complications such as arrhythmia, diabetes, deafness, and neurological diseases is a challenging task that is generally tackled resorting to drugs. Nevertheless, some diseases are resistant to drug-based treatments, which leads to a demand for alternative solutions. One of these can be the use of implantable devices, which play a fundamental role in monitoring and treating diseases in modern medicine. However, prior to their use in humans, extensive and rigorous tests in animal models must be performed to assess their safety and efficacy.

In a first stage, these tests are performed in lab animals, usually rodents. For an implantable medical device to be tested in rats, it must be as small and lightweight as possible and not have wired connections to the exterior. This is desirable to minimize its impact in the rodent's normal behavior, which can influence the experimental data. As such, it is necessary to implement wireless communication and power transfer modules in the implant. This avoids problems related with the device's size, shape, weight and biocompatibility. Additionally, wirelessly recharging the battery maximizes the implant's lifetime and eliminates the need to perform surgical procedures to change batteries, thus reducing shock and infection risk for the animal.

An implantable device for the treatment of epilepsy, developed in the scope of an ongoing research project, must be implanted and tested in rats. As such, a base station that allows to compensate the aforementioned issues was required. Due to the inexistence of communication and wireless powering systems that are suitable to the problem at hand, these were proposed, developed and tested during this dissertation's work.

The developed communication system allows sending and receiving data with OOK modulation at a 1 GHz frequency, with a communication distance of up to 1.5 meters which can be extended with the use of amplifiers. This system is regulated by a microcontroller and it is composed of several blocks, which facilitates its modification to tackle problems with diverse specifications.

The wireless power transfer system is based in a two-element antenna array which allows for the maximum power to be focused at the implant through a tracking mechanism, thus maximizing the power transfer. The tracking system resorts to a feedback mechanism that receives information from the implant concerning the amount of power it is receiving at any given moment. With this information, an algorithm controls the phase difference of the excitation signals of the antenna array to ensure that maximum power is transferred to the implant. The system resorts to this information at a rate of 1 kHz,

and wireless power transfer occurs at a 2 GHz frequency with a theoretical maximum tracking speed of 3.41 m/s.

Since it is also necessary to supply power and recharge the batteries of implants placed at a considerable depth inside the human body, it is useful to study the power distribution inside biological tissues. In order to do this, a system capable of mapping power distributions inside liquid phantoms was developed. Knowing that biological tissues interact with and absorb electromagnetic radiation, it was necessary to study its dosage. To achieve this, a specific absorption rate (SAR) mapping system for biological tissue liquid phantoms was developed, allowing to conclude if the RF exposure safety limits are respected or not. This system was then validated resorting to electromagnetic simulation tools.

TABLE OF CONTENTS

Agradecimientos	iii
Resumo	v
Abstract	vii
Table of Contents	ix
List of Figures	xiii
List of Tables	xvii
List of Abbreviations and Acronyms	xix
1 Introduction	1
1.1 Device miniaturization constraints	2
1.1.1 Communications	2
1.1.2 Device powering constraints	3
1.2 Wireless power transmission	4
1.2.1 Subject mobility	5
1.2.2 Subject tracking for power delivery	6
1.2.3 Specific absorption rate	7
1.3 Motivation	7
1.4 Contributions	9
1.5 Dissertation organization	11
2 Wireless power transfer and communication	13
2.1 Wireless communication	13
2.2 Wireless power transfer	14
2.2.1 General architecture of WPT links	14
2.2.2 WPT applications	15
2.3 WPT for biomedical moving subjects	17
2.3.1 Adaptive and dynamic systems	18
2.3.2 Static systems	21
2.3.3 WPT considerations for biomedical applications	28

2.4	Electromagnetic safety.....	30
2.4.1	SAR measurement systems	30
2.4.2	Phantom selection.....	32
3	Wireless power and communications base station	37
3.1	Wireless power transfer system.....	37
3.1.1	System architecture.....	40
3.1.2	System's block diagram.....	40
3.1.3	Power budget.....	42
3.2	Wireless power beamforming system	44
3.2.1	Antenna array module	45
3.2.2	Array's phase control.....	47
3.2.3	RF signal generation.....	48
3.2.4	Feedback loop.....	50
3.3	Tracking system	52
3.3.1	Processing unit.....	53
3.3.2	Active tracking algorithm.....	53
3.3.3	Tracking validation.....	57
3.4	Wireless communication system	57
3.4.1	System architecture.....	58
3.4.2	Modulation block.....	59
3.4.3	Demodulation block.....	60
3.5	Communications processing unit	62
3.5.1	Received signal detection.....	62
3.5.2	Management software	64
3.6	System management and powering	65
3.6.1	Power module and PCB.....	65
3.6.2	Antenna	68
3.6.3	RF switch	69
3.6.4	Optional amplifiers	70

3.7	Complete system.....	72
3.7.1	Wireless power transfer	72
3.7.2	Wireless communication sub-system.....	74
4	Wireless power transfer and SAR evaluation setup.....	77
4.1	Measurement equipment.....	77
4.1.1	SAR measurement system.....	78
4.1.2	Wireless power link characterization.....	80
4.1.3	Wireless signal generator with beamforming.....	82
4.1.4	Phantom development and characterization.....	84
4.2	Measurement setup.....	85
4.2.1	Measurement chamber	86
4.2.2	Probe position control.....	87
4.2.3	Calibration issues	88
4.2.4	Complete characterization system	89
4.3	Measurement.....	90
4.3.1	Measurement protocol.....	90
4.3.2	Control and readout software.....	91
4.4	Measurement setup evaluation	95
4.4.1	Post processing software	96
4.4.2	WPT measurement validation	96
4.4.3	SAR measurement validation	98
5	Measurements and results.....	101
5.1	Wireless communication.....	101
5.1.1	Measurement setup.....	101
5.1.2	Measurements	102
5.1.3	Discussion and conclusions.....	104
5.2	Wireless Power Transfer	104
5.2.1	Measurement setup.....	105
5.2.2	Tracking algorithm validation	105

5.2.3	“Real” scenario validation.....	109
5.2.4	Discussion and conclusions.....	110
5.3	SAR.....	111
5.3.1	Measurement setup.....	111
5.3.2	SAR measured results	112
5.3.3	Discussion and conclusions.....	112
6	Conclusions and future work.....	115
6.1	Conclusions.....	115
6.2	Future work.....	117
	References.....	121
Appendix I.	Characteristics of the systems’ components	125

LIST OF FIGURES

Figure 1 - Developed WPT system.....	9
Figure 2 - Developed wireless communication system.	10
Figure 3 - Developed SAR and power distribution measurement setup.	10
Figure 4 - Diagram representing the essential parts of a WPT system.	15
Figure 5 – WPT system for a moving bus resorting to inductive coupling [39].	16
Figure 6 – WPT system for a moving car resorting to a phased array antenna [40].	16
Figure 7 - Schematic of the EnerCage-HC [5].	19
Figure 8 - System proposed in [28]. In a) is represented the moving platform with the coil and magnetic field sensors and in b) is represented the complete WPT and tracking system.	20
Figure 9 – Proposed mat-based system for WPT [30].	21
Figure 10 - On the left is presented a concept of the cage, while on the right is presented the cage along with the implantable device [44].	22
Figure 11 - On the left is presented the design of the cage, while on the right the implant along with the ferrite rods [45].	22
Figure 12 - System proposed in [46], open in a) and closed in b).	23
Figure 13 - On the top left is represented the power transfer efficiency on the cage, while on the top right is shown the interior of the cage along with the barriers. On the bottom is shown the complete system from outside [31].	25
Figure 14 - Concept of the complete system in a), along with the power transfer mechanism in b) and c) [48].	26
Figure 15 - Example of a complete SAR measurement system, made by April [56].	31
Figure 16 - Example of alternative, academic SAR measurement system [58].	32
Figure 17 – Permittivity (ϵ_r) and conductivity (σ) of human head and torso, adapted from [32].	32
Figure 18 - Relative permittivity (top) and conductivity (bottom) of Triton X-100, DGBE and deionized water over the frequency range.	35
Figure 19 - Free space path loss of various frequencies over the distance.	39
Figure 20 - Block diagram of the developed WPT system.	41
Figure 21 – Cumulative power budget of the developed system.	43
Figure 22 - Dual half-wavelength dipole array's radiation pattern.	46

Figure 23 - Developed antenna array and respective power amplifiers.	47
Figure 24 - Phase-shifter used to modify the phase value of the RF signal.	48
Figure 25 - Splitter used to generate two identical RF signals.	49
Figure 26 - VCO that was used as RF source for the WPT system.	50
Figure 27 - Power detector used to implement the feedback for the tracking system.	52
Figure 28 - Flowchart of the developed algorithm.	55
Figure 29 - Results of the simulation of the developed tracking algorithm (orange – simulated position, blue – phase obtained by the tracking algorithm).	57
Figure 30 - Block diagram of the developed communication system.	59
Figure 31 - OOK modulation.	59
Figure 32 - VCO used as the RF source for the communication system.	60
Figure 33 - Bandpass filter used in the demodulation block.	61
Figure 34 - Power detector used in the demodulation block.	61
Figure 35 - Protocol used to establish the wireless communication link.	62
Figure 36 - Diagram of the developed pulse detector, to convert the analog waveform to a digital one.	63
Figure 37 - Developed user interface for wireless communication with the available chip.	64
Figure 38 - Power supply used to supply the entire system.	66
Figure 39 - Developed PCB to interface with the Arduino board and the WPT system's components, layout on top and final result on the bottom.	67
Figure 40 - Developed PCB for the communication system, which interfaces the Arduino board and the communication system's components on the bottom, and its layout on top.	68
Figure 41 - 1 GHz monopole antenna.	69
Figure 42 - RF switched used for the modulation and managing the antenna access.	70
Figure 43 - Schematic of the switch used in the communication system.	70
Figure 44 - Optional amplifier for the transmission block of the communication link.	71
Figure 45 - Optional amplifier for the receiving block of the communication link.	72
Figure 46 - Developed WPT system and 3D printed box.	73
Figure 47 - Developed communication system, along with the power supply and an antenna.	74
Figure 48 - Block diagram of the SAR measurement system.	79
Figure 49 - The SAR probe is on the left and on the right, the modified Keithley multimeter, used to perform the acquisition (front view on top and back view on the bottom).	80
Figure 50 - Block diagram of the S21 measurement system.	81

Figure 51 - On the left is shown the developed probe along with the printed holder and on the right a close-up of its tip.....	81
Figure 52 - E5071C VNA used in this system.....	82
Figure 53 - Modifications made to the rodent implant WPT system to implement the SAR and S21 measurement system.	84
Figure 54 - Dielectric properties measurement setup, composed of the VNA, dielectric probe and phantom.....	84
Figure 55 - Phantom's relative permittivity and conductivity variation over time.	85
Figure 56 - Reference marks drawn on the cardboard.	86
Figure 57 - Interior of the anechoic chamber with the supports on top, and an example of the installed measurement setup on the bottom, where two transmitting antennas are being used.....	87
Figure 58 - Configuration of the two stepper motors, to position the probe, along with the wood rod to increase the range of the system.....	88
Figure 59 – Complete power and SAR distribution measurement setup.	90
Figure 60 - Measurement system program flowchart.....	94
Figure 61 - LabView interface, with the user inputs and current measurement information.....	95
Figure 62 - Models used for the simulations. On the left is represented the case where two antennas were used, at an angle of 60° from the normal and on the right the case where one antenna was used.....	96
Figure 63 - Simulation (on the left) and measurement (on the right) of the power distribution inside the phantom for one antenna.....	97
Figure 64 - Simulations (on the left) and measurements (on the right) of the power distribution inside the phantom for two antennas. On top with a 0 degree phase difference and on the bottom with a 60 degree phase difference.....	98
Figure 65 - Simulation (on the left) and measurement (on the right) of the local SAR levels for one antenna.....	99
Figure 66 - Simulations (on the left) and measurements (on the right) of the local SAR levels for two antennas. On top with a 0 degree phase difference and on the bottom with a 60 degree phase difference.	99
Figure 67 –Modulator block's test configuration.....	102
Figure 68 - Generated carrier signal, turned on (left), and turned off (right), on the output of the modulation block.	102

Figure 69 –Modulating and demodulating blocks’ test configuration.	103
Figure 70 - Generated and received square wave before the modulation on top and after the demodulation on the bottom.	103
Figure 71 - Sent (top) and received (bottom) "turn on" command, before the modulation and after the demodulation.....	104
Figure 72 - Algorithm test setup, with a coaxial cable feedback.....	105
Figure 73 - Power level (orange) and phase variation (blue) during the tracking with the receiving antenna stopped.....	106
Figure 74 - Power level (orange) and phase variation (blue) during the movement at a constant distance.....	107
Figure 75 - Illustration of the corners of the defined area.....	108
Figure 76 - Power level (orange) and phase variation (blue) during the tracking with the receiving antenna moving around the defined area.....	108
Figure 77 - WPT system setup, with the feedback horn turned away and the LED turned off on the left and the system fully working with the LED lit up on the right.	109
Figure 78 -900 MHz SAR measurement setup.	111
Figure 79 - Results of the simulations and measurements of SAR distribution for 900 MHz.....	112
Figure 80 - Example of a planar phased array antenna [78].	118
Figure 81 - MiniCircuits ZHL-10W-2G+ High Power Amplifier characteristics.	125
Figure 82 – Peregrine Semiconductor PE44820 Digital Phase Shifter characteristics.....	126
Figure 83 – MiniCircuits VAT-3+ SMA fixed attenuator characteristics.	127
Figure 84 - MiniCircuits ZAPD-2-272+ SMA Power Splitter/Combiner characteristics.	128
Figure 85 - MiniCircuits ZX95-3800A+ Voltage Controlled Oscillator characteristics.....	128
Figure 86 - MiniCircuits ZX47-60+ Power Detector characteristics.	129
Figure 87 - MiniCircuits ZX95-2150VW+ Voltage Controlled Oscillator characteristics.	130
Figure 88 – Delta PMT-24V350W1A Panel Mount Power Supply characteristics.....	131
Figure 89 – MiniCircuits ZX80-DR230+ SPDT RF Switch characteristics.	132
Figure 90 - MiniCircuits ZX60-33LN+ Low Noise Amplifier characteristics.	133
Figure 91 - MiniCircuits ZFL-1000LN+ Low Noise Amplifier characteristics.	134
Figure 92 - MiniCircuits VBFZ-925+ Bandpass Filter characteristics.....	135

LIST OF TABLES

Table 1 - Summarized review of the presented WPT systems.....	27
Table 2 - Human body phantom composition and properties	33
Table 3 - Components used in the system and correspondent gain.....	42
Table 4 - Price breakdown of the components and total WPT system cost.....	73
Table 5 - Price breakdown of the components and total wireless communication system cost.....	75

LIST OF ABBREVIATIONS AND ACRONYMS

ADC	Analog to Digital Converter
ASK	Analog Shift Keying
CMOS	Complementary Metal-Oxide-Semiconductor
DGBE	Diethylene Glycol Butyl Ether
FCC	Federal Communications Commission
FSK	Frequency Shift Keying
HFSS	High Frequency Structure Simulator
IEEE	Institute of Electrical and Electronics Engineers
ISM	Industrial Scientific and Medical
LED	Light Emitting Diode
OOK	On-Off Keying
PCB	Printed Circuit Board
PLA	Polylactic acid
RF	Radiofrequency
RSSI	Received Signal Strength Indicator
SAR	Specific Absorption Rate
SMA	Subminiature Version A
SPI	Serial Peripheral Interface
USB	Universal Serial Bus
VCO	Voltage-Controlled Oscillator
VNA	Vector Network Analyzer
WPT	Wireless Power Transfer

1 INTRODUCTION

Dealing with medical complications such as arrhythmia, diabetes, deafness, and neurological diseases is a challenging task. Reducing or even eliminating the need to prescribe drugs for the treatment of such disorders is of immeasurable importance, as these drugs often have many unpleasant and sometimes appalling side effects. With the advances of modern medicine, more specifically pathology, and the technological breakthroughs experienced in the recent past, biomedical devices are showing promise to become a cornerstone in the treatment and management of diseases. Fully implantable microsystems are becoming a reality and its growing market is expected to reach more than 54 billion dollars in value by 2025 [1]. Examples of such devices are pacemakers and cardioverter defibrillators, glucose biosensors, cochlear implants, bladder implants and nerve stimulators [2].

The development of biomedical devices must consider several design and implementation constraints, since these devices must fulfill several requirements. Firstly, the device's ability to stimulate, control and/or monitor a given biological function is of utmost importance, as it is the primary objective of these devices. Along with this, several design parameters such as size, shape, weight, biocompatibility, longevity, and safety, must be carefully planned and studied. This aims to guarantee that the device is suitable for implantation in an environment as sensitive and restrictive as the human body. Moreover, different diseases have distinct treatment approaches, which means that implant locations will vary. With this, the above-mentioned parameters, especially size and shape, will vary according to the application for which the device is being designed. For instance, the constraints for a head-implanted device are not the same as the ones for a thoracic implant where, for example, volume availability is much less restricting.

Since implantable devices have strict restrictions that must be met before their use in humans is approved, they must be thoroughly tested and validated in animal models prior to real-world application and widespread use as a medical treatment. Several laboratory animals can be used for research, nonetheless rodents are mostly preferred as a first model for biomedical research. This is due to the similarity of characteristics such as their anatomy, physiology and genetics, between them and humans [3]. Moreover, rodents are smaller, their cost is lower, and their maintenance is easier and cheaper than those of other human-like animal models, such as monkeys. Despite this, their size poses

a challenging task to evaluate and develop an implantable device, as volume and weight constraints are much stricter than those in human hosts.

1.1 Device miniaturization constraints

The miniaturization of implantable medical devices is one of the most sought-after objectives. With modern device fabrication technology, it is possible to greatly reduce the size of control and communication electronics, memory modules, and stimulation and monitoring electrodes. However, these components require a power source to perform their functions. Such power sources are usually either external, with power being delivered to the devices through wires, or resorting to batteries.

In several studies, wires were used to power and establish communication links with devices under test in rodent hosts, such as in the system proposed in [4]. Using cables to perform these trials regularly requires a high level of human operation to make sure the experiment flows correctly. Due to this restraint, the duration of the experiment is limited, as long-term trials become harder to accomplish [5]. Additionally, these kinds of setups, such as those presented in [6] and [7], impede experiments that involve freely moving animals as their mobility is severely hindered. The removal of the wiring would allow the animal models to move freely during the experiments, as well as eliminating the need to handle the animal beforehand. This can affect the results in behavioral studies, for example. Finally, percutaneous wires increase the risk of infection in the animal models, making it extremely desirable to eliminate them.

Having established that wires are cumbersome elements in animal experiments, their removal is most sought after. As previously established, wires are mainly used to deliver power to and establish communication links with the implanted device. Considering the wires will be removed, these functions must be made available to the device in some other way for them to perform as designed.

1.1.1 Communications

When removing wires from an implantable device, its communication platform must be reinvented. The implementation of a radiofrequency (RF) wireless communication system presents itself as a solution for the posed challenge. To achieve this, a communication module in the electronic system and two antennas are required: one on the implant and another one on the outside world, to

establish the communication link. As it is a widespread need, several RF wireless communication solutions have been developed, and numerous devices capable of performing it have been presented and described in scientific literature, e.g. blood pressure monitors for rodents [8], intraocular pressure monitors [9] [10]. Furthermore, commercial devices resorting to this technology have also been developed [11].

The implementation of a wireless data transfer link does pose some drawbacks, as any other technology. The most important one is the additional power requirement to the device. Nevertheless, carefully designed communication modules do not present a high power draw nor a high impact on the battery life, as the implant can transmit at a low power level. On the other hand, to make up for this, the external communication unit that establishes the link with the implant will have to be capable of capturing, amplifying and translating the weak RF signal. This is not problematic as size and power requirements of the external components are not nearly as restrictive as those on the implant side.

1.1.2 Device powering constraints

As stated before, an alternative powering method to wires would be the development of a battery powered system. A few devices that use batteries as a powering alternative, while data communication is done wirelessly, were developed [12][13]. Despite available electronic miniaturization technologies allowing for extremely small devices to be developed, batteries are limited by their energy densities. This means that a battery will usually be the largest component of an implantable device, especially if said device has a large power consumption or is intended for long-term use, as a battery capable of storing more energy (therefore with a longer lifetime) will necessarily be larger than a battery with a smaller energy requirement.

From the previous paragraph's statements, it becomes apparent that batteries have a high impact on the device's final weight and volume. These are limiting factors in small laboratory animals such as rodents, since, according to [14], the weight of the implant should not be more than 10% of the animal's total bodyweight. Assuming the weight of a mouse to be 20 g, the weight of the device should not surpass 2 g. In [15], the authors reported optogenetic devices that weigh up to 3 g, and that must be attached on a mouse's head that weighs just around 2 g. The weight and volume of the device have an impact on the amount of time that it can be attached to the animal, which in turn affects the reliability and conceivability of experiments that require long periods of data collection. Therefore,

depending on the device and experiment, a tradeoff must be made between the experiment's duration and the device's weight, as it can influence the animal's behavior and, consequently, the results.

The use of batteries implicates that once their lifetime is over, either the experiment is terminated, or a battery replacement surgery is required. Associated with such surgeries, exists a risk of infection to the animal [16][17] and all the logistics behind the procedure. A few examples of medical devices that use batteries that require recharging or replacement are pacemakers [18][19], deep brain stimulators [20] and hearing aids [21]. The same complications are acknowledged by current studies in which it is also concluded that a longer battery life could diminish these problems. [22], [23]. A possible solution would be the implementation of larger batteries; however, these prevent the highly sought-after miniaturization of implantable devices. As an alternative, these batteries could be wirelessly recharged instead, thus eliminating the need for battery replacement surgical procedures. Devices such as pacemakers and deep brain stimulators that can be recharged wirelessly have already been reported [18]–[20], [24].

1.2 Wireless power transmission

To surpass the previously reported limitations of battery use in prototypes for laboratory testing and research, an alternative powering solution is needed. This led to the proposal of wireless power transfer (WPT) systems that can provide power without the hassle caused by wires or large batteries. Such solutions culminate in devices that can be used with a very small battery or without one at all, which in turn makes possible lighter, less voluminous and more easily implanted devices. If the device has got low power consumption and the WPT system can provide enough power for the device to operate, no batteries are needed, and the device can be directly powered. Otherwise, if either the WPT link is not efficient enough or the device is too power-hungry, a battery can still be used, and a recharging procedure can be done wirelessly and in intervals, allowing for a smaller battery to be used and eliminating the need for battery replacement.

As animal models will be used to test the implants, they require a cage that is specifically designed to accommodate both their living needs and experimental requirements. A comprehensive study of housing conditions will be undertaken to understand how they influence the animal and, consequently, the experimental results. Additionally, it will allow to understand how the housing conditions the development of a WPT system.

1.2.1 Subject mobility

The conditions where rodents are embedded in are extremely important to reduce the impact of external events on their behavior and physiology, which in turn guarantees that reliable experimental results can be achieved. Anesthesia is an example of negative impact on experiments, as it affects the animal's vital signs and normal behavior, and consequently the experiment's results [25].

Housing conditions are also a crucial factor in terms of natural behavior of rodents, as its poor housing can stress the animal. Additionally, these poor conditions can also manifest themselves in other ways. If the animal feels a lack of control over its physical and social environment, an external aversive stimulus might cause a stressful reaction, which ultimately affects the outcome of the experiments, that would not occur if the animal felt in control [26]. According to [26], for the case of a rat that weighs up to 500 grams, its housing should have a rectangular base with a minimum of 387 cm² and 17.8 cm of height, while a mouse weighing up to 25 grams requires a housing with a height of 12.7 cm and a base of 77.4 cm²[27]. Moreover, its enclosure must contain sufficient bedding on the bottom to cover the whole floor. Several materials have been used for this, such as wood chips, paper towels, paper strips, shredded paper and wood wool. Fundamentally, the housing of the animals must be such that it allows for free movement, is stress-free and as natural as possible.

The implementation of a WPT system in a large rodent housing presents several advantages, such as allowing for free, untethered movement, thus facilitating natural behavior and more reliable experimental results. The development of such a WPT solution must consider that, associated with free-movement over a given area, power availability must be guaranteed all over the housing, to guarantee that the animal doesn't go into a spot where not enough power can be delivered to the implant, resulting in a device failure and, consequently, a failed experiment. To do this, a tracking algorithm can be implemented to know where the animal is and focus power transmission to his location. Although the rodent can move freely, its movement is confined to its enclosure. This, conjugated with their size and housing needs results in a small working area. This kind of animal's movements are mostly on a two-dimensional area and do not include jumping, although their head can move up or down. This limits the height at which they must be tracked, allowing for 2-dimensional or even 1-dimensional tracking systems. Nevertheless, WPT and tracking systems must account for the rodent's vertical movement, such as looking up, standing up or laying down, and must be able to transfer power to the device in all these scenarios. Along with this, the tracking system should also cope and keep up with the rodent's speed while it is moving, which was estimated to be around 7 cm/s [28], [29]. Considering a top speed

of 15 cm/s, with a system that can discern the rodent's position with a resolution of half a centimeter, according to Nyquist's theorem, it is necessary to sample its position and update the power transfer direction over 60 times per second.

1.2.2 Subject tracking for power delivery

As stated before, power must be available everywhere the rodent can go. It is then required for the system to transfer power within all the rodent's housing and to handle the unpredictability of where the power must be transferred to. Moreover, as the device must be always active, power must also be transferred while the animal is moving, even though its location will be constantly changing. To surpass this issue, one of two approaches can be undertaken: power can be sent equally all over the animal's cage, or it can be directed to where the animal is, thus requiring tracking capabilities. Examples of systems capable of tracking the rodent are the ones proposed in [28] and [30]. Although both resort to inductive power transfer, each of them uses a different approach. The first one aims to transfer power only to the position of the rodent and has an external system that mechanically adapts to it. The position of the rodent is detected by sensing a magnet that was placed in the implant, and a coil placed under the cage is moved accordingly, maintaining the transmitting coil always aligned with the rodent's position. The second system is a mat of coils placed under the housing and can use tracking through a camera and activate single transmitting coils. However, it is also an example of a solution that requires no tracking, as all coils can be activated at the same time. Another approach, presented in [31], is to always transfer power to a given part of the cage while physically blocking the rodent's access to the remaining housing areas.

As for the tracking capabilities of the systems, several factors must be considered. Firstly, the area in which the rodent is must be accounted for, considering its movement is confined to the area of the housing. Secondly, the dimensions of these aren't usually extremely big, which benefits the tracking system as it can be simpler and doesn't have to account for highly unusual behaviors. Lastly, due to the rodents' characteristics, and although they are unpredictable, their movement is not rapidly changing and completely uncertain. Moreover, since their range and speed of motion is limited by the housing, it allows for the development of more stable tracking systems.

1.2.3 Specific absorption rate

As biological tissues are a lossy medium, when RF waves propagate through them a portion of them is absorbed by it. The specific absorption rate (SAR) represents the rate at which energy is being absorbed by biological tissues and is measured in W/kg. This absorption by the lossy medium causes it heat up, which can be hazardous and put the subject in danger, therefore special care must be taken. SAR can be useful to assess how much the biological tissues heat up, and limits that prevent unsafe conditions are defined by the FCC. According to this organism [32], SAR values cannot surpass 1.6 W/kg averaged over a 1 g tissue sample and 2 W/kg in an averaged 10 g tissue sample. However, these values are defined for general usage and uncontrolled exposure, such as with mobile phones. When a device is being used in a controlled exposure, such as when a therapeutic device is used, these limits extend to 8.0 W/kg and 10 W/kg, respectively. SAR is calculated with the following formula:

$$SAR = \frac{\sigma |E_{rms}|^2}{\rho} \quad (1)$$

where E is the induced electric field and σ and ρ are the conductivity and density of the medium, respectively.

1.3 Motivation

An implantable device was developed, and it is going to be tested in rats. The core of the implant is an RFCMOS chip [33] that was developed parallel to this work. A bidirectional communication link was required between the outside world and said chip, to control and monitor the implant. The chip's communication protocol was not standardized, and an in-house protocol was established. Consequently, commercially available modules would require meticulous modifications in order to be able to communicate with the chip. Moreover, some of them can only transmit data and require further modifications or another parallel system to manage the reception of data. In this case, instead of resorting to unsuitable commercial solutions, reutilizing and adapting them, the bidirectional communication link was developed with various off the shelf components. These allowed to develop a modular, cable connected communication system. By using this approach, it is possible to easily tweak and adapt it, to any desired configuration. It is possible to modify the carrier frequency by changing the oscillator's tuning voltage, communication protocol and modulating signal frequency by modifying the software, and the emitted power level by using amplifiers.

Experimenting with and testing implantable medical devices on rodents, as explained before, has several complications due to size and weight constraints. It is already, by itself, a challenging task, but it is aggravated when high power draw devices must be powered. In this case, the device to be tested is a thermal neuromodulator that consumes power in bursts of up to 400 mW. When this amount of power is needed for 30 seconds, a battery with a capacity of at least 3.33 mWh is required for a single burst. For the sake of example, in a long-time experiment that requires 10 discharges per day, the value goes up to around 33.3 mWh per day. Also as an example, the GM301014H battery from PowerStream weighs half a gram and, as its capacity is only 51.8 mWh, it limits the device's lifetime to less than two days. When using the same device for longer periods, it becomes necessary to explore other powering solutions. Using more batteries makes the entire device bulkier and unusable by the rodent. By considering the solutions available and the already exposed problems, the focus shifts to WPT as the most promising solution.

As previously pointed, the free movement of the rodents is essential for the results' quality and reliability, yet it leads to an intricate powering solution. The main goal of this dissertation is to fulfill the necessity of a WPT system to power an implantable device to be tested in free rodents, along with a communication system that controls it. The chosen path was to develop a system that requires the minimum configuration to be done before the experiment, that can transmit power not only when the device is close but also over longer distances, and that concentrates power to where the rodent is. Ultimately, for this to be possible, a tracking algorithm was developed.

The propagation of RF waves on biological tissues is lossy, which leads to power loss when they propagate in this medium. As high amounts of power will be transmitted to power the device on the low-gigahertz range, the close presence of the rodents' tissues, just as humans', is a factor to consider. The presence of these lossy tissues will originate higher losses on the power transfer link, and consequently attention must be given to the RF dosage, by monitoring the SAR value. This phenomenon causes the tissue heat up, which can become unsafe after a certain power level. Given this, wirelessly powering the device becomes a challenging task, as the amount of power absorbed by the rodent must be such that it doesn't affect its comfort and well-being, while at the same time sufficing at powering the device. With the central task of this work being the development of the communication system and WPT system with tracking capabilities, these concerns had to be taken into account.

Moreover, by the same principle, the powering of devices inside a human head must also be carefully planned and tested, as safety is a key priority. Like rodent implants, SAR limits can impede the

WPT link to deliver the required power level to the implant. Keeping this in mind, the use of several transmitting antennas, rather than the traditional approach with a single one, was studied. The goal was to determine if it was possible to deliver more power using this approach, while still respecting the imposed safety limits.

1.4 Contributions

During the work of this dissertation, several contributions were made and will be listed below:

- A plug-and-play RF-based WPT system, shown in Figure 1, with an array of antennas capable of tracking and following the location of a device implanted in a rodent was designed, built and tested, and control software was developed in Matlab and C++;

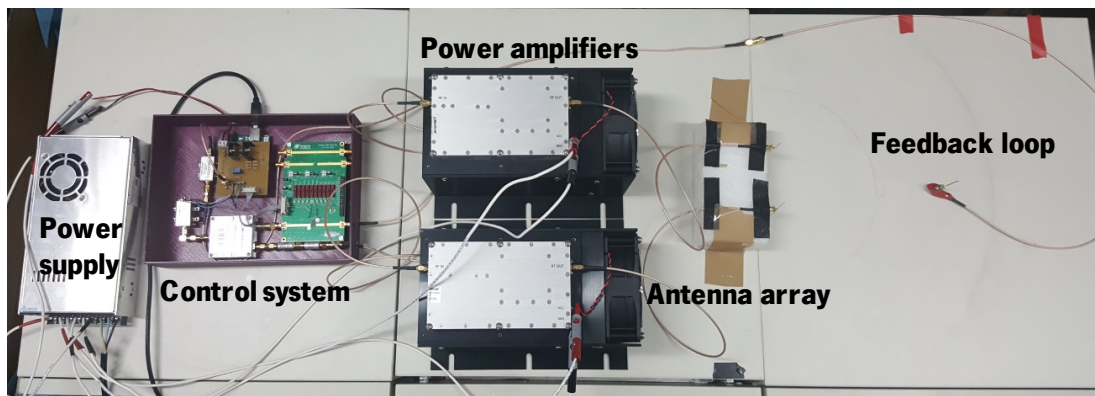


Figure 1 - Developed WPT system.

- An RF communication link, presented in Figure 2, along with an in-house communication protocol, was developed to communicate with a RFCMOS chip developed in a parallel work that will be used to control an implant. Both the hardware and software (LabView, C++) required for that communication link were developed in this work;

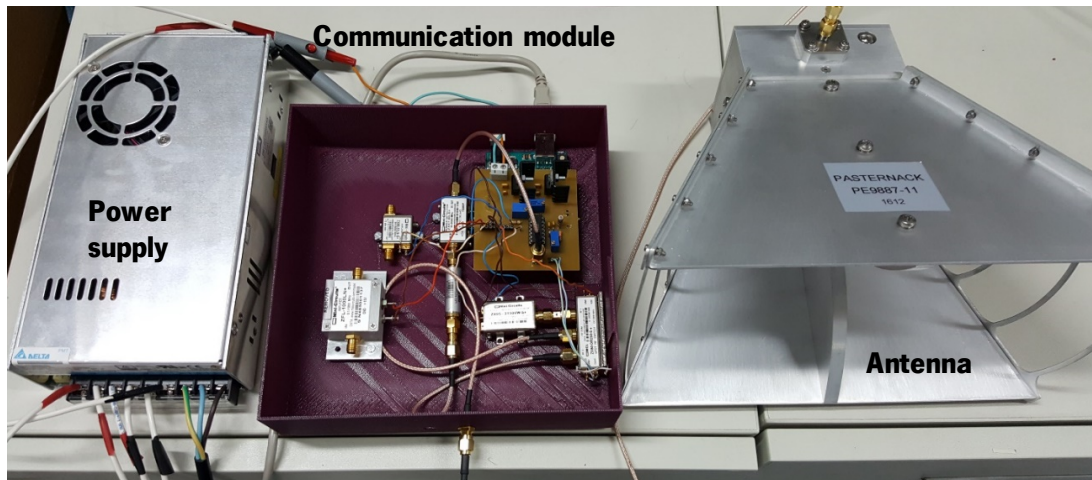


Figure 2 - Developed wireless communication system.

- A system, displayed in Figure 3, for measuring power distributions and SAR values inside a volume was proposed and designed. Both hardware and software (LabView, Matlab) were developed during this work. An in-house fabricated human head phantom was produced to evaluate power and SAR distributions, and simulation data (HFSS) were used to validate the results and, consequently, the measurement system.

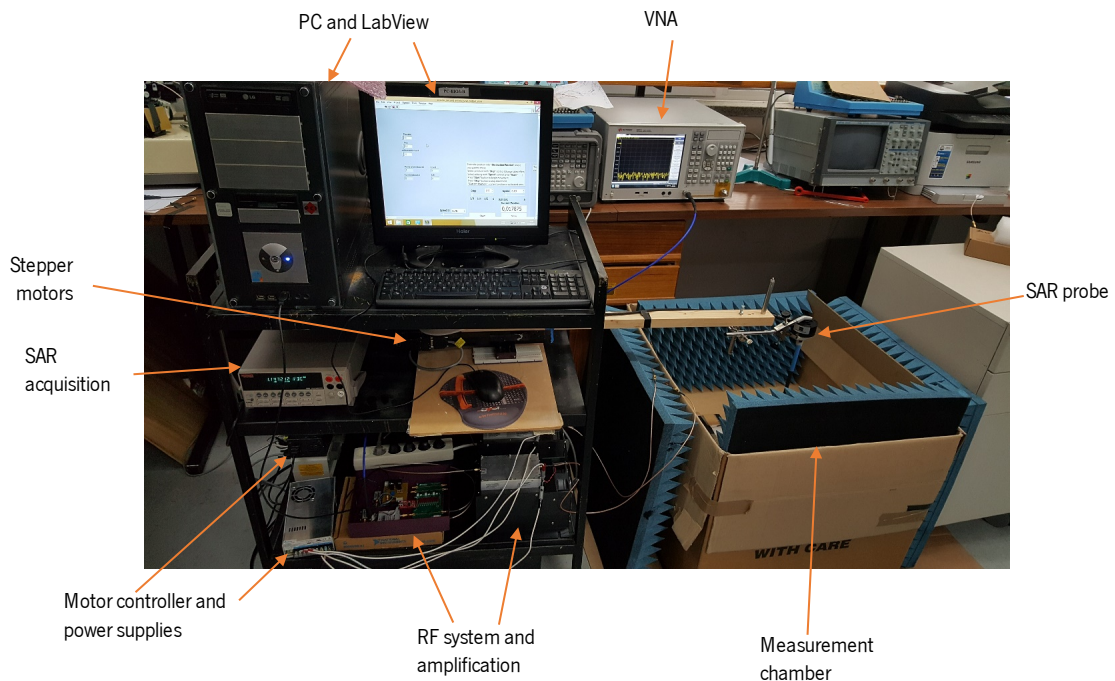


Figure 3 - Developed SAR and power distribution measurement setup.

The work of this dissertation contributed for the following articles:

- H. Dinis, J. Fernandes, V. Silva, I. Colmiais, P. M. Mendes, "Thermal modelling of an implantable brain focal cooling device," Coimbra, Portugal, February 16-18, 2017.
- H. Dinis, I. Colmiais, and P. M. Mendes, "A Multiantenna Approach to Maximize Wireless Power Transferred to Implantable Devices," 2017 International Applied Computational Electromagnetics Society (ACES) Symposium Firenze, Italy, March 26-30, 2017.
- H. Dinis, I. Colmiais, P. M. Mendes, "Extending the limits of wireless power transfer to miniaturized implantable electronic devices," *Micromachines Journal*, Special Issue on "Wireless Microdevices and Systems for Biomedical Applications, Accepted.

1.5 Dissertation organization

The first chapter is an introduction and establishment of the problems, constraints and limitations to be dealt with when an implantable device must be tested, and more specifically on rodents. The constraints of device miniaturization as well as WPT links to implanted devices on rodents are discussed. It also briefly reviews how similar problems were tackled and a solution to surpass those issues is presented. Following this, the motivation and contributions of this dissertation are presented.

The second chapter contains a state of the art on WPT systems for rodents, and a brief study of wireless communication links and SAR measurement systems.

The third chapter presents the designed WPT and wireless communication systems. In both cases, the implemented hardware and software are described.

The fourth chapter describes the developed system to characterize the SAR dosage, along with its software and system validation. Along with this, the power distribution measurement system is also assessed. The phantom that was used for these systems as well as the Matlab script are also described in this section.

The fifth chapter contains the performed measurements that characterize each of the developed systems presented in chapter three and four.

Finally, the sixth chapter contains the conclusion and future work.

2 WIRELESS POWER TRANSFER AND COMMUNICATION

In the previous chapter, device miniaturization, communication and powering constraints were highlighted, alongside possible solutions. The complications that result from allowing the rodents to freely move in their housing dictate the increase of the device's versatility by adding wireless communication and powering systems. A review of state of the art wireless power and communication solutions for biomedical applications will be presented in this chapter.

2.1 Wireless communication

Several solutions to implement a wireless communication system suitable for data acquisition in the biomedical field have been developed. Commercial and more widespread alternatives such as Bluetooth, Wi-Fi and ZigBee are available, but their implementation would often use up too much of the developed chip's area and, although low power alternatives exist, e.g. Bluetooth Low Energy, these still present a high-power draw. Alternatively, RF transceivers can be used to implement the required communication link. Examples of these are the RFM02 from Futurlec, and the nRF24L01 from Nordic semiconductor, which transmit and/or receive data at some ISM bands with frequency shift keying modulation [34][35].

Solutions to establish a wireless communication link with implantable devices has been deeply explored around the world, as a consequence of device miniaturization and implantation, the need to monitor and reduce the health risks associated to the usage of percutaneous wires. As a widespread need, several requirements are needed with different solutions being developed. Considering the implantable devices with wireless communication targeted by this work, many solutions have been developed and their approach will be reviewed.

The following devices are examples of small, implantable medical devices in which some of them use wireless powering. Nonetheless, for each system, a different wireless communication link was implemented. A blood pressure monitoring device is reported in [8] for remote monitoring in rodents. This device transmits the data at a rate of 48 kbps and for that, it operates at 2.4 GHz and resorts to FSK modulation. Another device that uses the same type of modulation is presented in [36], but was designed to communicate at 433 MHz, needing a larger antenna and measuring 3.16 x 3.16 mm². In [9] was presented a wireless implantable intraocular device and, as it has got several dimensional

constraints, it has a sub-mm³ design and implements a 2.4 GHz band wireless transmitter. Moreover, it uses OOK modulation for a transfer of up to 1.5 kb/s and at a power of -33.5 dBm, to transmit intraocular pressure values. In [10] was also developed a 700 x 700 μm² implantable intraocular pressure monitoring device that used OOK modulation at 2.4 GHz, has got a power output of -45 dBm and it managed to transfer data over 50 cm. It is worth noting that both works resorted to OOK modulation to reduce the power consumed for data transfer.

Lastly, commercial devices have been developed, such as [11]. However, this solution has a minimum dimension of 12.5 x 12.5 x 5.5 mm³ and presents a communication at 2.4 GHz over a range of 5 m, with several channels available for recording (4, 8, 16 or 32), requiring a high data rate.

2.2 Wireless power transfer

In this section, a review of wireless powering strategies will be conducted. Different approaches and features that can be helpful for the development of the system will be studied.

2.2.1 General architecture of WPT links

In Figure 4 are displayed the essential parts of the configuration of any WPT system. First, a power supply is required to power the entire system, including the oscillator which is tuned at the desired frequency for the WPT. It passes that signal to the transmitter, which depending on the application is usually preceded by a power amplifier. Its power output is dependent on the remote device's requirements and is needed for the system to be able to transfer enough power. The power transmission can be done resorting to inductive coupling, capacitive coupling, RF, ultrasounds or even light. Depending on the type of transmission, several kinds of transmitters, such as coils and antennas, can be used. The wirelessly transmitted power is then transferred to the receiver through the propagation medium. The receiver, in turn, collects part of the emitted power, which is then rectified, e.g. RF-DC conversion, and used to power the device.

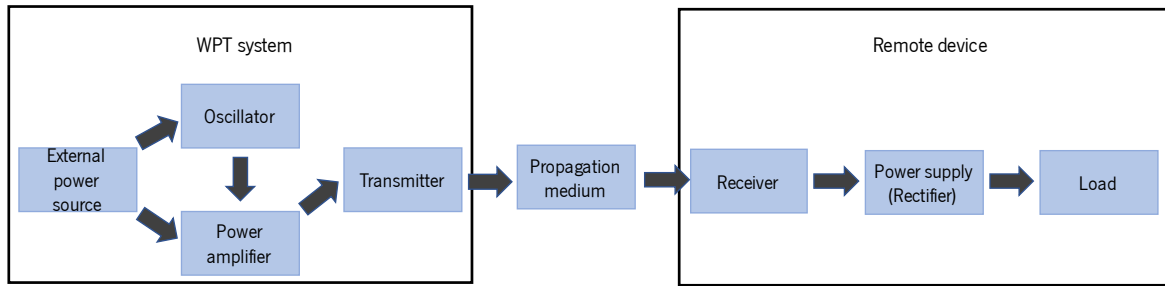


Figure 4 - Diagram representing the essential parts of a WPT system.

2.2.2 WPT applications

The research of WPT to moving devices is found across several fields of study. Although these systems follow similar structures, there are different ways of obtaining a WPT link. As each application must be studied to conclude which approach is the most suitable for the desired goal, a state of the art of WPT systems for both commercial applications and research studies will be presented and discussed.

Along with the wireless charging developed for mobile phones [37], the automotive industry, for example, is currently interested in allying WPT with electrical vehicles. Such a system has already been developed, and is called WiTricity [38]. It is capable to wirelessly charge a parked car, but the principle of operation could also be to transfer power from a WPT system installed along the road to circulating cars, allowing for on-the-move battery recharging. Solutions for this have been presented in [39] [40], and these rely on inductive coupling and microwaves, respectively. For the case of the inductive powering presented in [39] (Figure 5), a power transfer of 100 kW over an air gap of 26 cm, with a power transfer efficiency of 80% was experimentally achieved. However, this was done with a 0 cm lateral displacement. With a 15 cm displacement, the transfer efficiency is reduced to 70%, which means that either a vehicle guidance method to guarantee perfect coil alignment or a more versatile system are required.

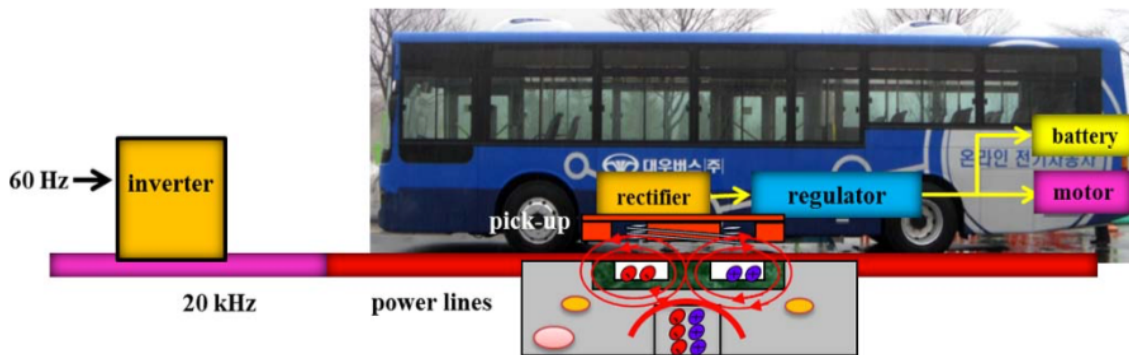


Figure 5 – WPT system for a moving bus resorting to inductive coupling [39].

The WPT system suggested in [40] and presented in Figure 6 transmitted 4 W and achieved a transfer efficiency of around 60% for nearly the same distance as the one in the previous paper, and increasing up to 75% for a distance of 40 cm. Although the latter transferred less power and achieved a lower power transfer efficiency, it was significantly smaller, as it had got a receiving rectenna that measured around 230 x 180 mm², compared to the previous receiving system of around 200 x 700 mm².

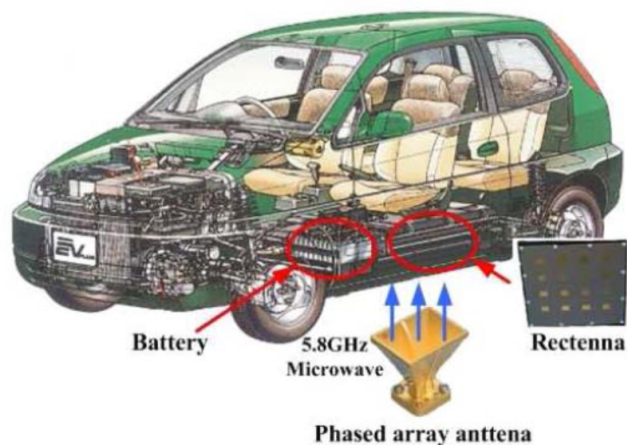


Figure 6 – WPT system for a moving car resorting to a phased array antenna [40].

Although these are different methods of WPT and have been developed for electrical vehicles that have different power requirements, both presented solutions that need to be installed under or along the side of the road to prevent the vehicle from eventually running out of power.

Another study on WPT was done for Google's project Loon, which aims to create a network with balloons and provide internet access to remote areas. Although the project considers solar powering for

this network, this is not a reliable method during the night. Moreover, the balloons are at approximately 20 km from the ground, which means that the power transmission must be done wirelessly from a great distance, rendering several methods inapplicable [41]. It is then necessary to resort to a long distance WPT system, and in [42] a system that relies on far-field WPT is proposed. It uses a beamforming array with four horn antennas to transmit a total of 4 W to the balloon at a frequency of 5.8 GHz. However, the received power by the implemented 4 by 4 rectenna is only 100 mW, at 1 meter. This means that at larger distances, and depending on the power requirements, it is necessary to improve this system by increasing the directivity of the array and transmitting more power.

2.3 WPT for biomedical moving subjects

The challenge of WPT to moving devices also finds application for biomedical devices, like experiments with different animals, where the problem may become more difficult since requirements are different when compared, e.g., with automotive applications. As most of the times rodents are the animal of first choice for in-vivo testing, we limit our analysis to systems where the WPT targets the rodents' housing living area. The previous principles of the systems presented before can also be used for WPT to rodents and, as such, several systems have been developed. However, as laboratory animals are confined to a smaller space, the WPT system can be smaller and more flexible. In addition, as the size of the device must be much smaller than the previously mentioned ones, to obtain the same power at the receiver, it is necessary to have a high-power density in the smaller receiving volume.

In [21], the authors propose a specially designed bowl that can recharge hearing-aid batteries that are placed inside it. Such a concept could be applicable to rodent implants, as the animal could be placed inside a special cage for recharging their implants' batteries. Nevertheless, such an approach was not found in literature for laboratory animals. This is likely due to the arbitrary position and behaviour of the animal under test, which prevents a desirable recharging. An alternative system that could be developed would rely on the water drinking system as a powering solution, as it is made of stainless steel and could be used as a WPT system. However, the amount of power transferred would be dependent on how long the rodent stays in that place and how it places itself relatively to the water supply mechanism, making this system unreliable. A study on RF exposure is presented in [43], in which the effect that the water drinking system has got on the rodent is evaluated. It aims to prevent temperature elevation in the drinking water, as it could influence the animal's own body temperature. It

also aims to prevent RF burns to the animal from high levels of SAR, which can discourage the animals from drinking water.

As the implantable device will be placed on a rodent with complete freedom of movement, the misalignment and random positioning of the implant relatively to the WPT source poses a challenging task. Systems to surpass this issue will be reviewed in the following sections, and they are categorized under adaptive/dynamic systems, which track the position of the implant, or static systems.

2.3.1 Adaptive and dynamic systems

The system proposed in [5], denominated EnerCage-HC and presented in Figure 7, uses a multi-coil approach to increase the power transfer efficiency and generate a homogeneous and high-power transfer in a 30 x 30 x 17 cm³ cage. It is comprised of a square shaped coil in the center of the bottom of the cage and four triangular shaped coils in the corners of it. The center coil forms a 3-coil power transmission link with two coils placed at the mobile device. The four triangular coils are open circuit and can form a four-coil link by connecting the specific coil with a resonant capacitor. This configuration allows for the controlled activation of the four triangular coils and the usage of only one power amplifier. Their activation is dependent on the animal's position, therefore a tracking capability is required. Moreover, several adjustment mechanisms are used, as this system uses the feedback from the device to control the transmitted power based on coil coupling and loading variations. For the tracking capability, a Kinect camera is used. It collects real-time images from the cage, while a normal camera tracks an LED indicator. These images are then processed to detect the animal's position, which can be stored and accessed later. A drawback of this solution is that preparation is needed before each experiment, as this tracking system works by comparing a previously taken image of the cage when it is empty. This information is processed in real time to control the activation of the four triangular coils. To transfer power, this solution operates at 13.56 MHz and can deliver 24 mW to the device with a maximum power transfer efficiency of 36.3% at a height of 7 cm. However, along with the image capture before the rodent is in the cage, this system requires a specific, crafted housing, as the bedding of the housing increases and limits the range of operation, since it increases the distance between the transmitting and receiving coils, and it requires a bulky external tracking system.

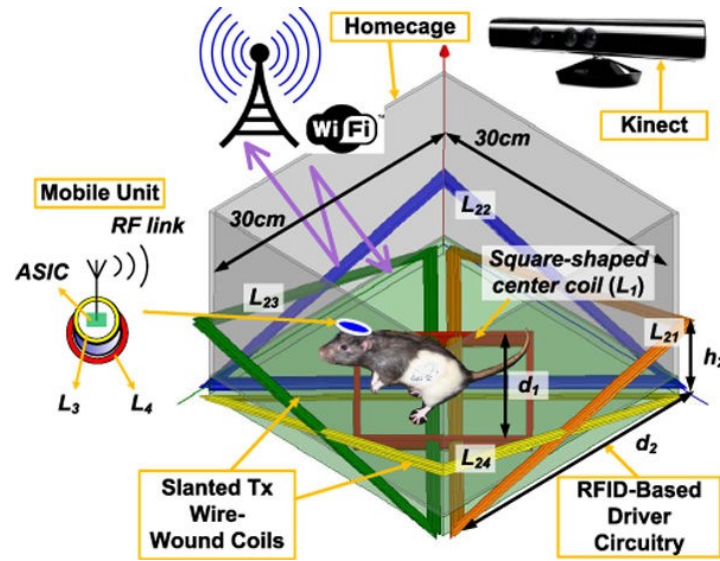


Figure 7 - Schematic of the EnerCage-HC [5].

In [28] is presented a WPT system, displayed in Figure 8 a), that includes tracking to avoid coil misplacement. It is an inductive system that transfers power at 13.56 MHz and is comprised of two coils: a transmitter outside the cage and a receiver that is placed on the device. The housing is in a fixed position, while the transmitting coil is placed on a positioning system. As this system is composed of 2 rails, the coil is moved in a plane of $18 \times 34 \text{ cm}^2$ under the housing to align it with the device. This system also has a feedback to regulate the power level. When power level adjustments are required at the implant, the power amplifier at the transmission side changes its output level. The maximum power transfer efficiency of this system is 17% in the center of the coil, with a load power of 1.7 mW. Tracking is achieved by using a magnetic position detecting system. The device has a permanent magnet attached to it, while the moving assembly, Figure 8 b), with the transmitting coil below, has five magnetic field detectors. These sensors track the permanent magnet with the objective of maintaining it their center and, consequently, aligned with the powering coil. An analog-to-digital converter (ADC) board obtains the values measured by the magnetic sensors, which are then processed by a field programmable gate array which in turn controls the position of the motors. However, this tracking solution is not feasible in some applications, such as applications where power levels over 200 mW must be transferred, since the detection of the permanent magnet becomes impossible as the transmission coil generates a stronger magnetic field than that of the magnet. This is one of the systems with the least preponderant drawbacks, but it still is worth noting that it is limited in terms of

power transmission, of vertical power transfer, and it is a bulky system which makes it hard for moving around and swapping housing.

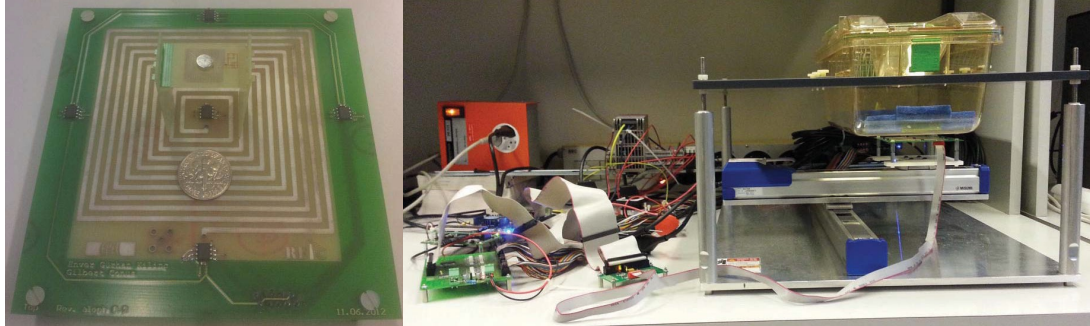


Figure 8 - System proposed in [28]. In a) is represented the moving platform with the coil and magnetic field sensors and in b) is represented the complete WPT and tracking system.

Instead of a moving coil that can move everywhere an animal can go, such as the one in the system presented before, the solution proposed in [30] places several coils covering the whole housing area, suggesting that this is capable of generating a nearly flat magnetic field distribution in the desired area, which leads to a more stable power output in that area. This system resorts to inductive coupling and is a mat-based WPT system, represented in Figure 9, operating at a frequency of 29 MHz. The coil size allowed them to be hexagonally arranged to build the transmitting mat to be placed under the cage, above it, or both. The mat system therefore covers the entire area of motion of the rodent, allowing its device to be powered anywhere inside the cage. To power it, in the case where only one or few animals are used, the coils can be individually activated to transmit power only where it is necessary. To achieve this, a tracking system composed of a camera is required. Eventually, all the transmitting coils can be activated, originating a fully powered mat and neglecting the adaptability of the system. This system, however, is unpractical as it must be placed in the housing, requires a camera for tracking, could be complicated to setup due to the camera versus mat orientation and is limited in terms of vertical power transfer.

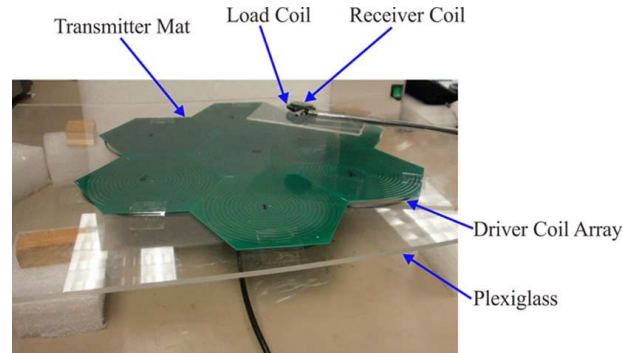


Figure 9 – Proposed mat-based system for WPT [30].

2.3.2 Static systems

As opposed to the previously studied solutions, static systems do not require tracking of the power receiving device's location. Examples of such systems will be presented next.

The usage of two coils, one on top and one on the bottom of the housing was explored in [44]. A cage that measures $15 \times 20 \times 15 \text{ cm}^3$ was developed with a resonator-based inductive WPT system. This system works at 2,4576 MHz and two coils, placed on the top and bottom of the cage, were used as transmitters. This approach was used to make the WPT link immune to vertical position changes. Furthermore, it makes it unnecessary to have a horizontal tracking system, as power is made available to the entire volume of the cage. As this is a resonator-based inductive link, apart from the transmitter and receiver coils there are two more separate coils that are used to improve the power transfer efficiency. The developed resonators for the transmitter are rectangular and column-shaped, while the transmitting coils are planar. By using two of these transmitters, the power transfer efficiency variation is lower. For a single transmitting coil, power transfer efficiency varies 93% when the rodent moves, but when two transmitting coils are used, it only varies 28%, therefore being a more consistent strategy. The implemented system, with the cage and the transmitters on the top and bottom of it, is shown in Figure 10. The power amplifier had a power of 3.3 W and the system achieved a WPT efficiency of 19,3%. Although this system tackles several drawbacks related with inductive power, it still presents a small unstandardized housing and a high coil size mismatch.

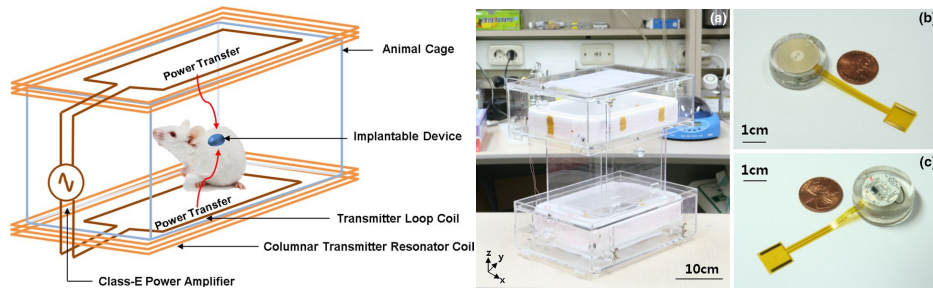


Figure 10 - On the left is presented a concept of the cage, while on the right is presented the cage along with the implantable device [44].

As mentioned before, coil misalignment is a huge problem for inductive WPT. Therefore, the work of [45], Figure 11, focuses on increasing the magnetic flux on the secondary coil and consequently enhancing the power transfer efficiency. Moreover, it aims to reduce the effect of misalignment between the transmitting and receiving coils. The cage measures 25 x 12 x 15 cm³ and has the transmitting coil wrapped around it while the receiving coil is wrapped around a printed circuit board (PCB) that measures 13.25 x 20.25 mm². This system does not require a tracking component as it transfers power to the entire cage. The result of their experiment was the increase of magnetic flux on the secondary coil by installing ferrite rods. Depending on their usage and configuration, the system operates from 2.057 to 2.302 MHz. The placement of the ferrite rods on the corners is important as if they were placed in the middle, their effectiveness would be lower. The results obtained demonstrated that using ferrite rods improved the power transfer efficiency when the coils were placed at any orientation. A power of 28 mW was transferred when it was at 60°, while a power of 113 mW was managed to be transferred when the secondary coil was parallel to the primary, resulting in a power transfer efficiency of 1.5%. Lastly, the downsides of this system are having a very small area for the housing and not being easily transportable.

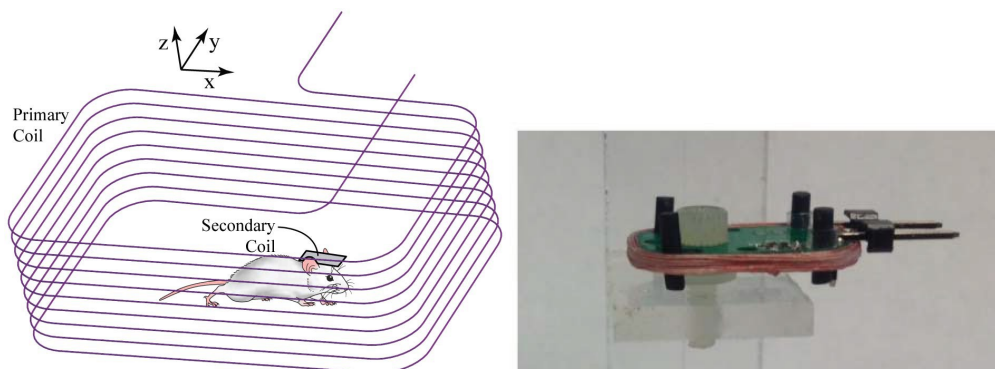


Figure 11 - On the left is presented the design of the cage, while on the right the implant along with the ferrite rods [45].

Another solution to the coil orientation problem for inductive systems was explored by [46]. A square biphasic pulse is applied to the excitation coil, which in turn produces a triangular current waveform and consequently a triangular magnetic field intensity. The power is inductively transferred to the implanted coil. Due to the movement of the animal, a problem that affects all systems, the device will not be perfectly aligned throughout the entire experiment, which results in a variable amount of transferred power. The method used on this system, Figure 12, was wrapping the coils around the cage ($16 \times 16 \times 17 \text{ cm}^3$) in different orthogonal orientations. This prevents the device from being completely misaligned, guaranteeing that misalignment is, at most, 45° . To achieve steady powering, the coils were sequentially activated on each orthogonal orientation, also ensuring that at any time, the device will always receive at least one pulse per cycle. However, when coil misalignment is 45° , the induced voltage will only be 50% of the maximum achievable when perfect alignment is observed. The power transmitted is pulsed with a peak of 531 W, generating a peak of 5 mW on the receiving coil, resulting in a power transfer efficiency of 0.0009%. Besides being an extremely small cage, a prohibitive issue of this solution is that this is a closed system. Due to the amount of current passing through the coils, dielectric heating occurs, and several holes as well as a fan were installed to help cool the housing. This is a serious issue, as not only it can cause discomfort to the rodent, but the fan can also cause unwanted neurological signals, due to excitations on the whiskers [47].

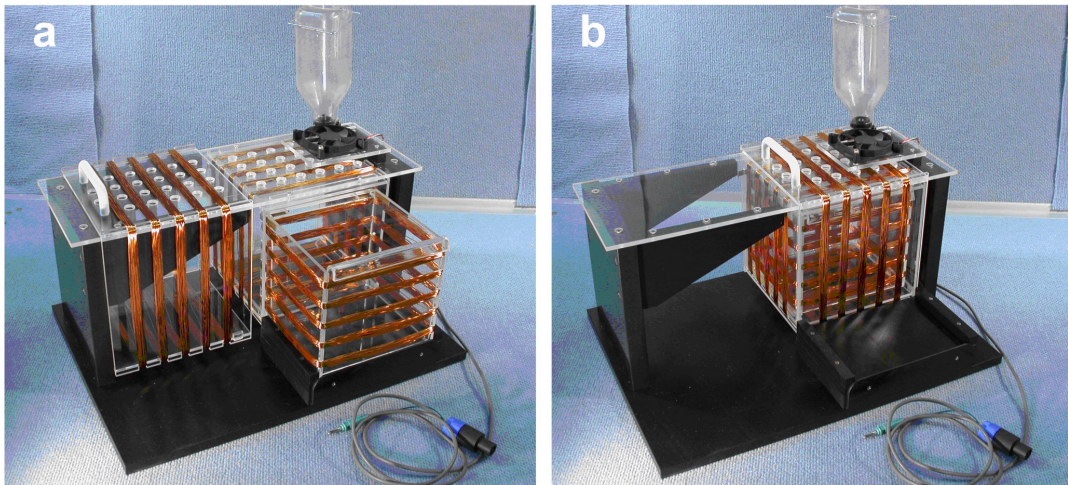


Figure 12 - System proposed in [46], open in a) and closed in b).

The work reported in [31] did not follow the same approach as the systems before and resorted to a cavity resonator. A cavity resonator is a conductive enclosure that contains electromagnetic waves reflecting back and forth between the walls. The developed WPT system, presented in Figure 13, like

the ones shown before, powers the device on the entire area of the cage, making it suitable to use when implanted on a freely moving rodent. This was done by developing a cavity resonator (60.96 x 60.96 x 30 cm³) that is made of aluminum. The characteristics of the cage make the system work at 347.99 MHz and the excitation used is the transverse magnetic TM₁₁₀ mode, which is representative of the standing wave pattern originated inside the chamber, represented in Figure 13, with the excitation probe placed in the middle of the cage. It is possible to conclude that there are five areas where the field strength is low, and to prevent the animal from going to those blind spots, electromagnetic-transparent barriers were placed. To avoid orientation issues, the device had a biaxial receiver and an impedance matching system to increase the power transfer efficiency. To accommodate the rodents and regulate the cage's temperature and humidity, several 2.1 cm wide slits were opened. The achieved power transfer efficiency is 14% without the presence of the rodent. However, as there is a moving animal inside the cavity resonator and the rodent's tissues are lossy, the chamber's resonant frequency drops and the power transfer efficiency decreases to 10%. This problem is recognized by the authors and is enlarged when there are several moving animals, as the medium characteristics will be highly modified. They also acknowledge that to solve this, a tuning solution is needed for parts of the system such as the probe's length and on-board capacitors. Lastly, although this is a very spacious housing, its space was limited with transparent barriers and it is very heavy and extremely hard to transport as it is made of metal. Furthermore, it is very sensitive to its contents, which alter the optimal frequency of operation.

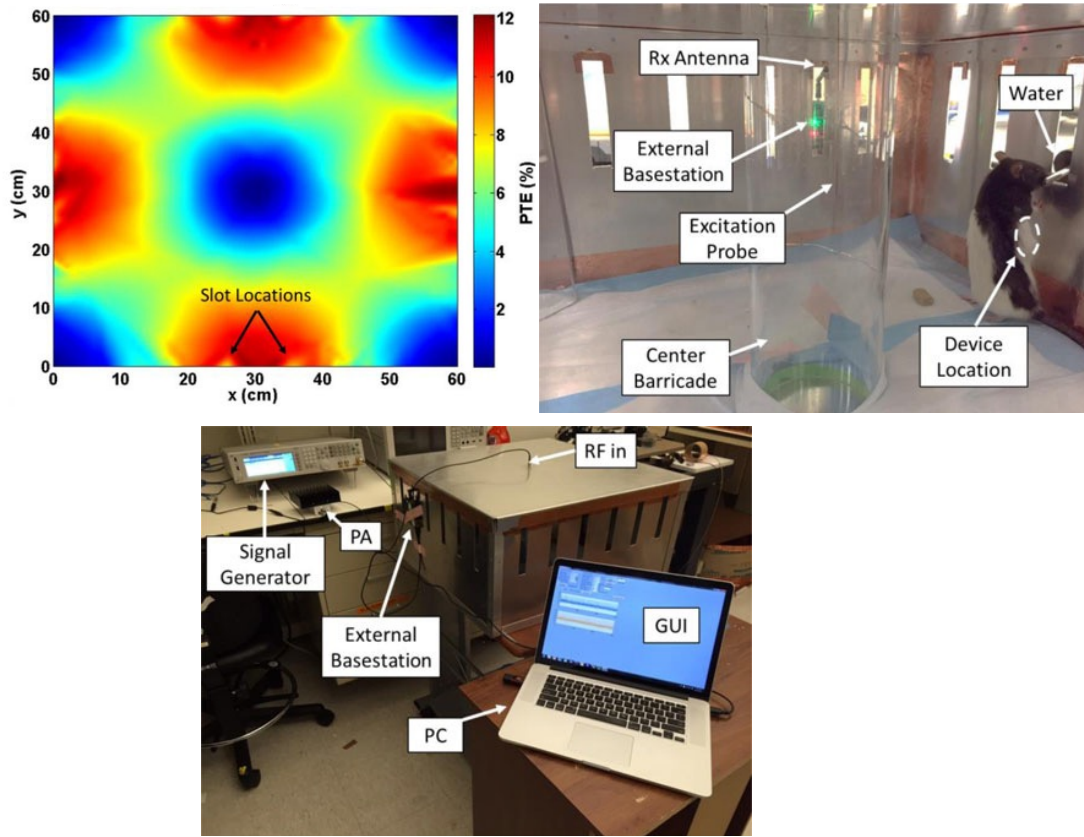


Figure 13 - On the top left is represented the power transfer efficiency on the cage, while on the top right is shown the interior of the cage along with the barriers. On the bottom is shown the complete system from outside [31].

The system presented in [15] and [48], shown in Figure 14, is another cavity resonator based WPT system. It is a cylindrical structure with a 21 cm diameter where a resonator chamber tuned to work at 1.5 GHz was built under the cage. The boundary between the cage and the chamber is metallic and has hexagonal sub-wavelength apertures. In the presence of a dielectric object, such as a rodent, energy resonates through the animal and is delivered to an implant inside its body. The way this system works allows for a self-tracking system as the power is always transferred to the rodent, not requiring a dynamic system that adapts to its location, since energy coupling only occurs where the dielectric volume, i.e. the rodent, is present. A three-turn coil on the implant, also tuned to 1.5 GHz with a 4 pF capacitor, is powered through the rodent's body. To prevent any alignment issues, the excitation had a circular polarization, originating a maximum power transfer efficiency of 0.075%. This results in an average of 15.7 mW of power transferred from a 4 W source for a 20% duty-cycle. This is a heavy system, as its made of metal and, unlike the previous systems, this cage has got a very small diameter, which can make it unsuitable to be used in experiments where natural rodent behavior is expected, as explained in the previous chapter.

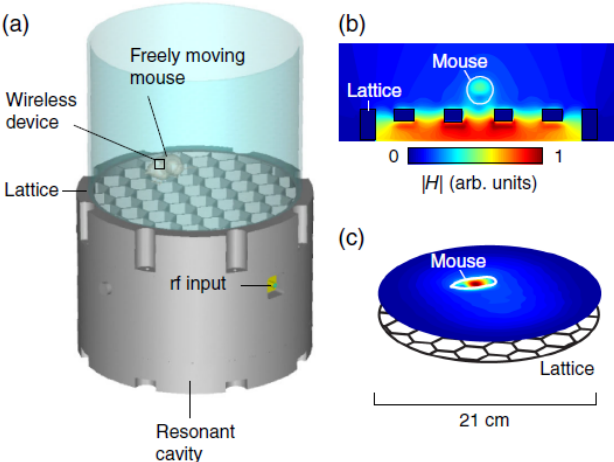


Figure 14 - Concept of the complete system in a), along with the power transfer mechanism in b) and c) [48].

Table 1 - Summarized review of the presented WPT systems

Ref.	Author	Year	Wireless comm.	Area (cm ²)	WPT Freq. (MHz)	Dynamic tracking	Static	Tracking method	Max. eff. (%)	Cons
[5]	Byunghun	2015	✓ (Wi-Fi)	30 x 30	13.56	✓	X	Kinect and camera	36.3	Nonstandard housing. Increased distance due to the bedding. Bulky external tracking system.
[28]	Kilinc	2014	✓ (869 MHz)	18 x 34	13.56	✓	X	Magnetic field sensor	17	Limited power transmission. Bulky and hard to swap housing.
[30]	Xu	2013	X	Undefined	29	✓	✓	Camera (Optional)	-	Unpractical installation. Tracking requires a camera.
[44]	Eom	2014	X (Future work)	15 x 20	2.4576	X	✓	-	19.3	Small and unstandardized housing. High coil size mismatch.
[45]	Badr	2015	✓ (Unknown)	25 x 12	2.057 - 2.302	X	✓	-	1.5	Small housing area. Not easily transportable.
[46]	Millard	2007	X	16 x 16	0.002-0.02	X	✓	-	0.0009	Extremely small cage. Closed with forced airflow with a fan.
[31]	Mei	2017	✓ (2.4 GHz)	60.69 x 60.69	347.99	X	✓	-	14	Space limited with transparent barriers. Extremely heavy. Optimum operating frequency very sensitive with its contents.
[48]	Ho	2015	X	21†	1500	X	✓	-	0.075	Round, small diameter cage. Heavy system.

† - Diameter in centimeters

It is noticeable that in most of the presented WPT systems, summarized in Table 1, the authors choose to neglect housing conditions in favor of a small or limiting area to facilitate establishing a stable WPT link. The majority of the reviewed systems do not resort to tracking systems, yet the latter achieve higher link efficiencies. All solutions, however, are bulky and dependent on the cages, i.e., they are not suitable to be used in different housings, thus not being a universal solution. All the systems resorted to inductive coupling for WPT purposes, however, this method is limited mostly due to misalignment between coils. This problem usually contributes the most to the housing constraints, as direct, external and bulky workarounds to prevent or manage those misalignments are explored. It is possible to verify that when the system uses power in the GHz region, the power transfer efficiency is significantly reduced. These systems only implement a wireless communication link when required, which can be based on standard communication systems or not. However, none of these implement the communication link through the powering link. In the case of [44], the possibility of implementing such link was only analyzed and suggested as future work.

2.3.3 WPT considerations for biomedical applications

The most commonly used method of power transmission to medical devices is inductive coupling, which is done by passing an alternating current in the transmitting coil. This generates a varying magnetic field that couples with the receiving coil and consequently generates power through the induced electromotive force. This type of transmission is the least absorbed by the body tissue, as it is done at lower frequencies. On the other hand, this type of powering is greatly influenced by the system's characteristics. Firstly, the transmitter coil is generally much larger than the receiver, as the latter must fit in the implantable device, which decreases the antenna's quality factor and coupling between the transmitter and receiver [17].

The second issue with this kind of powering encounters is the distance and alignment. Usually these systems are placed below the rodents' housing, which leads to the distance between the device and transmitting coils to include the distance of the bedding, which is around 3 cm and the height of the rodent, creating a large transfer distance. Inductive power transfer links degrade considerably over distance and, to tackle this, a WPT system used a two-transmitter approach [44] and in another, a

matching circuit was designed to improve coupling in varying distances [49]. However, even with these alternatives, lateral and angular misalignments are still present. Despite these problems, one of the presented systems managed to partially avoid them, but the housing became too small, of difficult access and generated a considerable amount of heat [46].

Far field WPT can be a solution for these problems. For the cases in which the dimension of the device is much smaller than the depth it is placed at, WPT is the most effective in the low gigahertz range [50]. Implantable devices could benefit from RF WPT, as sub-cubic millimeter biomedical implants are being developed [51]. The miniaturization of these devices leads to even more limited sized antennas, for which a higher frequency WPT system would be more advantageous. Moreover, WPT using RF not only has the highest power density per unit area but also allows for long distance powering [52].

Some of the aforementioned systems present various alternatives and methods to track and power the device implanted on a rodent, but there are still some to be explored. Most of the systems resort to optical tracking by using a camera or a Kinect for tracking the rodent to transfer power. In the same kind of tracking, a blinking LED could be used, however in all these solutions high computing power is required, as they resort to image processing.

On a different perspective it could also be possible, as suggested before, to use far-field RF for a WPT system. As a tracking technique, a radar system could be developed, however, as rodents are small, it could perform poorly. Alternatively, the solution that will be explored in this dissertation, will be the implementation of a tracking system that uses a feedback whose only information is the amount of power that the device is receiving. This system will be similar to that of [28], as the housing used will be a standard one (allowing a universal solution), requires low computation power and the external system adapts to the rodent's position without affecting it's well-being and housing conditions. This work will be a significant improvement over the other presented solutions, as they implemented their own cages, had to change the rodent's housing, block some of its cage area and use bulky tracking apparatus.

Instead of using inductive coupling, this system resorted to a steerable beam by beamforming, which led to assembling an antenna array. Furthermore, as larger housing volumes are made possible with the proposed system, it could also be used to power implantable medical devices that are being tested on larger animals, such as monkeys.

The proposed system must be capable of delivering power to an implant being developed in parallel that requires up to 400 mW of power [53], which is a value well within those of other reported

implantable devices (several devices were reported to require under 50 mW, with some in the μW range and others going up to 2000 mW [14]. The main problem with WPT using far-field RF waves is the transfer medium, along with the high amounts of power required, as with the increase of frequency the tissue absorption becomes higher and SAR limits can't be exceeded, which can limit the amount of power available at the implant.

2.4 Electromagnetic safety

Due to the ease with which RF energy can heat up biological tissues, the exposure levels to which an individual is exposed must be controlled. Exposure to high power levels of RF radiation such as those that will be used in the WPT system, can cause discomfort and be unsafe. To avoid these complications, and as explained in the previous chapter, SAR regulations were implemented. These define safety thresholds that must not be surpassed to guarantee the safety and well-being of the implanted subject. SAR measurements can be done in order to guarantee electromagnetic safety, for which measurement systems are required. A system that allows to verify if these levels comply with the regulations must be used, for which these systems will be analyzed in the following subsection.

2.4.1 SAR measurement systems

As explained in the previous chapter, SAR evaluation can be done by measuring the electric field strength and calculating the corresponding SAR value. As its distribution must be analyzed, it is necessary to map the electric field point by point. Measurement systems are composed by an electric field measuring probe, its acquisition electronics, a probe positioning system, and a central unit that controls these components.

Complete SAR measurement systems are commercially available. These systems have got several parts available, such as the one from Aprel, whose complete system is exemplified in Figure 15, and contains the previously enumerated parts. Several manufacturers, such as Aprel, Speag, IndexSAR, and MVG [54]–[57] have got the same parts for sale, which must follow international standards. The SAR probes have got different frequency ranges, with the lower limit starting from 4 MHz and the upper ending at 10 GHz. For the dosage levels, these probes can detect levels as low as 0.01 W/kg and up to

100 W/kg, while having an isotropy of 0.3 to 0.5 dB. Each of these probes have got correspondent acquisition electronics to convert the probe's output to an electric field value.



Figure 15 - Example of a complete SAR measurement system, made by Aprel [56].

To map the SAR distribution, these systems use a positioning system to locate the SAR probe in the measurement area. This is usually a robotic arm with 6 degrees of freedom, that is attached to the measurement container, for calibration purposes. Only for the case of the IndexSAR system is implemented a 6 degree of freedom positioning system that is not a robotic arm. In this case, three cartesian axis are provided rotational axis on the probe, on a side dipole, and the measurement table itself. These commercial solutions also provide phantoms for various frequency ranges, measurement tables, and device positioning solutions, which in this dissertation's work were not used. By using these components, alternative SAR measurement setups can be developed, such as the one shown in Figure 16, which rotates the phantom container and the probe at the same time, mimicking the measurement of SAR levels on the surface of a sphere.

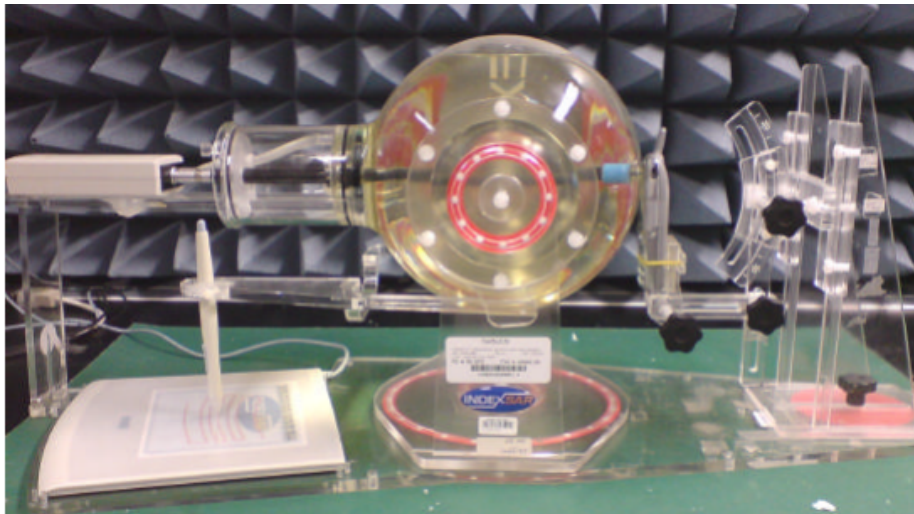


Figure 16 - Example of alternative, academic SAR measurement system [58].

2.4.2 Phantom selection

As noted above, to calculate SAR values, it is necessary to use the tissue's properties. As for these measurements it is almost impossible to use the real tissue, it is necessary to use a phantom that mimics them. Gabriel et al. [59]–[61] studied the permittivity and conductivity of several biological tissues, becoming the references for the Federal Communications Commission (FCC), which in turn defined values, Figure 17, for these properties for the human head and torso. The permittivity and conductivity are frequency dependent, with the first decreasing with frequency and the latter increasing with it.

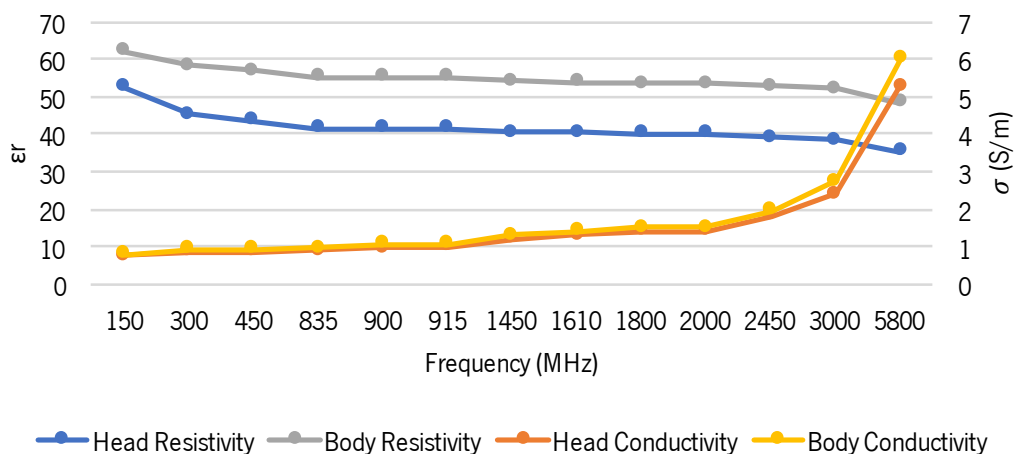


Figure 17 – Permittivity (ϵ_r) and conductivity (σ) of human head and torso, adapted from [32].

These values dictate the characteristics that a phantom should present, and to replicate them at 2 GHz, a research for recipes was made. Several were found, however, to select which is more adequate, their viscosity, stability and durability were considered along with the permittivity and conductivity of the solution.

An example of a phantom that is adequate for this frequency is proposed in [62]; it has a large bandwidth (500 MHz-2 GHz), has a long 9-week stability and can be used to mimic several tissues but it is solid. However, it uses 7 different reagents with some of them being hazardous, resulting in an extremely complex, risky recipe. Another solid phantom was proposed in [63], also having a large bandwidth (300 MHz-20 GHz), capable of mimicking several tissues, similarly to the previous one. However, this is more suitable as its reagents are not as dangerous, resulting in a more desirable recipe. Two more phantoms were proposed in [64] [65] with these being also solid, and having a bandwidth of 1 GHz to 4 GHz. Nevertheless, these are specific for different tissues of the brain such as white and grey matter.

For several experiments, the phantom had to be used with a setup in which a SAR probe is placed inside it and moved, which is a long process that takes several hours to complete. Moreover, the previous recipes were for solid phantoms, making them unfit to use with a probe moving inside them. A liquid phantom was proposed in [66], for 0.9 GHz to 3 GHz and using only four safe reagents: Deionized water, mineral oil, Triton X-100 and NaCl. Other reagents, including water and alcohol, were proposed for a recipe in [67], resulting in a phantom suited for the frequency of 2.45 GHz. The FCC also presents recipes that rely on the same reagents as the phantoms presented before [32]. These solutions, however, offer the possibility to modify the quantities of each reagent, in order to tweak the final solution's dielectric properties to the desired value. In Table 2 is presented the percentage of contents to obtain phantoms at 1.9 and 2.45 GHz.

Table 2 - Human body phantom composition and properties

Ingredients (% by weight)	Frequency			
	1900		2450	
	Head	Body	Head	Body
De-ionized water	54,9	40,4	62,7	73,2
NaCl	0,18	0,5	0,5	0,04
Sugar	0	58	0	0
HEC	0	1	0	0
Bactericide	0	0,1	0	0
Triton X-100	0	0	36,8	0
DGBE	44,92	0	0	26,7
Dielectric Constant	39,9	54	39,8	52,5
Conductivity	1,42	1,45	1,88	1,78

In [68], the authors studied the properties of some of the most common ingredients in liquid phantoms, diethylene glycol butyl ether (DGBE) and Triton X-100. It was concluded that, independently, these present undesirable characteristics, such as volatility, in the case of DGBE, and high viscosity, flammability and the generation of bubbles when mixed with water, in the case of Triton X-100. However, the proper conjugation of these reagents allows for the development of a solution with the desired physical properties. Mixing de-ionized water, DGBE, Triton X-100 and salt results in a phantom that has got low viscosity, is stable and that allows air bubbles generated during its mixing to disappear quickly. To aid in the development of this phantom, the dielectric properties of these reagents, along with deionized water, were measured and are presented in Figure 18.

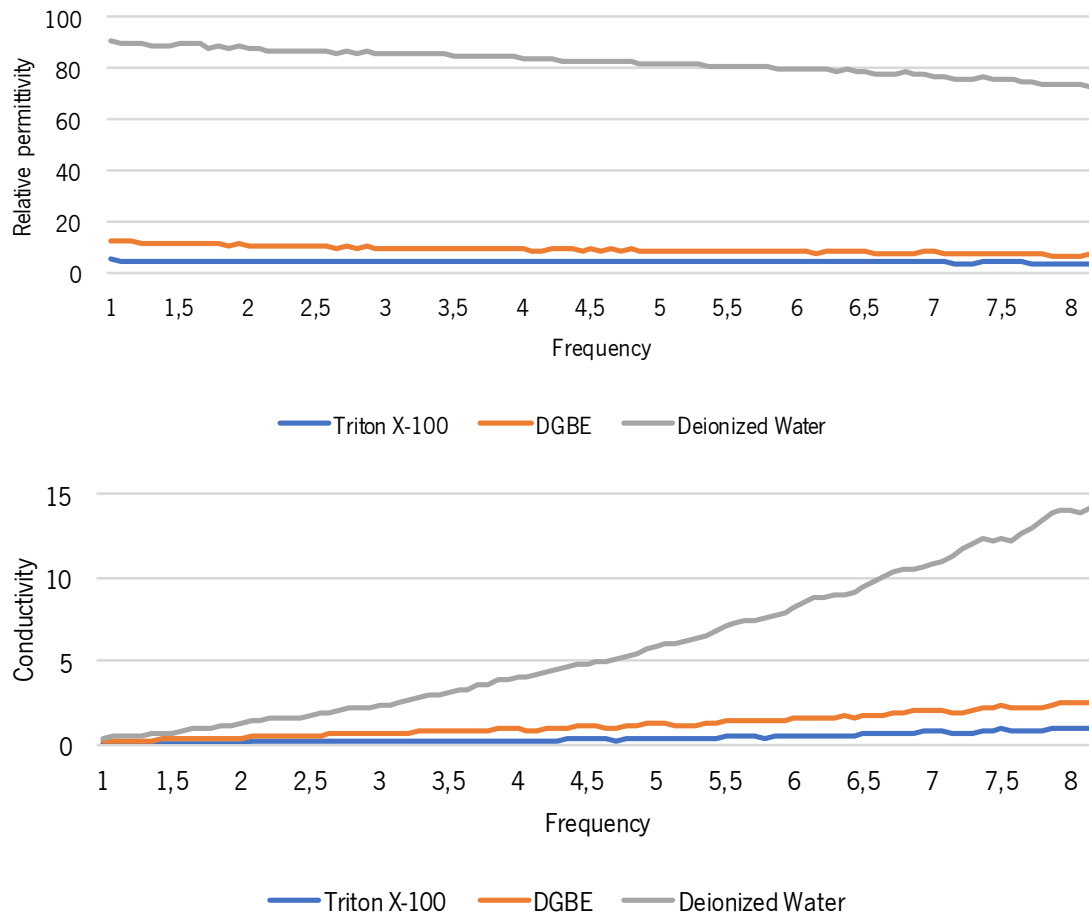


Figure 18 - Relative permittivity (top) and conductivity (bottom) of Triton X-100, DGBE and deionized water over the frequency range.

This study is useful as it is possible to more easily understand the preponderance that each constituent has got on the phantom, allowing to make small adjustments of its characteristics and producing the desired phantom. By analyzing the measurements, it is possible to conclude that deionized water has got a very high permittivity; by adding the DGBE, as its permittivity is lower, it is possible to reduce the resulting solution's permittivity. The mixture of this with Triton X-100, not only further helps to obtain the desired properties, but also prevents the evaporation of the DGBE, making the phantom more stable over time. As the conductivity still has to be adjusted, NaCl is added, to increase the solution's conductivity and obtaining the desired phantom's dielectric properties.

3 WIRELESS POWER AND COMMUNICATIONS BASE STATION

3.1 Wireless power transfer system

Several methods to implement a WPT system to transfer power to devices implanted in rodents have been reported in the literature and reviewed in the previous chapter. As most of them resort to inductive coupling, several constraints were identified. Decoupling due to transmitter and receiver sizes, misalignment due to the receiver coil's orientation, and efficiency loss due to height displacement are examples of such constraints. Moreover, these systems either transmitted power blindly to the whole cage or required a bulky and high processing-power tracking system. Finally, the systems that track the rodent's position and transfer power to it either required a setup step before the experiment or required heavily modified and/or unique housing.

The objective of this dissertation is the implementation of a WPT system to be used with an implanted device on a rodent, that is easily adaptable to any circumstance and without needing a camera or similar tracking method. The path chosen to develop such system came from the necessity to have a flexible system that doesn't require custom housing for the rodents. It was planned to be placed on the side of the rodent's housing, and due to the rodent's desirable free mobility, it must be able to transfer power all over the housing's volume. This means that it must be capable of powering the device in both short and long ranges. Another requirement was having a system that didn't limit the area where the rodents could be at, such as the cavity resonator from [31]. It used physical barriers to prevent the animals from going into low power spots. In this dissertation's work, instead of imposing such constraints it was opted to track the rodent's location.

Long distance WPT can be achieved with approaches such as optical wave power transfer or far-field RF power transfer. The National Aeronautics and Space Administration (NASA) have developed in 2003 a laser beam power transmission for unmanned aerial vehicles, and Wi-charge is a commercial alternative for long distance powering, as it aims to transmit power by using infrared beams of light [69]. These are examples of optical power transfer links, however, if the path of the light is blocked, it becomes impossible for the powering to be done. Furthermore, using high power light beams can lead to severe health complications, such as blindness. Far-field powering based on RF links is starting to be commercially available. Ossia, for example, developed the Cota transmitter and receiver, which

implements a link in which one of the devices transmits its location and the other one transmits power to it. This allows for WPT to be done to several targets, even while they are moving [70]. Another example of a commercial system is AirFuel, which, just as the Ossia's system, allows for multi-device wireless powering through RF waves, and claims to be capable of charging the device anywhere within a radius of up to 4.5 m [71].

It was opted to develop a RF WPT system as it allows for a more flexible solution comparatively to other possible methods. Moreover, by using RF in the low-gigahertz band, it is possible to transfer power wirelessly while overcoming some constraints associated with inductive coupling. As low power zones can exist due to the antenna's radiation pattern, along with the fact that the surroundings can affect the link's efficiency, the developed system resorted to beamforming to prevent these complications. This also allowed to direct the beam and transfer more power to where it was needed, consequently achieving a higher power transfer efficiency [72]. In addition to this, by using two transmitters instead of one, it is possible to transfer up to four times the amount of power compared with one antenna, depending on the power output of each antenna. As the implantable device must have a small size, the frequency at which the WPT system will operate is 2 GHz, allowing for a small antenna to be used on the implant. From Figure 19, it is also possible to verify that due to the free space path loss, the higher the frequency, the more severe is the attenuation over the same distance. By transmitting power at 2 GHz, it is possible to circumvent a higher power loss that can exist if higher frequencies are used, due to the free space path loss, while also allowing for small antennas to be used on the implant.

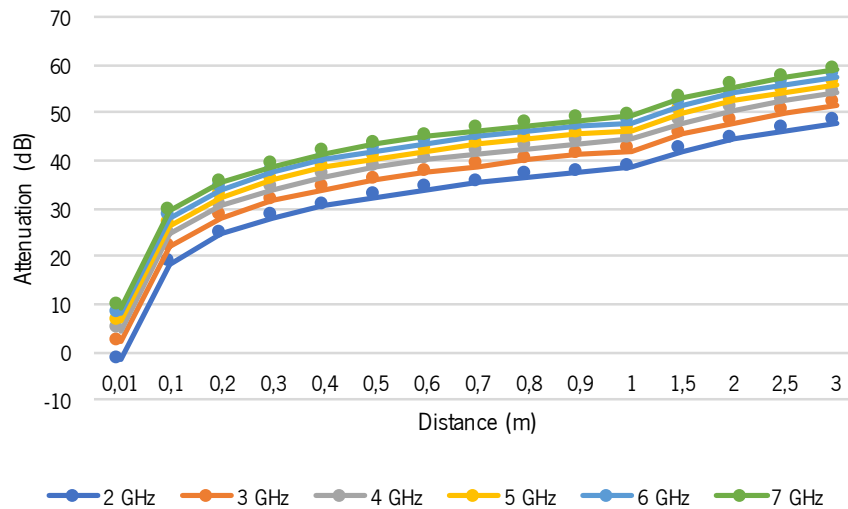


Figure 19 - Free space path loss of various frequencies over the distance.

As stated, the beamforming technique can be used to implement the power transfer system to direct more power to the rodent's position. The tracking system, however, instead of relying on a camera feedback and requiring high amounts of computational power, uses a wireless feedback to track the rodent's position.

Due to the impossibility of directly assessing the real and absolute position of the rodent through the developed approach, it was necessary to implement a method to indirectly determine it. The WPT system's feedback was implemented resorting to the amount of power transferred by a secondary antenna system that operates at a frequency that is double of the WPT one. By switching the WPT beam's direction through the manipulation of the phase of one antenna, it is possible to change the amount of power transferred to the implant. Since the received feedback power is proportional to the power at the receiver, it was possible to implement a tracking algorithm to follow the rodent's relative position. This was attained by resorting to a relative comparison of the power transferred throughout the powering.

As through this method it is not possible to directly determine its position, it was planned to work at 1 kHz sampling frequency. Lastly, the designed system does not require any planning before the experiment, any external tracking, high-power processing unit and doesn't limit the rodent's movement in any way.

3.1.1 System architecture

The implemented system was based on key elements, which are the beamforming system to direct the beam direction, tracking system to control that direction in each instant, and the feedback loop that allows for the system to determine in which direction to aim the beam. For the beamforming system, it was necessary an RF system that generated two similar signals with a defined phase difference. In order to achieve this, a splitter was used to divide the RF wave from the power source into two equal waves, and then the phase shifter was used to control the phase of one of them. For the feedback loop, a splitter was used at the implant side to divide the received RF signal. Part of this signal was used to power the implant, while the remaining part was sent back to the external transmitter's power detector at a frequency of 4 GHz. This frequency was chosen to avoid interference from the WPT system in the feedback loop, which would happen if both operated at the same frequency. For this feedback mechanism to be possible, a secondary pair of transmitting and receiving antennas was, as two wireless links were necessary: one for transmitting power and another to receive the wireless feedback. For the implementation of each of these parts, it was necessary to select components that allowed to build the final system, along with the tracking system. These building-blocks originate a system that meets the previously described requirements, for which it was also necessary to implement a power management block. The implementation of this system will be described in the following sections.

3.1.2 System's block diagram

A diagram of the complete system is presented in Figure 20. The powering interconnections of the system are represented in black. When there is not only power but there also is a control or data signal, the connection is represented in blue. The RF circuitry is represented in orange and lastly, in yellow, is represented the RF feedback of the WPT link. The presented blocks and their interaction will be described subsequently.

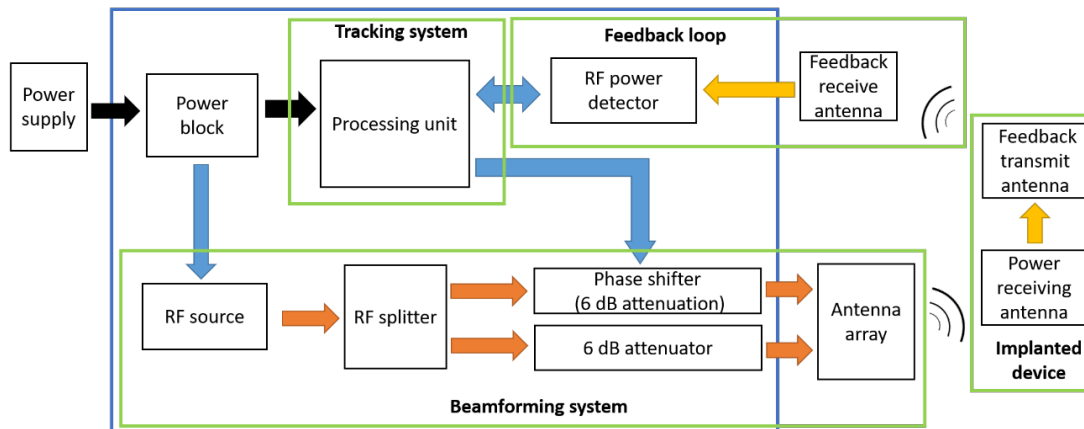


Figure 20 - Block diagram of the developed WPT system.

Three main parts of the developed system can be highlighted: the beamforming system, the feedback loop and the tracking system. It was necessary to control the phase difference of the RF signals, which means that one high-precision 2 GHz generator for each signal path would be necessary. These would have to generate the exact same signal, with the same amplitude and phase, which is problematic due to factors such as phase noise and amplitude. Instead, a single generator and a splitter were used to divide the generated signal into two identical signals. For the control of the relative phase, it was necessary to use a phase shifter in one of the signals branch. The phase shifter presented a 6-dB insertion loss, which was compensated in the other signal path by using a 6 dB attenuator, maintaining the power level of both signals equal. With the beamforming signals generated, they were fed to the antenna array. The configuration of the system doesn't allow for a single high-power RF source, as both the splitter and phase shifter are not suited for use with high input power. Consequently, power amplification must be done on the output of the phase shifter and of the 6-dB attenuator, which means that two identical power amplifiers were required. Moreover, if a single RF source was used, the system would incur on a high power loss due to the attenuation generated by the phase shifter.

As explained before, since a feedback was necessary to perform the tracking, a power feedback loop was implemented. By using the transmitted 2 GHz signal, a 4 GHz signal was generated with a power level that is dependent on the power received by the WPT link at 2 GHz. It was then wirelessly transmitted back to the system and input to a power detector. To control the system and run the

tracking algorithm, a processing unit was required. Lastly, as several supplies were needed, it was necessary to develop a power management block, as the selected power supply only outputs 24 V.

3.1.3 Power budget

To power the device implanted in the rodent and recharge its battery, it is necessary to transfer a certain amount of power. In this case, according to [33], the device needs at least 1 mW for recharging. It is then required to determine the system's characteristics and estimate how much power it is necessary to transmit to achieve an effective wireless powering. In Table 3 are presented the gains of the components used, where free space path loss is calculated for 2 GHz and a distance of 40 cm, and the gain is presented in dB or dBi for the case of the dipoles.

Table 3 - Components used in the system and correspondent gain

Component	Gain (dB or dBi)
RF splitter	-3.2
Phase shifter/ attenuators	-6
Coaxial cables	-2,3
Power amplifiers	44.4
Transmitting dipole	2,1
Free Space Path Loss	-30,5
Receiving dipole	2,1

This information was used to determine the cumulative power budget of the system, which is presented in Figure 21.

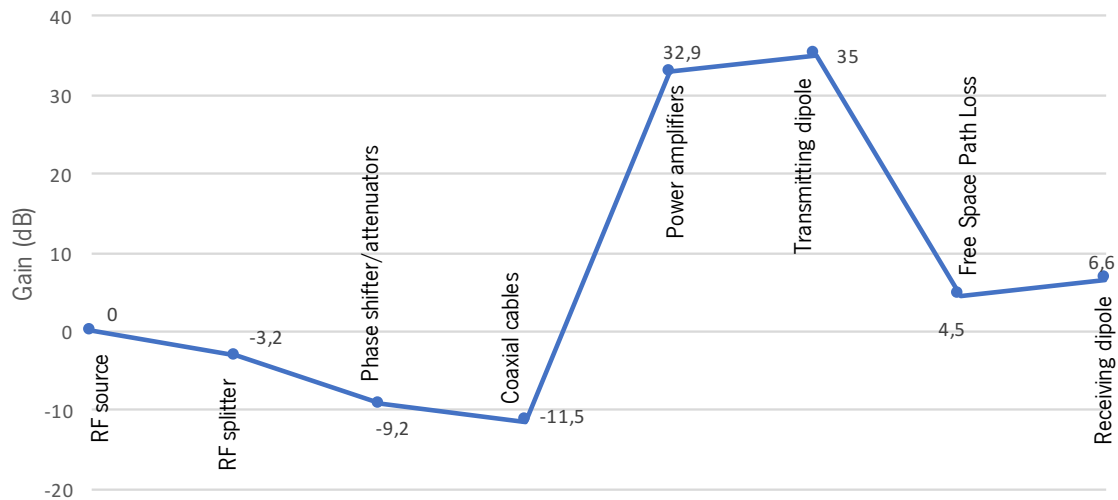


Figure 21 – Cumulative power budget of the developed system.

As this system resorts to beamforming, it is necessary to take the array effect into account. In this system, two elements were used for the antenna array and, as their signals are always in phase due to the tracking algorithm, the signals' recombination on the receiving antenna results on a higher amplitude, which is dependent on the array's directivity. According to [73], the directivity (D) of the array for a broadside configuration is given by:

$$D = 2 \frac{Nd}{\lambda} \quad (2)$$

where N is the number of elements of the array, d the separation between them, and λ the wavelength. By using an end-fire configuration, it is possible to further increase the gain of the array, as it is defined by:

$$D = 4N \frac{d}{\lambda} \quad (3)$$

The placement of the antenna array makes this system operate between both conditions, broadside when the rodent is between the antennas and end-fire when it is close to one of the extremities of the housing. However, as the array will be spaced at half wavelength, the end-fire radiation exists in both directions [73], which results in a lower directivity. Due to this, the broadside configuration will be considered to calculate the power budget.

In this case, the array is composed of two elements separated at half-wavelength, which results in a 3 dB extra gain. Given this, to the resulting power budget of 6.6 dB, it is necessary to add that gain, due to the aggregate factor of the antenna array, resulting in a 9.6 dB gain.

It is possible to conclude that to power the device, it is necessary a minimum power source of -9.6 dBm, if an efficiency of 100% by an RF-DC conversion at the receiver is considered. However, as this is not possible, an RF source with a power output of 4.1 dBm was used, resulting in a transferred power of 13.7 dBm (23.4 mW).

For higher power draw devices, it is possible to replace the dipoles by more directive horn antennas. For example, if a gain of 5 dBi is considered, it would result in a received power of 16.6 dBm (45.7 mW). Replacing the RF source by one with a higher power output can also result in a higher power delivery. As the power output is limited by the power amplifiers (40 dBm), the maximum RF source that can be used can have a power output of up to 7.1 dBm, resulting in an expected received power of 19.6 dBm (120.2 mW), for the case where the horn antennas are used.

3.2 Wireless power beamforming system

The radiation pattern of a single element is usually wide, providing low values of directivity (gain). Obtaining more directivity is only accomplishable by increasing their electrical size. An alternative is the assembly of several individual elements, without increasing their individual size [73]. This creates an array of antennas, in which although not required, its elements are usually identical, as it is simpler, more convenient, and practical. By combining several elements, it is possible to obtain higher directivity, as the fields generated by its elements interfere with each other either constructively (add) or destructively (cancel each other). It is possible to define in which directions these interferences arise, making the constructive interferences occur in the desired directions while keeping the destructive interactions on the remaining ones. Through this approach, it is possible to obtain a higher directivity with a faster beam direction control unlike with a single high directivity antenna, which is heavier and must be physically oriented [73].

In an array of identical elements, it is possible to shape its pattern by manipulating five variables: the geometrical configuration, the displacement between the elements, the excitation amplitude of each element, the excitation phase of each element and the relative pattern of each element [73]. Considering an array of two infinitesimal dipoles, the total field radiated by them is given by:

$$E_t = E_1 + E_2 = \hat{a}_\theta j\eta \frac{kI_0 l}{4\pi} \left\{ \frac{e^{-j[kr_1 - (\beta/2)]}}{r_1} \cos\theta_1 + \frac{e^{-j[kr_2 + (\beta/2)]}}{r_2} \cos\theta_2 \right\} \quad (4)$$

with β being the difference in phase excitation between the elements and considering an identical magnitude of excitation. When assuming far-field observations, according to [73] that equation is reduced to:

$$E_t = \hat{a}_\theta j\eta \frac{kI_0 l e^{-jkr}}{4\pi r} \cos\theta \left\{ 2 \cos \left[\frac{1}{2} (kd \cos \theta + \beta) \right] \right\} \quad (5)$$

Thus, the array factor of the two-element array is given by:

$$AF = 2 \cos \left[\frac{1}{2} (kd \cos \theta + \beta) \right] \quad (6)$$

This is a function of geometry of the array and excitation phase, which by varying the separation d and the phase β , it is possible to control the array's characteristics. The directivity of the entire array is then defined by the multiplication of the array factor by the directivity of the individual elements:

$$D_{array}(\theta, \phi) = AF \times D_{element}(\theta, \phi) \quad (7)$$

For this WPT system, it is necessary to generate and manipulate the RF signals, as it is the chosen mean of powering. The method used to transfer power will be based on the beamforming technique. Although several factors can be used, such as the radiation pattern of the elements, their displacement and geometrical configuration will be kept constant. Moreover, as previously shown, it is possible to control the generated beam's direction by modifying the phase, for which the amplitude of excitation was also kept equal for both elements. As such, in this subsection, the devices used for the generation and handling of the RF signals as well as the phased array are described.

3.2.1 Antenna array module

From Figure 22 it is possible to conclude that by using more than one element, it is possible to obtain a higher directivity than by using only one. However, if a larger number is used, the cost of the system is immensely increased. By using high directivity antennas and more elements, more power amplifiers are necessary for each ramification, and the space occupied by the entire system becomes too large. As such, taking the technical and economic aspects into account, a two-element phased array was implemented. Two dipoles oriented along the Z axis were placed on the Y axis half-wavelength away from each other, originating an array with a total gain of 6 dBi, according to [74]. Simulations were

performed in HFSS to verify this, where the maximum gain obtained was approximately 6.1 dBi, as shown in Figure 22. This configuration originated the higher gain, when comparing to two dipoles separated at half wavelength on an end-fire configuration. Moreover, it also produces a higher gain when compared to a quarter wavelength separation, either on a broadside or end-fire configuration. Lastly, for other applications, these dipoles can be replaced by more directive antennas, such as patch or horn antennas, obtaining a higher directivity.

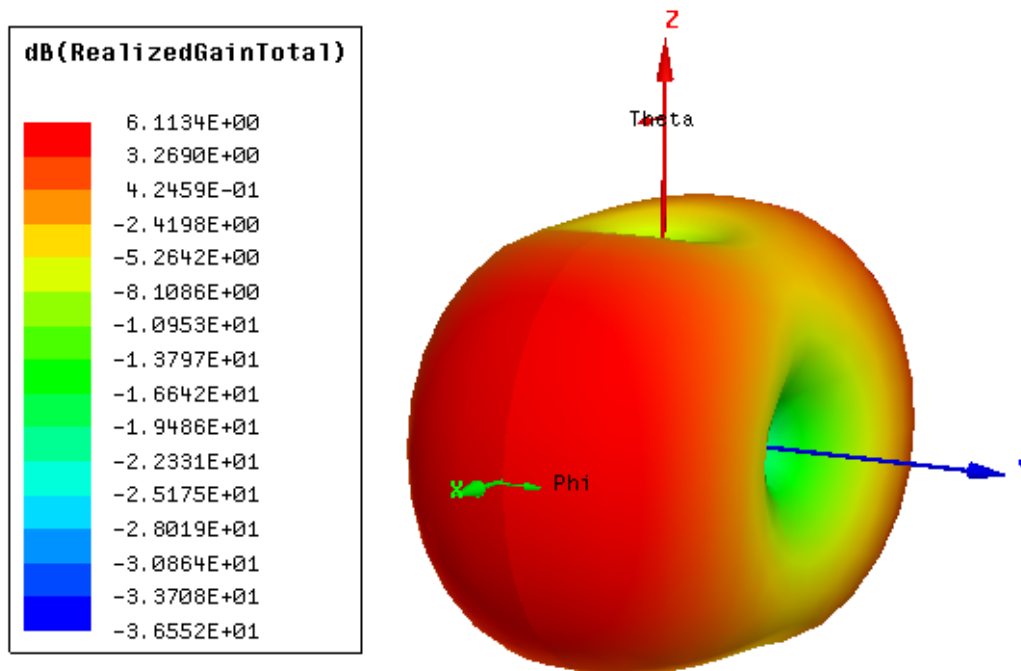


Figure 22 - Dual half-wavelength dipole array's radiation pattern.

The antenna array developed was comprised by two elements, which had to operate at 2 GHz. The radiating elements developed were two half-wavelength dipoles separated by a distance of half a wavelength in free space (7.5 cm), as displayed in Figure 23.

As high-power RF signals would have to be generated and handled, the beamforming module would have to be able to withstand them. Although the used splitter can support input power levels of up to 10 W, the remaining components, i.e. phase shifter and attenuators, can only withstand 630 mW and 1 W, respectively. The solution to implement the high-power system was to use two power amplifiers after the RF signals have been generated and phase shifted. The power levels generated are only attenuated by 1 dB due to the coaxial cables connecting the amplifiers to the antennas, and allowing for almost all the power generated to be transmitted.

To transfer the required amounts of power, it was necessary to use RF power amplifiers. These had to operate at the desired frequency of 2 GHz, for which high power amplifiers which had the lowest cost were chosen. The selected ones, one for each antenna, were the ZHL-10W-2G+ from MiniCircuits® which have to be supplied 24 V at a maximum current of 5 A each. These have got an operating frequency range from 800 to 2200 MHz, a 44.45 dB gain and a maximum power output of 10 W at 2 GHz, making them suitable for this application.

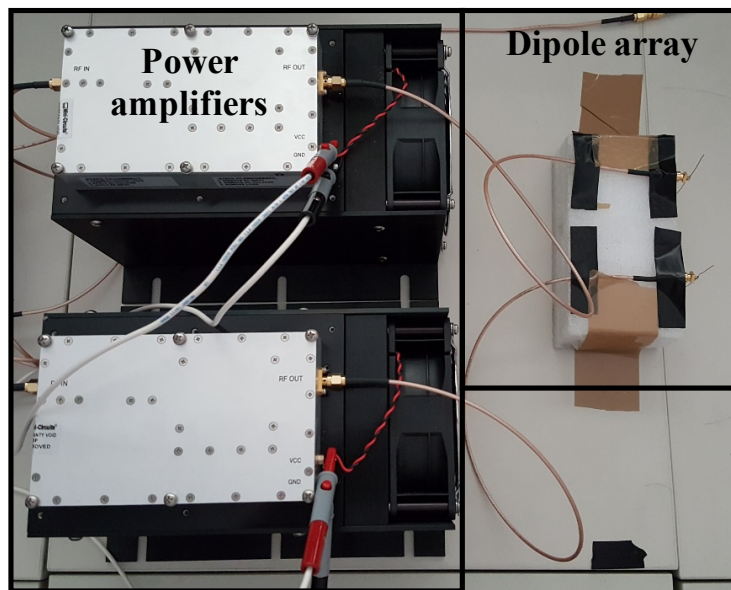


Figure 23 - Developed antenna array and respective power amplifiers.

3.2.2 Array's phase control

To control the array's beam direction, it is necessary to control the phase difference between the elements of the array. As this is a two-element array, only the phase of one of the elements had to be changed. Therefore, to modify the phase difference between the two previously generated signals, it was necessary to use a phase-shifter. It was required to have a high resolution to modify the beam direction in small steps and allow tracking the rodent, while maintaining the highest power transfer possible in each position.

The one that fulfilled the requirements was the PE44820 from Peregrine Semiconductor, shown in Figure 24. It is capable of operating in a frequency range from 1.7 to 2.2 GHz, which makes it suitable to work at the desired frequency, and requires a supply of 3.3 V and 200 μ A. Moreover, it is a full range shifter, which means that it can change the phase value of the signal from 0 to 358.6

degrees. As it is digitally controlled by 8 bits, it has got a 1.4 degree resolution. This is required as small phase increments allows the beam to be directed more precisely. Besides, it can be controlled through SPI and has got a maximum 25 kHz switching frequency, which allows to track the rodent at the desired frequency of 1 kHz. However, this phase shifter has got an insertion loss of 6 dB, making it necessary to balance the power level between the two antennas. Two VAT-3+ 3 dB attenuators from Minicircuits®, were used to compensate the phase shifter's insertion loss. The phase unbalance generated by different paths from the splitter to the antennas (one through the phase shifter, the other through the attenuators) is not problematic, as the algorithm developed is adaptive and compensates this difference.

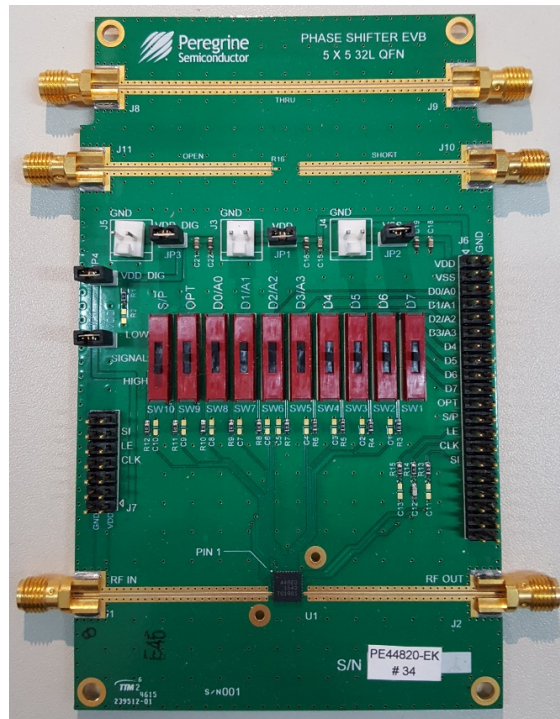


Figure 24 - Phase-shifter used to modify the phase value of the RF signal.

3.2.3 RF signal generation

As the implemented solution relies on beamforming, it is necessary to have two RF signals, one for each of the elements of the array. Instead of using two RF sources, it was preferred to split the RF signal the required number of times, to prevent amplitude and phase variation during the system operation, obtaining more reliable phase control, and consequently a more stable system. In this case, as it is a two-element array, a single 2-way splitter was necessary. The main requirement for this splitter

was to have a low power unbalance, managing to divide the power equally in two, to each of the antennas. For the phase difference, it is only required that this difference is stable over time, as it can be compensated by the algorithm and phase shifter.

The used RF splitter was the ZAPD-2-272-s+, from MiniCircuits®, presented in Figure 25. This component is a two-way splitter and at 2 GHz presents a 0.3 dB insertion loss, 0.24 degree phase unbalance and a 0.02 dB amplitude unbalance, being capable of splitting into two signals with low amplitude difference. This makes it suitable for this application and for the generated signals to be used in the phase shifting and beam directing part of the system.



Figure 25 - Splitter used to generate two identical RF signals.

By using a splitter, it becomes possible to use a single RF source. In this case, it must generate an RF signal at 2 GHz, while also presenting a small size in order to be implemented in a portable system. The generated signal does not have strict requirements such as high precision and performance, which are required in several communication links. As it will not be used for data transfer, it must only generate the RF signal to be processed by the beamforming module, amplified, transmitted and received by the antennas. Given this, the voltage-controlled oscillator (VCO) is not required to have an extremely low phase noise, as the beamforming module uses a splitter to generate two signals from the VCO's one, which would approximately have a zero phase difference between them.

The ZX95-3800A+ VCO, from MiniCircuits®, displayed in Figure 26 was the RF source selected. It can generate an RF signal from 1900 to 3700 GHz. More specifically, it can generate a 2 GHz signal at a power of around 4.1 dBm. This device presents a very small size, which is perfect to develop a small and portable system. Moreover, the power supply needed must be of 6 V DC and 55 mA, allowing for an easily implementable power source. Lastly, to obtain the 2 GHz signal, it is necessary to control the VCO by using a specific tuning voltage, which was of 1.74 V and obtained by

implementing a voltage divider with a multiturn potentiometer and a resistor. The generated RF signal was then passed on to the RF splitter.



Figure 26 - VCO that was used as RF source for the WPT system.

3.2.4 Feedback loop

A feedback of the amount of power received by the device was needed, such as a Received Signal Strength Indication (RSSI), for the tracking algorithm to adapt the beam direction. However, other alternatives for the implementation of the feedback are possible.

An example of a feedback implementation would be the control of a VCO by the amount of power received on the receiver side. That power level is converted to an analog value which in turn would control the oscillation frequency of the VCO present in the device. Lastly, it would be transmitted wirelessly and detected by the management system, which would convert the frequency to a power level value.

Another alternative would be implementing a modulation of a specific carrier wave which would vary according to the amount of power received. An example of this is the sigma-delta modulation, which would be transmitted by the device and converted to an analog value by the feedback module for the tracking mechanism.

However, these were not used, as the variable frequency feedback would require an oscillator generating the feedback and a frequency to voltage converter receiving it. The second approach would require a sigma-delta modulator generating the feedback and a demodulating circuit on the outside. None of the presented options for the feedback loop were used as they would make the device for the experiment bulkier and require the implementation of a powering solution for them. Alternatively, a

wireless power feedback similar to the RSSI used in wireless communication systems was implemented. The method used for the feedback resorted to transmitting a signal with a power level correspondent to the received power, but in another frequency band to avoid interference from the WPT system. Although this makes the system bulkier, it is of simpler implementation, not requiring the development of a more intricate feedback generation system.

As it was not yet possible to use the developed chip (developed parallel to this work) to test the feedback loop, another system was implemented. The energy received by the antenna on the implant-side was split in two equal signals by the ZX10-2-42+ splitter, from MiniCircuits®. As it divides the input signal in two with approximately the same power, half of that power was used to light up an LED with an RF-DC converter, which represented the implantable system, and the other half was used for the feedback loop. To use another frequency for the feedback, that signal was input in the frequency multiplier, ZX90-2-50-S+ from MiniCircuits®, which doubled its frequency. A 4 GHz signal is generated with a power level related with the power received at 2 GHz, allowing for a relative assessment of the power transferred. On the tracking system, a feedback antenna receives that feedback power and inputs it to a power detector. Its output is an analog value, representative of the amount of power transferred which is then used in the tracking system.

The power detector needed for the feedback had to have a response time of at least 1 ms, as the feedback was projected to be done at 1 kHz. Moreover, it had to have got a resolution that could differentiate power levels varying under 1 dBm. As power is lost on the powering link and feedback link, a power detector that could detect low power levels was chosen.

To implement the feedback, the power detector used was the ZX47-60-LN-S+ from MiniCircuits®, presented in Figure 27. It is a wideband device (10 to 8000 MHz) and requires 5V DC at 120 mA to perform its task. The lower detection limit of this device is -60 dBm and the power received from the feedback loop can attain power levels that are close to that limit. For the tracking algorithm to be run, it was necessary to amplify the received feedback signal from the antenna to generate a reliable feedback. For this, the ZVA-183-S+ amplifier was used, whose output was directly connected to the power detector to measure the power received.

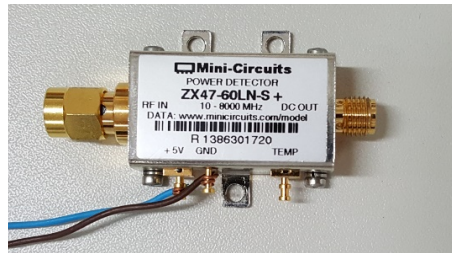


Figure 27 - Power detector used to implement the feedback for the tracking system.

To perform as a feedback, the power detector outputs a DC voltage according to the input power. It is then connected to an analog input in the control module board, through a coaxial cable. The generated voltage has got a response time of 800 ns (rise time) and 400 ns (fall time), making it suitable for mimicking the 1 kHz feedback for the tracking algorithm. Furthermore, its DC output varies 20 mV/dBm, making it suitable for a high precision power measurement.

The measurement power range of this device is comprised from -60 dBm to 5 dBm, having the performance required for the system, as the expected power level is in that range (approximately 0 dBm to -50 dBm). These values consider the power level transmitted, 40 dBm maximum, to which free space path loss for 2 GHz, which is 18.46 dB at 10 cm and 30.5 dB at 40 cm, and free space path loss for 4 GHz, which is 24.48 dB at 10 cm and 36.52 dB at 40 cm, are subtracted. Additionally, it was considered that there could be extra losses rounding 20 dB due to the feedback antennas' orientation, to the conversion loss from the multiplier, and cable losses. This allows for the power level to be detected in the rodent's housing area, and for the tracking system to be implemented. The detected power level is dependent of the temperature. However, the absolute value of power transferred is not needed for the tracking algorithm, and the temperature varies slowly. As only relative values between each iteration can be used, the temperature value was not considered.

3.3 Tracking system

With the beamforming system and the feedback loop implemented, it was necessary to develop a way to use the generated feedback to control the beamforming system. A tracking system to control power transfer to the rodent's position was required. To manage the feedback loop information, it was necessary to resort to a processing unit, which used the feedback information to perform the tracking and to control the beamforming system. The processing unit had to be able to read the analog value

from the power detector, execute the tracking algorithm, and control the phase shifter to perform the tracking.

The implemented position feedback does not allow for a direct absolute position assessment. Instead, it requires an iterative process to determine the position of the rodent. The developed tracking algorithm used the feedback provided by the power detector to control the power transmitted to the position of the rodent. The algorithm modifies the phase difference of the beamformer in real-time and detects the position of the rodent by searching for the maximum amount of power transferred to the implantable device.

3.3.1 Processing unit

To control the WPT system and allow it to perform the tracking, it was necessary to have a processing unit. This had to be able to control the phase shifter through a Serial Peripheral Interface (SPI) connection, to read the analog voltage generated by the power detector with a resolution of under 20 mV, and to be able to process the algorithm.

The used processing unit was based on the Atmega328 which has a clock of 16 MHz and is an 8-bit microcontroller, making it suitable to perform the tracking and run the algorithm at 1 kHz, while controlling the 8-bit phase shifter. The microcontroller was used to measure the feedback signal from the power detector and control the phase-shifter through SPI, requiring only three connections: slave select, clock, and MOSI. Moreover, the analog to digital converter used 10 bits, which approximately results in a 4 mV resolution (correspondent to 0.2 dBm), with the 5 V reference. It is only necessary to power the processing unit with 12 V, as the microcontroller is embedded in an Arduino board, which manages the power for it with onboard voltage regulators.

3.3.2 Active tracking algorithm

With both the processing unit that handles the generated RF signals and the feedback loop from the amount of power transferred implemented, it is now possible to develop a completely autonomous system. As explained before, it must be able to track the rodent, with an indirect indication of the amount of power transferred being the only information available to it. For the development of the algorithm, it was considered that part of the energy transferred to the device is directly used in the

feedback loop, without requiring the battery to have a minimum power level to be detected, i.e., it can operate even when the battery to be recharged is completely empty, as long as external power is reaching the implant. Moreover, at the start of the algorithm, the position of the rodent is completely unknown and must be discovered. Considering these conditions, the developed algorithm consisted in two major parts: brute force and active tracking. The developed algorithm for this specific application is presented in the flowchart in Figure 28 and will be described subsequently.

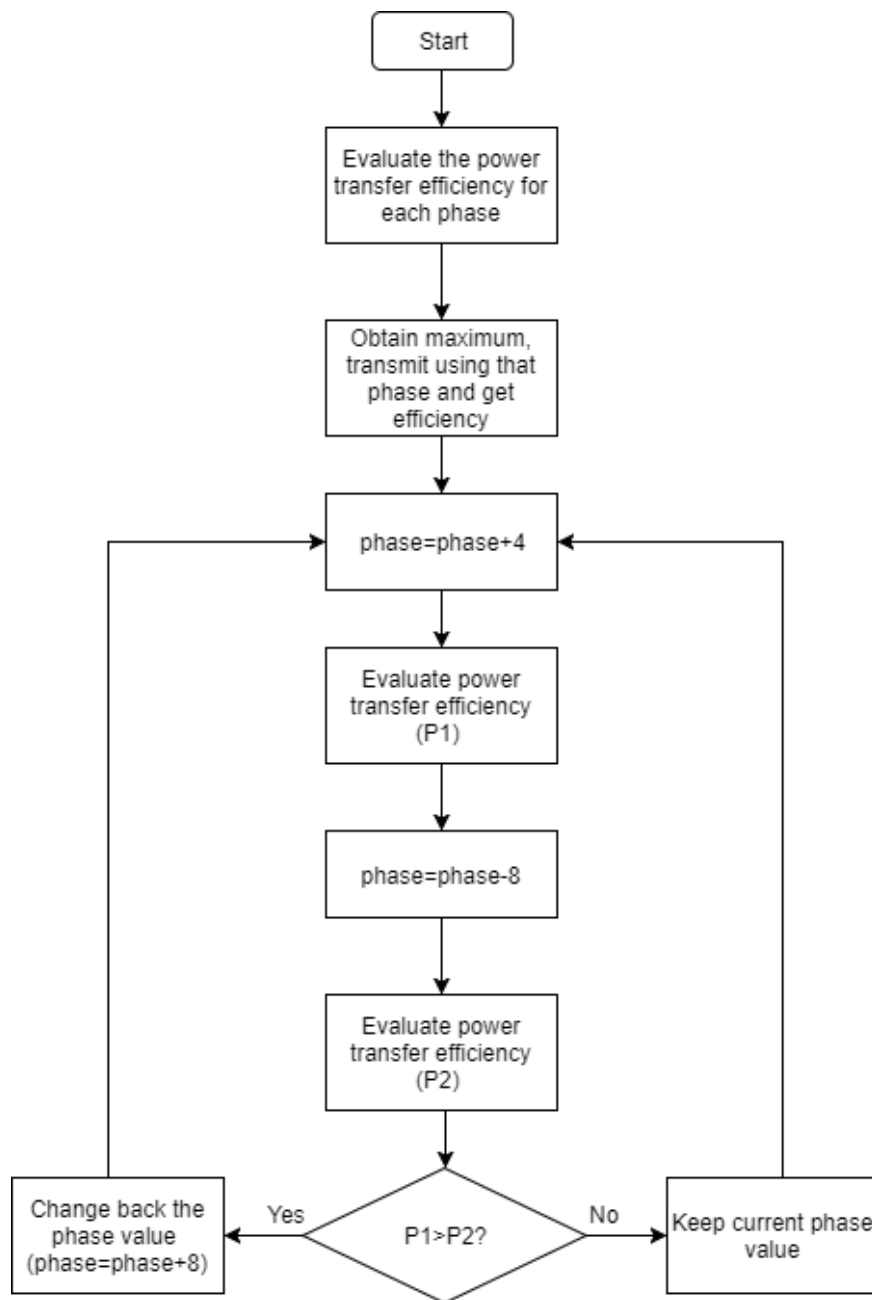


Figure 28 - Flowchart of the developed algorithm.

It was intended for the developed tracking algorithm to require low computing power, allowing it to be implemented on a microcontroller, and to perform tracking at high speeds. Given this, the developed algorithm was based on the Hook and Jeeves direct search algorithm, which is a simple, derivative-free direct search method that is convergent and doesn't require high computing power [75]. This algorithm is used to search for the maximum or minimum of a function by searching the

neighboring elements and selecting the highest or smallest one as reference. When the central point is the chosen one, the window of the search is narrowed down to elements that are closer to the center, eventually finding the maximum or minimum. In this case, the function to be maximized is the power distribution for each phase value, which is defined by the angular position of the rodent in relation to the antenna array. By varying its position in time, it also modifies the function to be maximized, consequently changing the value and coordinates of the maximum. However, the implemented initialization helps to skip the search and consequent reduction of the size of the window.

As stated before, it is considered that the initial position of the device is unknown and that it always transmits the feedback signal. For the algorithm to track the device, it was necessary to search and detect its position. For this, it was opted to follow a brute force approach for the initialization procedure. All phases (beam direction) were swept to detect which one transferred the highest amount of power, avoiding local maximums. As there is only one variable, this approach can be performed in under 300 ms. After having determined which of the phases obtained the highest transfer efficiency, the starting point for the implemented tracking algorithm was defined.

The value of the phase that was determined in the brute force initialization is used and then the tracking is iteratively done by directing the beam to each side of the detected position. This is done by modifying the phase of the RF signal to two neighboring values, next to the current iteration's phase. These phase values are separated by 5.6 degrees which is correspondent to 4 from 0 to 255, to control the phase shifter. This value is incremented and decremented to the current iteration's phase, covering the movement to both sides. The amount of power transferred is compared by aiming the beam to each of the sides and, finally, whichever is greater is defined as the current position and central phase value for the next iteration.

This algorithm is in constant operation and performing the tracking of the rodent. As the 360 degrees of phase allow to control the array's direction in 180 degrees, and considering that the variation of the phase is directly proportional to the variation of beam direction, a variation of 1.4 degrees (correspondent to the value of 1 to control the phase shifter) corresponds to a modification of the beam direction of 0.7 degrees. As the phase is changed 5.6 degrees in each iteration, and both sides are checked, it corresponds to a maximum variation of 5.6 degrees in three iterations. In terms of beam direction manipulation, it achieves a maximum velocity of 1306 degrees/s. Theoretically, with this algorithm, at a distance of 15 cm it is possible to track an object that is moving at 3.41 m/s, a velocity that is much greater than the estimated speed of the rodent in housing [28], [29].

3.3.3 Tracking validation

The developed algorithm, including the initialization by brute-force and the active tracking, were tested using Matlab. To simulate and validate the algorithm, an angle change in relation to the transmitter that varied at 3 Hz was generated and tracked at 1 kHz. The implemented feedback was dependent on the result of the difference between the simulated angle and the angle detected by the algorithm. To this difference (diff) was attributed a score (score) by using the equation:

$$\text{score} = e^{-|\text{diff}|*0.05} \quad (8)$$

The results of the simulation and testing of the developed algorithm are presented in Figure 29, where in orange is represented the simulated position, while in blue is represented the phase obtained by the tracking algorithm. It is demonstrated that the developed algorithm can perform its function and will be implemented on the final system.

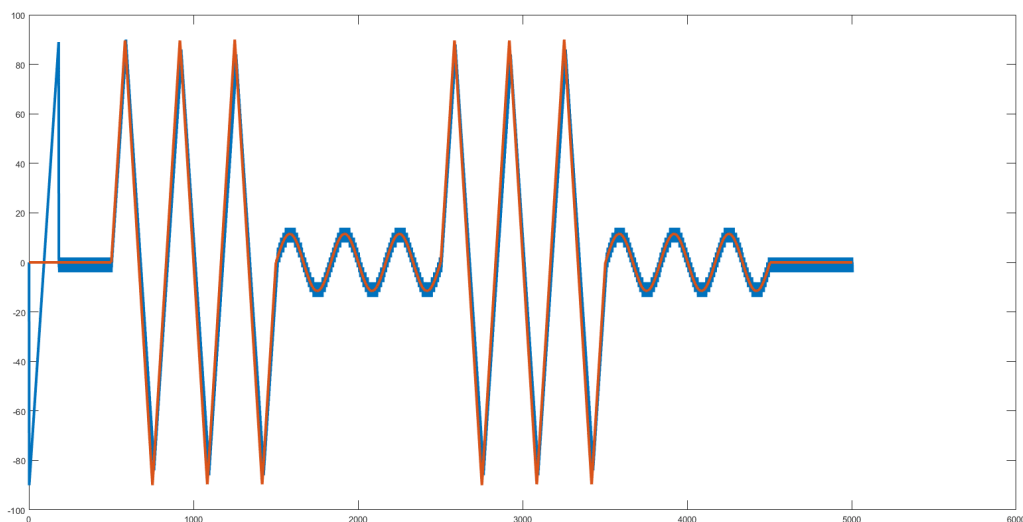


Figure 29 - Results of the simulation of the developed tracking algorithm (orange – simulated position, blue – phase obtained by the tracking algorithm).

3.4 Wireless communication system

In addition to the need to power up the implantable device, it was necessary to communicate with it, and as such a wireless communication system had to be developed. Several communication solutions for short-range communication systems such as WiFi and Bluetooth are available. However, as for the developed chip (parallel work developed under the same project) it is required a communication link with a specific communication protocol, an in-house communication system had to

be developed. The design and implementation of a unique wireless communication link is, therefore, the objective of this subsection.

A bidirectional communication system was necessary and was projected to work on a different frequency band from the WPT system. As it doesn't require a high data transfer rate and it must allow for the implementation of relatively small antennas, it was projected to operate at a frequency of 1 GHz, using an OOK modulation. Given this, it was necessary to implement a transmission block that could transmit the data at that frequency and modulation to the chip, and a receiving block that can detect the response from it, which has got the same characteristics. Lastly, it is necessary to combine these two and obtain the desired bidirectional communication link. The blocks required for this system will be explored in the next section.

3.4.1 System architecture

Several parts were required to build the communication blocks. For the transmission block, it was necessary to generate a 1 GHz carrier signal to modulate the information and transmit the modulated signal. For this, an RF source and an RF switch were used to generate the carrier signal and the modulation, respectively. For the demodulation block, as the modulation transmitted by the implantable device will also be OOK, an envelope detector can be used to detect that transmission. A power detector was used as an envelope detector to identify the transmitted data, for which its output had to be processed to regenerate the original digital data.

The blocks of this system are presented in Figure 30, for which several off-the-shelf components were used. In black are represented the interconnections between power parts and management of the system, in blue are represented the connections where there is not only power, but also a control or data signal. Lastly, in orange are represented the RF links for both transmission and receiving blocks. These blocks and their interaction will be described in the following section.

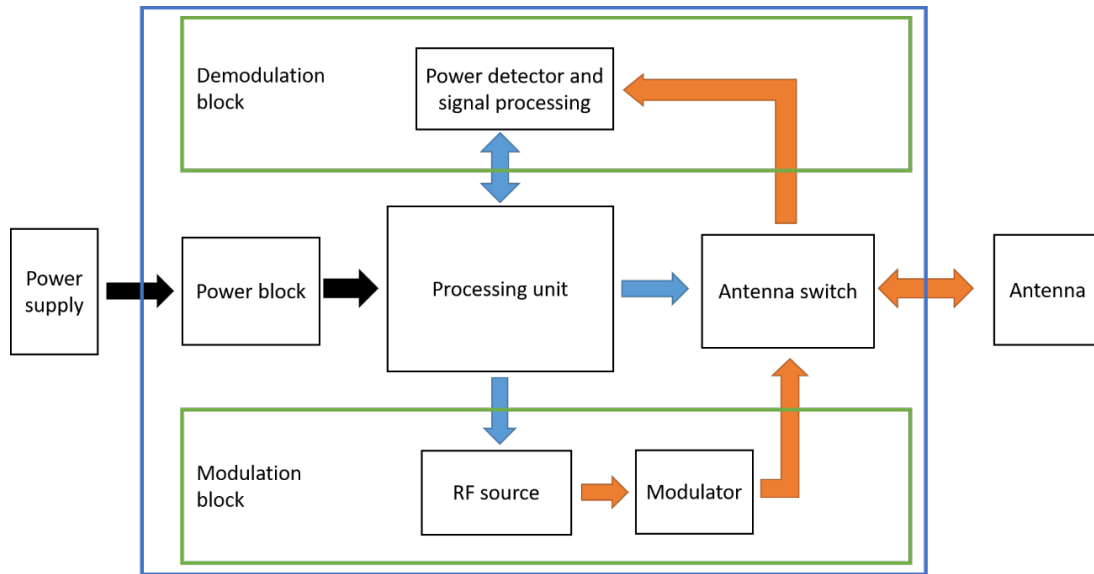


Figure 30 - Block diagram of the developed communication system.

3.4.2 Modulation block

For this block, it was necessary to modulate the carrier signal with the modulating signal. In this case, the communication link was designed to have a carrier signal of 1 GHz and a modulating signal to be decoded by a clock at 621 Hz. The modulation used was the OOK which is a simpler form of ASK modulation. In the case of OOK, as shown in Figure 31, the modulation relies on the presence of the carrier signal that represents a binary ONE, or on its absence that represents a binary ZERO.

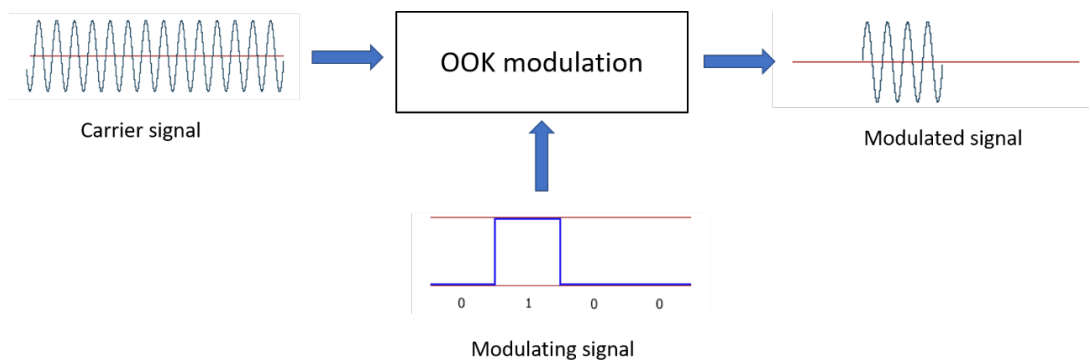


Figure 31 - OOK modulation.

It is possible to conclude that the modulating signal determines whether the carrier signal is turned on or off, to obtain the modulated signal. To perform this modulation, it was necessary to implement a switch that could turn the carrier on or off. In this case, the RF source was left on and the

modulating signal would determine whether an RF switch transmitted it to the antenna or to a 50 Ω load. The RF source used will be discussed in this subsection, while the RF switch will be addressed in the auxiliary components.

To implement the communication link, it was necessary to generate the carrier wave at a frequency of 1 GHz. The carrier wave's characteristics requirements are not strict, as the modulation is simple, the chip's detection band is wide, and the data transmission rate is not very high. Therefore, the generator is not required to have an extremely low phase noise, as this system does not resort to frequency modulation nor phase modulation. The necessary carrier wave can be easily generated by almost any VCO. These requirements were met by the ZX95-2150VW-S+ VCO, from MiniCircuits®, displayed in Figure 32. This device can generate an RF signal from 970 to 2150 MHz, and at 1 GHz outputs a power of around 3.75 dBm. The power supply needed by it must be able to output 26 mA at 5V, and to generate the 1 GHz signal, it was implemented a voltage divider to generate a tuning voltage of 2.77 V.



Figure 32 - VCO used as the RF source for the communication system.

3.4.3 Demodulation block

This block had to demodulate the RF signals transmitted by the chip, which has OOK modulation with a 1 GHz carrier wave. For its implementation, it was first necessary to filter the received signal, as several communication systems are used everywhere and, more importantly, the developed WPT system transfers high amounts of power at 2 GHz. As this system was projected to be used at the same time as those, it is necessary to filter unwanted signals from different frequency bands.

The filter used was the VBFZ-925+, from MiniCircuits® and presented in Figure 33. This is a bandpass filter with a passband from 800 to 1050 MHz, for which it has a typical insertion loss of 1.6

dB, up to a maximum of 2.3 dB, while presenting an insertion loss of at least 30 dB on the stopbands, allowing for the communication signals to be detected, while filtering out unwanted ones.



Figure 33 - Bandpass filter used in the demodulation block.

With the received signal filtered, and as an OOK modulation is being used, its demodulation can be done by using an envelope detector, much like the one used in the WPT system. The power detector used was the ZX47-60-S+, from MiniCircuits®, displayed in Figure 34. It operates at 5 V, consumes 100 mA and has got an operating frequency of 10 to 8000 MHz. This one is similar to the one used in the WPT system, however, it has got lower response times. Its rising time is 400 ns and its fall time is 10 ns, it has got the needed response time to be used as an envelope detector and demodulate the data that will be transferred with a pulse width of approximately 1.6 ms. Its output varies according to the input RF power and ranges from around 2 V to 0.5 V, lower and upper power limits, respectively. This allows for the detection of the two power levels used in the modulation, for posterior processing and obtaining the demodulated data. The modulated signal, already filtered, is then input on the power detector and, as its DC output is correspondent to the input power, it is possible to obtain the demodulated signal.

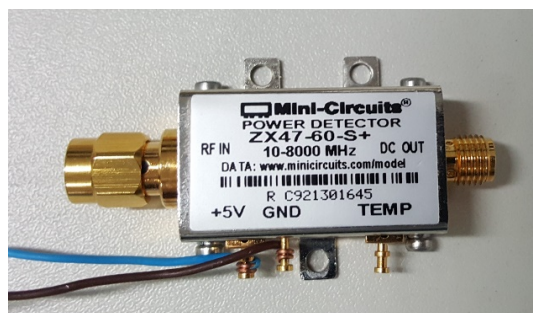


Figure 34 - Power detector used in the demodulation block.

3.5 Communications processing unit

For this communication system, it was necessary to implement a processing unit that could manage all communications to establish the bidirectional communication link with the chip. A processing unit along with the respective software was necessary to manage the transmission and reception of the commands and data. It was used to perform the modulation by controlling an RF switch, as well as to control the access of the modulating and demodulating blocks to the antenna.

The used unit was the same as the one in the previous system, the Atmega328 microcontroller, which came with an Arduino board. The already described microcontroller's characteristics allow for the implementation of the bidirectional communication link at the desired data rate.

The available chip controls the activation of eight current sources. To use each of them, as several functionalities are necessary, a protocol was implemented. First, as there are eight different current sources, it is necessary to define which of them will be used. Next, after programming which current sources will be used, it is necessary to turn them on or off. As it can be necessary to verify the state at which the chip is at, i.e. verify which current sources are activated, a command can be sent for the chip to report on this state.

This protocol can be resumed in five different commands which are: programming current sources (along with 8 bits that define which of them will be activated), turning them on, turning them off, communicate the device's program state, and resetting that state. The protocol is presented in Figure 35.

Reset state	1	0	1	1	0	0	0	1	1
Program				0	1	0			+8 bits
Turn on				1	1	0			1
Turn off				1	1	0			0
Communicate state				0	0	1			1

Figure 35 - Protocol used to establish the wireless communication link.

3.5.1 Received signal detection

When it is required for the chip to send the data outside, it is necessary to detect it with the communication system. With the demodulation block developed, it is necessary to recover the digital signal. The output generated by that block depends on the input power level. For a very low (less than -

60 dBm) RF input power level, a 2.2 V DC signal is output. When this power level increases, the DC output of the power detector decreases down to 0.5 V (for an RF input of 5 dBm). This means that the power detector outputs 2.2 V when a binary ZERO is received, but when a ONE is received, the DC output will vary according to the WPT link's efficiency.

It was therefore necessary to obtain a signal that had got a standardized high or low level for which a detection block was developed to filter, amplify and convert that signal to a digital waveform with a high or low level of 5 V or 0 V, respectively.

The developed detection block is presented in Figure 36 and generates an inverted logic signal. The signal generated by the power detector is passed through a low-pass passive RC filter to reduce the high frequency noise. This was composed by the resistor R1 with a resistance of 12 Ω and capacitor C1 which has got a capacitance of 100 nF, resulting in a cutoff frequency of approximately 132.6 kHz. Afterwards, the signal is buffered and is then filtered by another passive RC filter, which in this case is a high pass, to remove the low frequency components of the signal, such as the DC level, to allow for easier amplification. Resistor R2 has got a resistance of 270 k Ω and capacitor C2 has got a capacitance of 100 nF, resulting in a cutoff frequency of approximately 6 Hz. After filtering the signal, it was necessary to amplify it and, as such, a non-inverting amplifier was implemented. As an adjustable gain was desired, a multiturn potentiometer (R4) of 47 k Ω was used along with a 3.3 k Ω resistor (R2), resulting in an approximate variable gain of 1 to 15. Lastly, to obtain a digital signal, a non-inverting comparator was used for which a variable voltage reference was generated by implementing a voltage divider. These blocks had got a non-inverting configuration as it was desired to use a single supply operational amplifier, which in this case was the LM324DP.

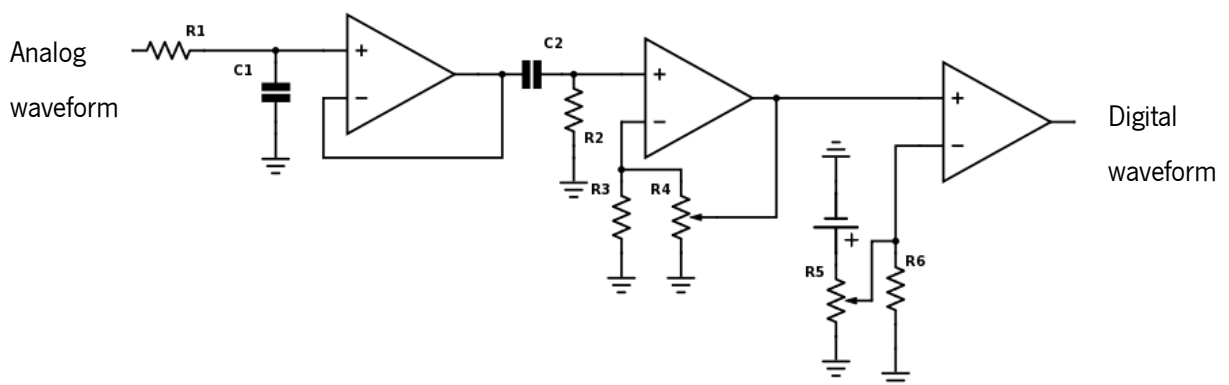


Figure 36 - Diagram of the developed pulse detector, to convert the analog waveform to a digital one.

3.5.2 Management software

With the hardware developed for the communication system, it was necessary for the microcontroller to receive information about which commands had to be sent to the chip. It was now necessary to implement the software that manages it and allows for the wireless communication link to take place. Moreover, as an easy way to use this communication system was needed, instead of typing the commands by hand, a user interface was developed. This was done resorting to LabView. A script was developed to allow the establishment of communication between a computer and the developed chip. With the communication between the Atmega324 microcontroller and chip already implemented, the RS232 serial port was used to establish the connection between the microcontroller and the computer, for which a protocol was implemented. The interface developed in LabView is presented in Figure 37.

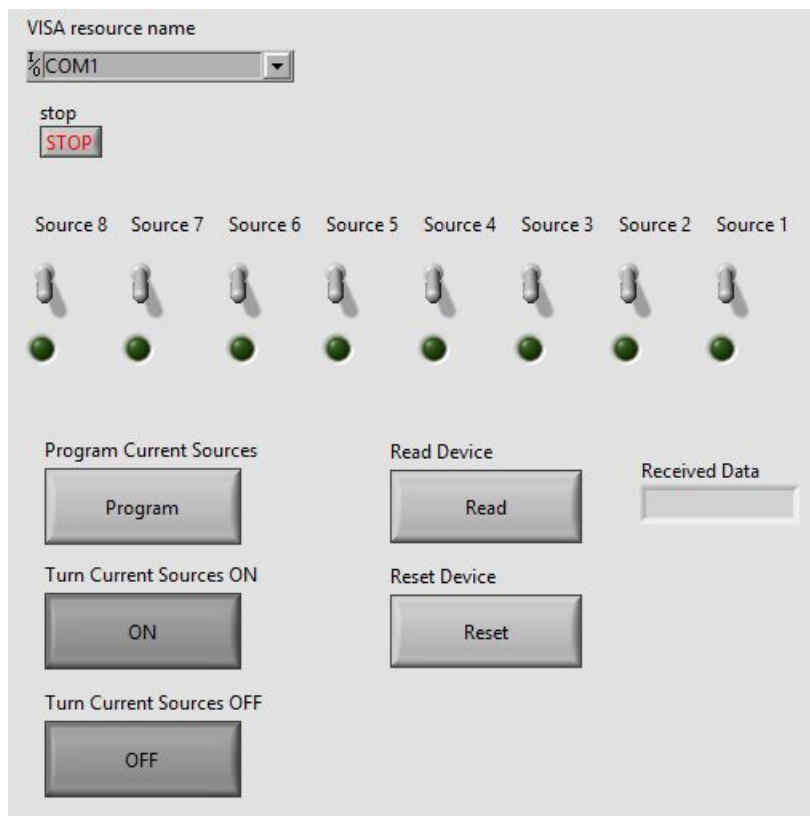


Figure 37 - Developed user interface for wireless communication with the available chip.

The microcontroller is connected through its serial interface via USB, to be selected on the list of COM ports provided on the interface. After it connects, it verifies if the connected device is the microcontroller to perform the communication with. For each of the commands to be sent to the chip, it

was implemented a different codification to communicate with the microcontroller. Every time a command has to be sent to the chip, this interface makes it possible by just pressing the corresponding button and sending a serial instruction for the microcontroller to transmit it. These instructions rely on sending two consecutive bytes that define which command will be sent. When the current sources have to be turned on, the ASCII equivalent to the letter "O" is sent twice; to turn them off, "FF" is sent; and to reset the chip, "RR" is sent. To request for the configuration, "CC" is sent and afterwards the chip's response will be detected by the microcontroller, sent back to the computer and displayed in the field "Received Data". Lastly, to program which current sources will be turned on, only a "P" is sent, along with another byte that dictates which current sources will be turned on. All these commands are translated to the ones explained in the previous subsection and transmitted to the chip with the required modulation, allowing for the control and communication with the chip through the developed user interface.

3.6 System management and powering

For the development of these systems, several complementary components such as system powering blocks were required. In the WPT system, not only was it necessary to power the components, but also to establish a link between them and the microcontroller. Moreover, it was needed a tuning voltage for the beamforming module's VCO, and to modify the logic level for the phase shifter communication. For these components, a printed circuit board (PCB) was designed.

For the case of the wireless communication system, it was necessary to implement external components to complement the described blocks. The powering and control signals for these components were implemented on another PCB along with the signal processing block from the baseband module and with the RF source tuning voltage circuit. Lastly, RF amplifiers were added in the system for a possible future use. Both PCBs served as an interface that connected the power source, Arduino board, and the components of each system.

3.6.1 Power module and PCB

To power the entire system, several voltage levels were required: 3.3 V, 5 V, 6 V, 12 V and 24 V. The most power-hungry components are the RF power amplifiers used in the WPT system, consuming

10 A both, while the rest of the components do not present a high-power draw, consuming only 170 mA. For the case of the communication system, it consumes 150 mA totaling 10.32 A at 24 V. The available power source that was used was the PMT-24V350W1AK from Delta Electronics, displayed in Figure 38, which outputs 24 V at a maximum current of 14.6 A, making it suitable for powering both systems.



Figure 38 - Power supply used to supply the entire system.

The selected power source converts the electrical grid's power to a 24 V output. As there are different power sources required for both systems' components, it was necessary to implement circuitry that generates multiple voltages. For each system, a power module that can generate them from the same 24 V supply was developed.

For the WPT system, the power module was designed on a PCB and required two voltage regulators. The first one was the L7812CV from STMicroelectronics, which converted the available 24 V to 12 V to power the Arduino board. The second one was the L7806CV, also from STMicroelectronics, which was used to power the VCO. Lastly, it was necessary to power the power detector and the phase shifter. As the Arduino board has got two onboard voltage regulators, one that outputs 5 V and another that outputs 3.3 V, they were used as a power source for the power detector and phase shifter, respectively.

The designed PCB, presented in Figure 39, not only was used as the power block, but also as an interface from the Arduino board with the rest of the components. Firstly, as the voltage generated from the power detector is accessible through a coaxial cable, a through-hole SMA connector was soldered to directly connect it to the microcontroller's analog input. Secondly, as the frequency

generated by the VCO is controlled by a reference voltage, it was necessary to generate it, which was accomplished by applying 5 V to a voltage divider. Lastly, as it was necessary to control the phase shifter at a 3.3 V logic level and the microcontroller uses a 5 V logic level, it was necessary to step it down. As this was for a low communication speed, the step down was obtained by implementing three voltage dividers. The three resulting signals as well as the power were transferred to the phase shifter through a ribbon cable.

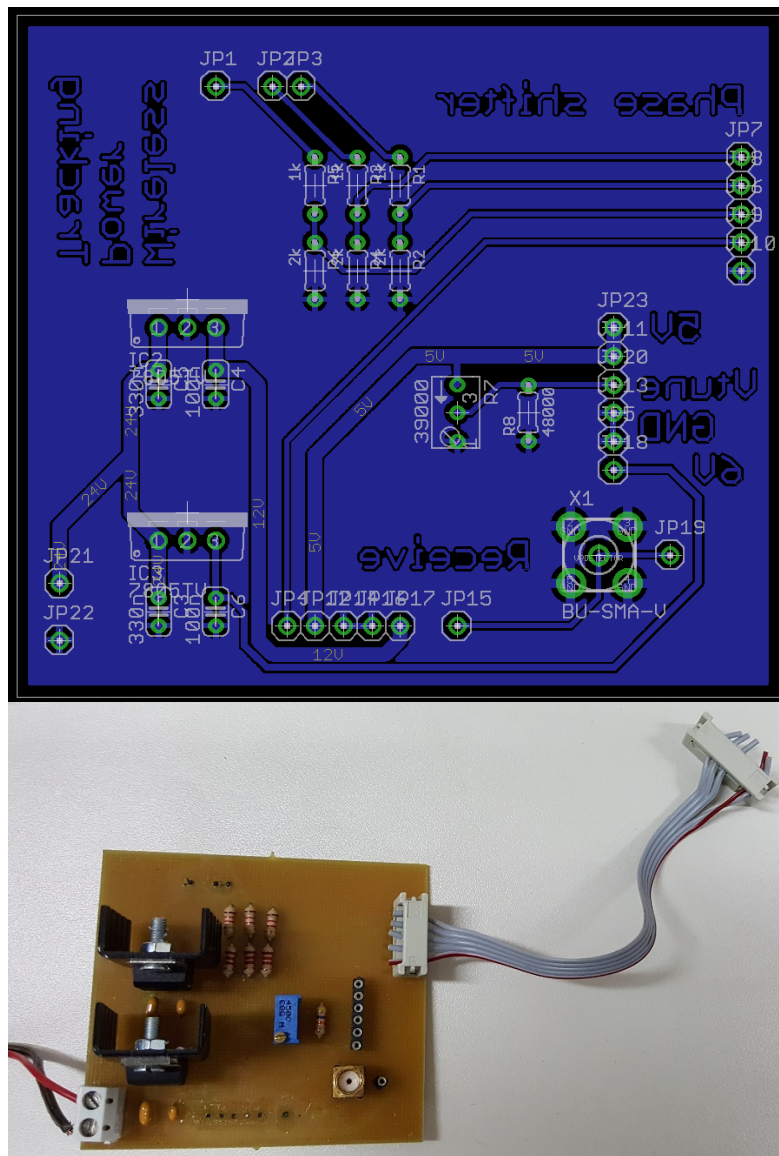


Figure 39 - Developed PCB to interface with the Arduino board and the WPT system's components, layout on top and final result on the bottom.

For the case of the communication system, three voltage levels were required: 5 V, 12 V and 15 V. Like the WPT system, it was necessary to provide several voltage levels from the same supply, for which voltage regulators were used to generate them. As one of the RF amplifiers required 15 V to operate, the L7815CV from STMicroelectronics was used to convert the 24 V to 15 V. Similar to the WPT system, the L7812CV, also from STMicroelectronics, which converted 24 V to 12 V, was used to power the Arduino board. For the 5 V, the previous system's approach was taken, as the voltage regulator present on the Arduino board was used to power the remaining components.

For this part of the system, a PCB, shown in Figure 40, was also designed to hold the powering module, signal processing circuits, and to be used as an interface between the Arduino board and the system's components. To regulate the frequency generated by the VCO, it was necessary to obtain a voltage to tune it and, as such, a voltage divider was used. The control of the RF switch was done by a 5V logic level generated by the pins 5 and 6 of the Arduino board, which were available on two pin headers. The detected power level generated by the power detector is accessible through a coaxial cable, for which a through-hole SMA was used to connect it to the signal processing circuit.

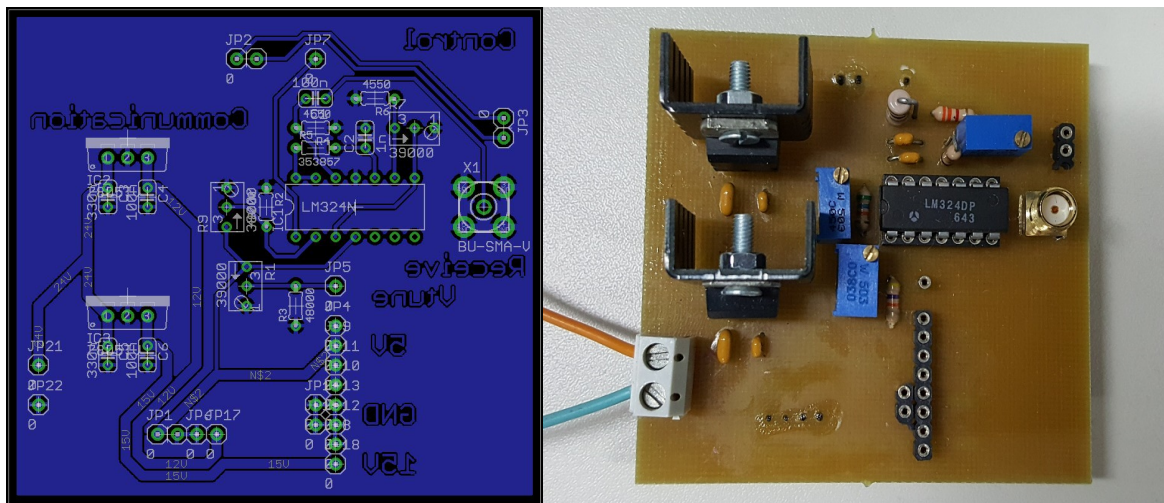


Figure 40 - Developed PCB for the communication system, which interfaces the Arduino board and the communication system's components on the bottom, and its layout on top.

3.6.2 Antenna

For the communication system, it was necessary to use a monopole antenna (Figure 41) to establish the communication link which either transmitted or received RF signals at 1 GHz. As this antenna will be used only to establish a communication link, it is not required to have a high gain as it

is not aimed to establish a high distance and performance link. However, if necessary, higher gain antennas such as a horn antenna can be used, to allow for lower power levels to be transmitted or received or even to increase the communication distance.

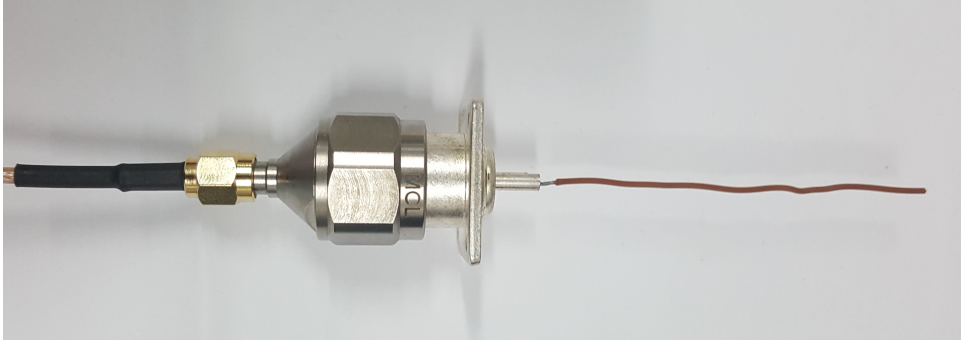


Figure 41 - 1 GHz monopole antenna.

3.6.3 RF switch

It was necessary to implement an OOK modulation, and a device that could generate it was needed. As this modulation is based on the presence or absence of the carrier wave to encode a binary 1 or a 0, respectively, this modulation could be achieved by a RF switch that could either transmit the RF signal or not. This modulation could be attained by simply turning the RF source on or off, or by using a switch with a dual output that could transmit the RF signal to the antenna (on) or to a termination (off). However, the RF source can't be turned on or off to modulate the signal and none of these solutions allow for the incorporation of the receiving system, which requires using a receiving antenna or an extra switch. Instead of using an extra antenna, a switch that allowed to obtain the modulation and to switch between the modulating and demodulating modules was necessary.

The RF switch used to implement this communication system was the ZX80-DR230-S+, from MiniCircuits®, shown in Figure 42. This device allows for the implementation of the bidirectional communication system with only one antenna by switching between the modulation and demodulation blocks. To generate the desired modulation, as it is not possible obtain it by controlling the VCO, the switch's internal load was used. It has got an operating frequency from DC to 3000 MHz, and requires a 5 V power source, while having a current draw of 1 mA. It has got an insertion loss of 0.9 dB which is low enough to implement a short-range communication system. Moreover, it has got a switching time of 2 μ s, which is adequate to generate the modulation and to switch between the transmitting and receiving blocks.



Figure 42 - RF switched used for the modulation and managing the antenna access.

This device's architecture, presented in Figure 43, allows for three possible different states, which are controlled by two input pins: (1) the RF1 port can be connected to the RFCOMMON, while the RF2 is connected to an internal $50\ \Omega$ load; (2) the RF2 can be connected to the RFCOMMON while the RF1 is connected to another internal $50\ \Omega$ load; or (3) each of the three ports can be connected to an internal $50\ \Omega$ load. By controlling the ports interconnection, it is possible to connect an antenna to the RFCOM which can be used to transmit and receive the data, connect the RF2 to the demodulating circuitry and connect the RF1 to the VCO. The modulation can be done by connecting the RF1 to the RFCOMMON to transmit a binary 1 or by connecting all the ports to the internal $50\ \Omega$ load, transmitting a binary 0. Lastly, by connecting the RF2 to the RFCOM, it is possible to connect the antenna to the demodulation block.

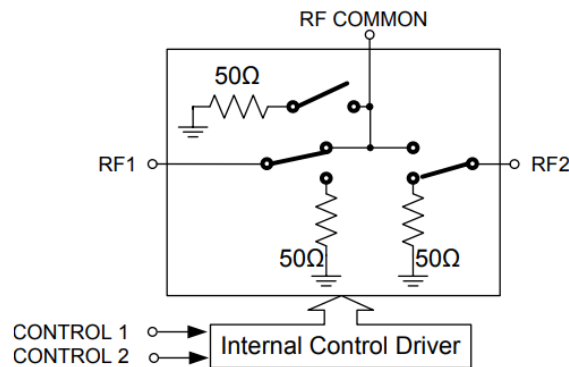


Figure 43 - Schematic of the switch used in the communication system.

3.6.4 Optional amplifiers

The chip's transmitted, received and detected power levels haven't been measured at this stage of development of the systems of this dissertation. Therefore, two amplifiers for the communication system that can be easily connected or disconnected were added as a preventive

measure, in which one is for the transmission and one for the reception. For the transmission, an amplifier that had a high output power was needed, while for the receiving part it was necessary to have a high gain, low noise amplifier. For the first case, the chosen amplifier was the ZX60-33LN+ from MiniCircuits®, presented in Figure 44. This amplifier requires a supply voltage of 5 V and draws 70 mA, and has an operating frequency of 50 to 3000 MHz. This amplifier was used due to its low noise figure of 1.1 dB at 1 GHz, to its gain (18.8 dB), output power at 1 dB compression of 16.5 dBm and maximum input power of +13 dBm, which increases the output power of the VCO and allows to transmit at a power of up to 16.5 dBm.



Figure 44 - Optional amplifier for the transmission block of the communication link.

For the second case, where it can be necessary to detect low power levels transmitted by the chip, the amplifier used was the ZFL-1000LN+ from MiniCircuits®. This amplifier, shown in Figure 45, has an operating frequency of 0.1 to 1000 MHz and requires a power supply of 15 V and 60 mA. It has got a 3.11 dB noise figure, but as it has got a higher gain, 23.32 dB at 1 GHz, it was used to amplify the received signal, allowing to theoretically detect power levels up to -75 dBm.



Figure 45 - Optional amplifier for the receiving block of the communication link.

3.7 Complete system

After having all the sub-systems implemented, they were placed together, resulting in the desired WPT and communication system, which were required for the base station. Their final state is presented followingly.

3.7.1 Wireless power transfer

The previously described components were combined with each other as described, resulting in the complete WPT system, displayed in Figure 46. To implement a portable WPT and tracking system, a box was 3D printed to enclose the components. This was done resorting to a BQ Witbox 2, with polylactic acid (PLA) filament. The developed system can be programmed once to perform the power transfer wirelessly and with tracking. Then, it only needs the power supply, and the USB cable can be removed as it becomes unnecessary. However, it can still be used, as this system can also be a development and testing platform for tracking algorithms.

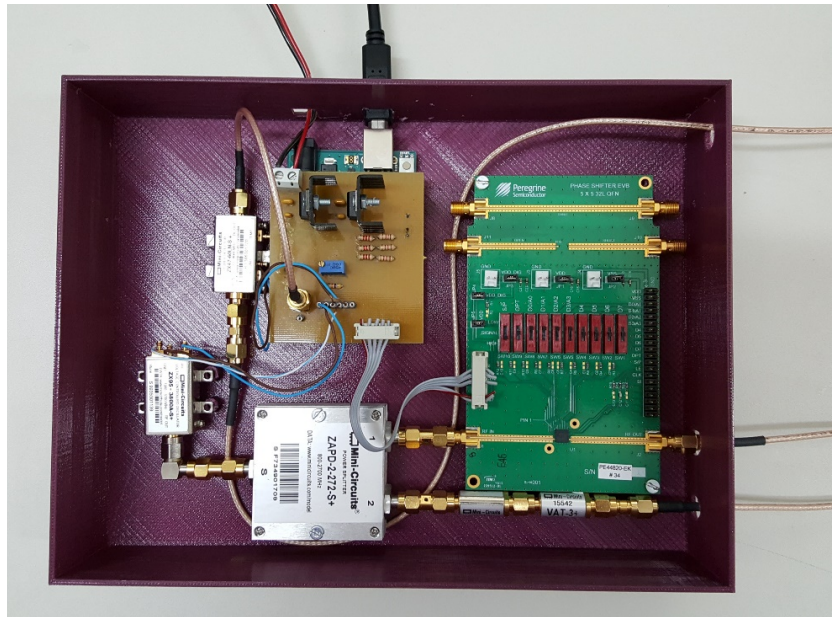


Figure 46 - Developed WPT system and 3D printed box.

The total cost of this system, as well as the price of each component, is presented in Table 4, totaling a cost of 2982.18 €. For this, the cost of the shipping, 3D printing, connectors, PCB and its components were not considered.

Table 4 - Price breakdown of the components and total WPT system cost

Component	Price (€)
ZX95-380A+	35.58
ZAPD-2-272+	63.56
PE44820ds	350
VAT-3+ x2	23.66
ZHL-10W-2G+ x 2	2366.11
ZX47-60+	76.28
Arduino Board	19.87
PMT-24v350w1ak	47.12
Total	2982,18

3.7.2 Wireless communication sub-system

The described parts of the system were assembled to form the complete communication system, which is shown in Figure 47. A PLA box was 3D printed on the BQ Witbox 2 where the communication system's components were fitted. In it are present the optional amplifiers that were previously reported. These already have connections for their DC supply and can be connected to the remaining system components. For the developed system to work, it only requires a 24 V power source, which is also used for the WPT system, an antenna and an USB connection. Lastly, Labview has to be installed in the computer to which the system is connected.

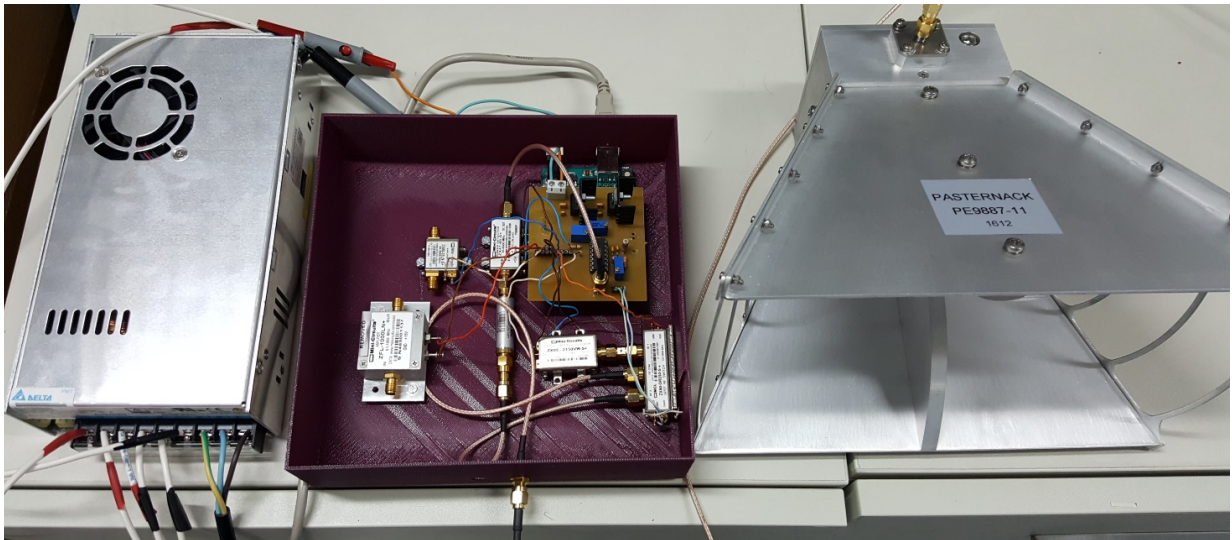


Figure 47 - Developed communication system, along with the power supply and an antenna.

The price of each component and the cost of this system presented in Table 5. It adds up to a total of 399.96 € in which the cost of the shipping, 3D printing, connectors, PCB, antenna, power supply, and its components were not considered.

Table 5 - Price breakdown of the components and total wireless communication system cost

Component	Price (€)
ZX80-DR230+	51.49
ZX95-2150VW	47.19
ZX60-33LN+	85.84
ZFL-1000LN+	84.98
VBFZ-925+	34.31
ZX47-60+	76.28
Arduino Board	19.87
Total	399.96

4 WIRELESS POWER TRANSFER AND SAR EVALUATION SETUP

Beyond the ability to track a device on a rodent, the WPT system should also be able to power devices that are implanted inside its body. Additionally, the WPT system used for implants in rodent testing should also be capable of being used in human applications, as this is the ultimate goal of biomedical device development. Due to the depth at which the implant can be placed inside the human body, where several centimeters of tissue can exist between the device and the outside world, it was necessary to determine where the power is transferred to in such scenario. As RF electromagnetic waves interact with biological tissues, part of that radiation is absorbed. The previously described and developed WPT system transfers high amounts of power at 2 GHz. Consequently, to prevent any damage and/or discomfort to the human host, it was necessary to evaluate the SAR dosage. Since the implant being developed in a parallel project is aimed at being used in the human head, an evaluation setup was developed to generate a mapping of the power and SAR distribution inside a human head phantom.

To determine SAR levels, it is necessary to measure the electric field's strength and calculate SAR through the medium's dielectric properties. Along with this, a positioning system is necessary to accurately place the probe and measure the distribution of that field on a certain predefined area, to verify if the regulations are met. Several commercial SAR measurement systems are available, however, they cost tens of thousands of euros. As these systems are very expensive, an in-house SAR measurement system that had a lower cost was necessary, and as such it was developed. The cost of this system was reduced by replacing a robotic arm with two stepper motors, replacing the commercial phantom with an in-house phantom and developing the positioning and measurement software.

The developed positioning system can also be adapted for other measurements inside the liquid phantom. Replacing the SAR probe with an antenna allows for a mapping of power distribution and availability inside the phantom. Instead of the SAR acquisition system, a vector network analyzer (VNA) is used to measure the transmission loss.

4.1 Measurement equipment

The objective of this part of the dissertation's work was to implement a SAR and power distribution measurement system for WPT to the human head. The measurements were done by

resorting to either one or two antennas, and were performed inside a human head phantom, which was placed inside a measurement chamber.

These systems required two different types of measurements to be made, for which specific probes were necessary. For the SAR levels, it was required a probe that measured the electric field level according to established international standards. On the other hand, for the S21 parameter measurement, an antenna that radiated at the desired frequency was necessary. For each of these probes, different readout electronics were necessary, for which a SAR acquisition system and a VNA were used, respectively. To map the SAR and power distributions inside the phantom, two different systems, although with common parts, were necessary.

The components of both systems were computer-controlled and, as such, software was developed to obtain the measured values from the instruments (SAR acquisition system and VNA). The used positioning system was the same for both cases, which was comprised of stepper motors and motor controllers, to position the probes in a plane. Moreover, in the case where two antennas were used, this setup also controlled the phase difference between them. The different configurations of each setup will be described subsequently.

4.1.1 SAR measurement system

For this system, it was necessary to connect the components that belong to the SAR acquisition system to the those that are common to the power mapping system. The block diagram of this part of the system is shown in Figure 48.

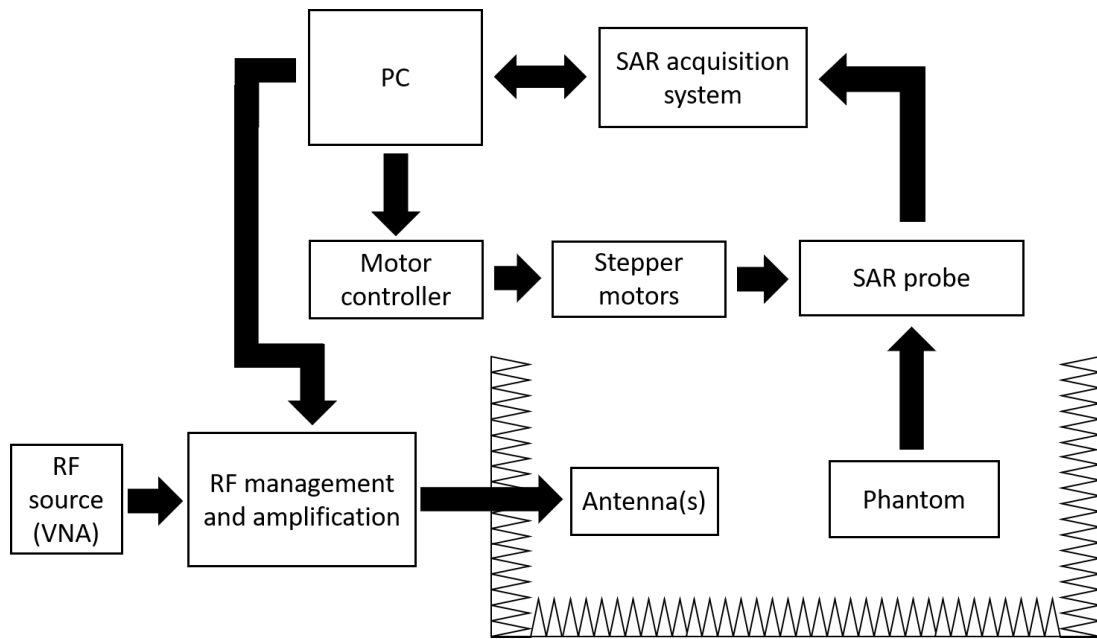


Figure 48 - Block diagram of the SAR measurement system.

The computer communicated with the SAR acquisition and motor controller to locate the SAR probe and perform the measurements. The VNA was used only as an RF source for the management and amplification block, which for the case where two antennas were used, a phase shifter was necessary to control the phase difference between them.

To measure SAR, it is necessary to use a probe that can measure the electric field strength inside the phantom, which must meet several requirements such as those imposed by the IEEE: it should be isotropic, much smaller than the wavelength of the propagating wave in the tissue simulating liquid, their diameter should be less than 8 mm, respond linearly to the square of the electric field strength, and be transparent to the field. These probes consist of three orthogonally placed short dipole antennas with a diode detector at the dipole feed point, which is then used to obtain an electric field strength value. The probe used was the SSE5 from MVG, which was built in accordance to the IEEE 1528, OET65 Bulletin C, and CEI/IEC62209 standards.

To perform measurements with this probe, it is necessary to use the respective acquisition system, which consists of a probe holder that interfaces the probe with a manufacturer-modified Keithley multimeter. This, in turn, is connected to the computer through a GPIB interface, to perform the measurements and obtain the electric field strength and consequently SAR values. In Figure 49 are presented the probe along with its holder on the left, and the Keithley multimeter (SAR acquisition system) on the right.



Figure 49 - The SAR probe is on the left and on the right, the modified Keithley multimeter, used to perform the acquisition (front view on top and back view on the bottom).

4.1.2 Wireless power link characterization

The same setup can be used for the measurement of the power distribution inside the phantom head which is controlled by the same computer. In this case, the same components as the ones in the SAR measurement system were used, with exception of the acquisition system, and SAR probe, which were replaced by a VNA and a probe-like antenna, respectively. Besides acting as the RF source, the VNA was also used to measure the S_{21} parameters. The block diagram of the developed system is presented in Figure 50.

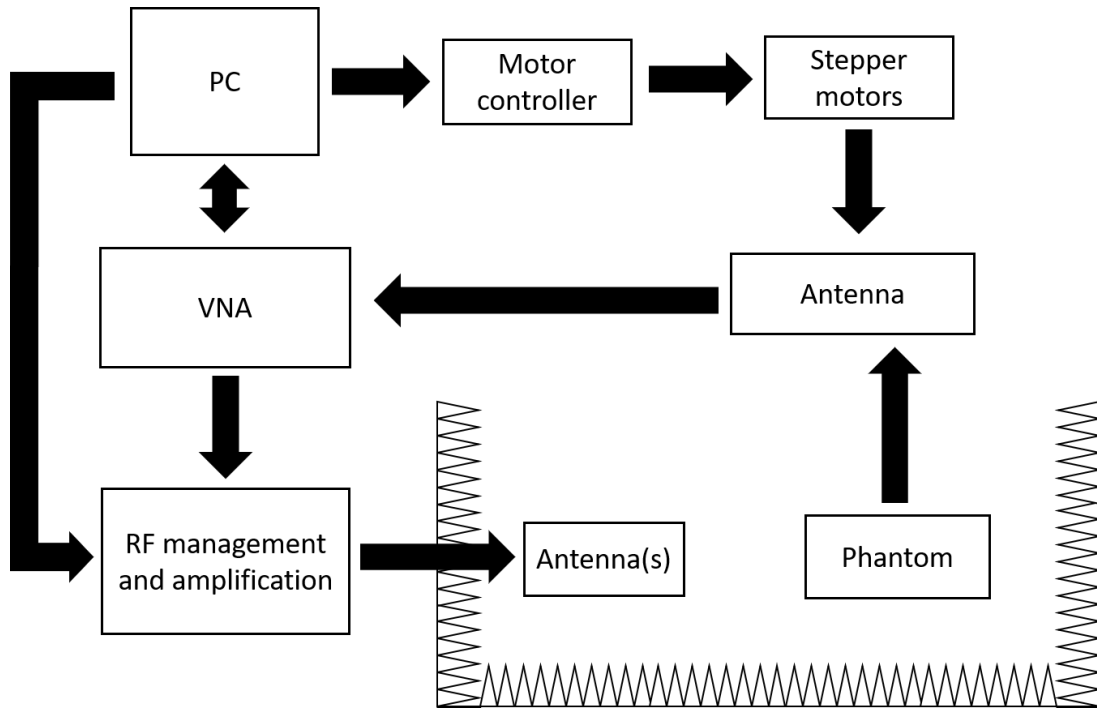


Figure 50 - Block diagram of the S21 measurement system.

To measure the S21 parameters, the probe-like antenna was made by using a semi-rigid coaxial cable that was modified to create a small dipole antenna that operates at 2 GHz inside the phantom. Moreover, as it cannot be easily held, a support for it was 3D printed (in red). The set of these two is shown in Figure 51, along with a close up of the probe tip.

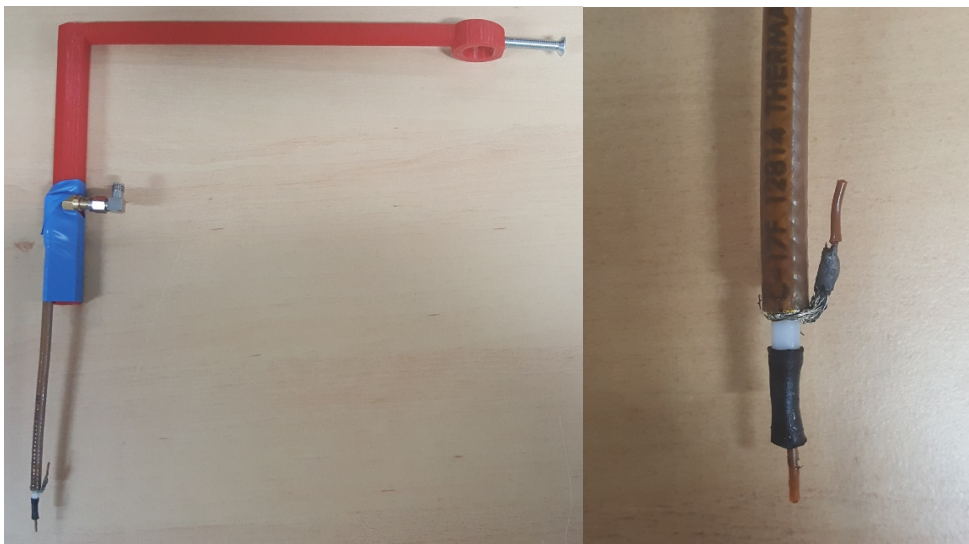


Figure 51 - On the left is shown the developed probe along with the printed holder and on the right a close-up of its tip.

The S21 parameters were measured resorting to Keysight's E5071C VNA, displayed in Figure 52. This measurement requires the VNA to generate a 2 GHz RF signal at one of its terminals, which goes into the developed system. After being radiated by the antenna, it is received by the probe inside the phantom and returned to the VNA, which then calculates the signal loss along that path. Since relative measurements were required for the power distribution mapping, the variation of the S21 parameter according to the position of the probe inside the phantom is a translation of the power distribution on the selected area. To automate the system, the VNA was controlled through USB.

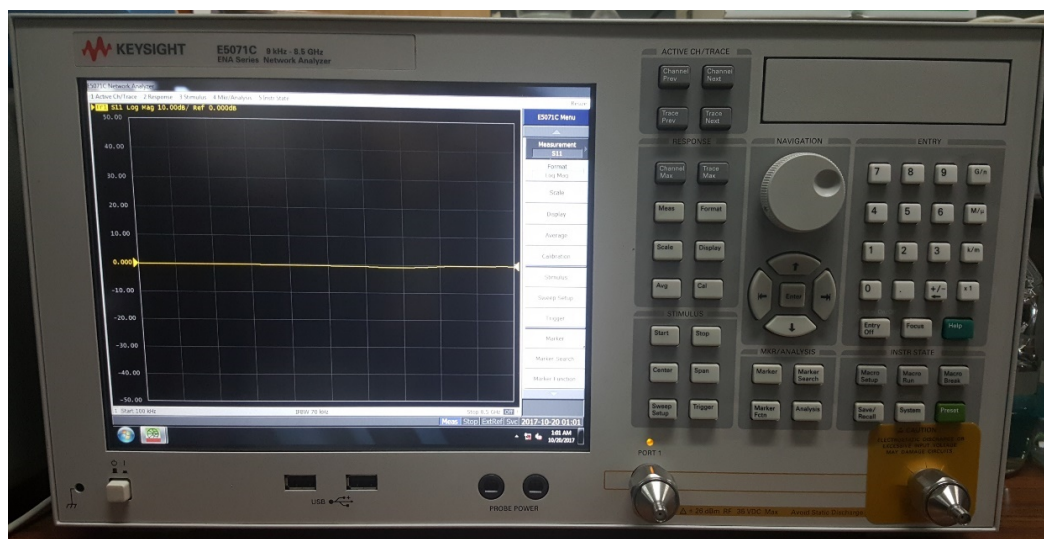


Figure 52 - E5071C VNA used in this system.

4.1.3 Wireless signal generator with beamforming

As previously mentioned, the developed system was required to measure the S21 and SAR distributions at 2 GHz. In the transmitting end of the system, an antenna was used. Nevertheless, the system should also be easily adapted to be used with two transmission antennas, to allow a study of the effect of multiple transmitter use on power and SAR distributions. This system, however, was already implemented and described in the previous chapter. As mentioned, it has got an output for two antennas in which it is possible to control their phase difference. The same amplifiers and power supply were also used in this case. However, for the scenario in which it is necessary to use only one antenna, in the output of the phase shifter, instead of placing an amplifier and its respective dipole antenna, a 50 Ω termination was used.

To perform the measurements where two antennas were used, it was necessary to modify the phase value of the signal, but instead of resorting to the microcontroller to control the phase shifter, the Peregrine Semiconductors USB controller was used. This allowed for the computer to control the entire system, including the required instrumentation, eliminating the need for a microcontroller to be implemented.

Lastly, instead of using the VCO incorporated in the previously developed beamforming system as an RF source, a VNA was used. This replacement was due to the necessity of measuring how much of the power was received by the probe inside the phantom in relation to the power that was input in the system, which is possible through the S21 parameter measurement. Although the VCO could be used along with a spectrum analyzer to measure the amount of power received, the latter has got a much slower response time through the computer, which would make experiments take longer. Since the phantom's properties slowly change over time, such was not acceptable. Therefore, the VNA was used instead, which measured S21 parameters instead of absolute power, while providing faster and more stable measurements. The S21 parameters also allow to easily obtain the transmitted power by adding the transmission loss in dB to the RF source's power in dBm. Additionally, the VNA can generate a 2 GHz signal, but unlike the VCO, the power emitted by the VNA can also be controlled. This was necessary as it was required to modify the power transmitted in either one or two antennas scenario, where it was desired to evaluate the power transmission and SAR levels by using one antenna with a certain power level, or two antennas with half that power each.

The modification of the RF source (VCO for the VNA, through the blue coaxial cable) and phase shifter control (red PCB instead of the flat cable) can be visualized in Figure 53.

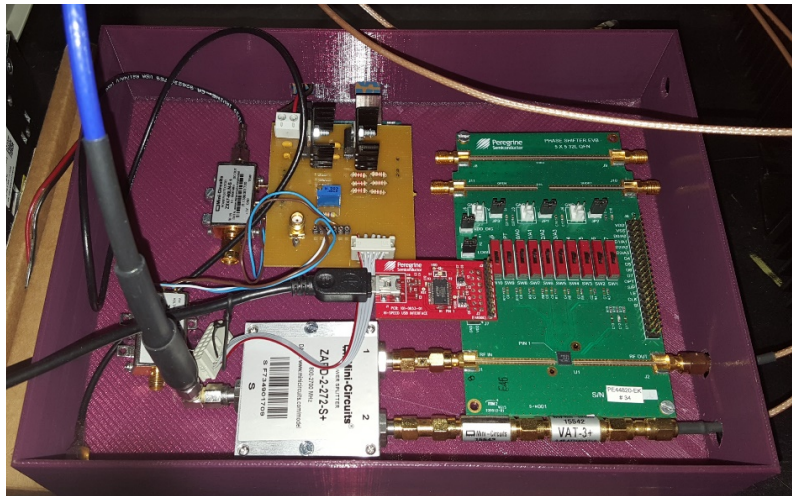


Figure 53 - Modifications made to the rodent implant WPT system to implement the SAR and S21 measurement system.

4.1.4 Phantom development and characterization

As mentioned in the second chapter of this dissertation, to perform the mapping of SAR and power inside the head phantom it was necessary to fabricate an in-house phantom for these measurements. During this process, dielectric properties measurements were possible resorting to the 85070E dielectric probe kit, Figure 54, along with the Keysight E5071C VNA.

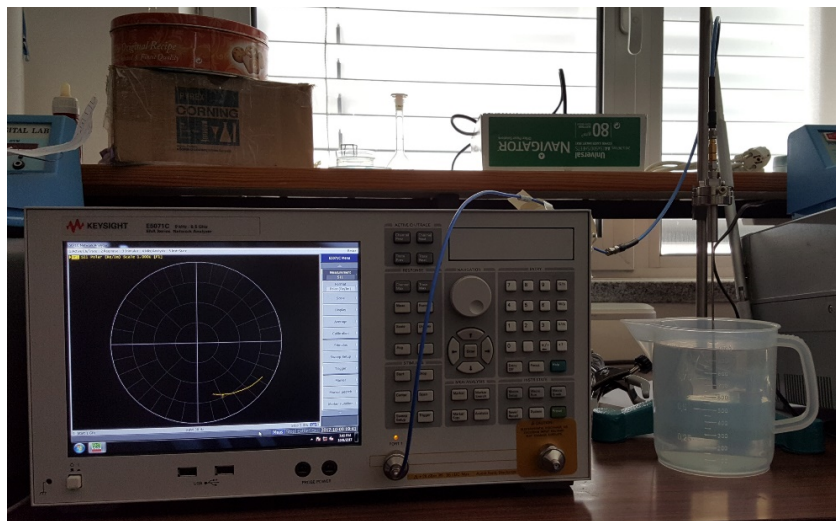


Figure 54 - Dielectric properties measurement setup, composed of the VNA, dielectric probe and phantom.

After analyzing the recipes and ingredient properties presented in Chapter 2, work began on the development of the in-house human head phantom, bearing in mind the dielectric properties (permittivity and conductivity) that the human head presents at 2 GHz. Several iterations to obtain the

final composition of the phantom were performed, concluding that the DGBE has to be mixed and stirred in the water, followed by the Triton X-100 and, lastly, the NaCl. The recipe must be followed in this sequence, to avoid creating a thick and gelatinous paste and bubble formation, minimizing the time it should sit after the procedure. Moreover, it was concluded that for the desired phantom, it had to be composed of 56% of deionized water, 39% of DGBE and 5% of Triton X-100 in volume, along with 0.05 g of NaCl per 20 ml of phantom. This originates a phantom with a permittivity of 40.6 and a conductivity of 1.4353 S/m. The FCC suggests that the phantom's permittivity and conductivity must be 40 and 1.4 at 2 GHz, respectively. As it is necessary to conclude if the phantom is reliable during the measurements, its longevity was studied, and the results are presented in Figure 55. It is possible to conclude that, as the measurements do not last longer than a few hours, the phantom's stability is adequate for the measurements, as its properties do not vary significantly in such a short amount of time, as expected.

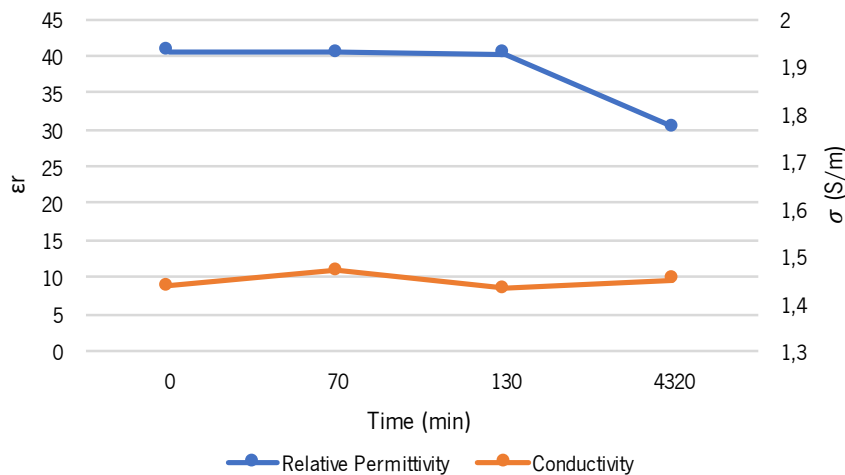


Figure 55 - Phantom's relative permittivity and conductivity variation over time.

4.2 Measurement setup

To measure power and SAR distributions inside the phantom, it is necessary to use the developed wireless signal generator along with the control computer and the acquisition equipment. To avoid interferences on the measurements, such as reflections and external RF signals, a measurement chamber where the experiments could be done was developed. To perform them, it was necessary to place the probe inside the head phantom and accurately make measurements point by point, inside

that chamber. The positioning systems used are usually robotic arms, such as the TX60L from Stäubli. This one in particular is the lightest of its kind and weighs 52.5 kg, has a repeatability of 0.03 mm and 6 degrees of freedom [76]. However, as the measurements will be done on a plane, that many degrees of freedom are not needed, with two stepping motors sufficing for the task.

4.2.1 Measurement chamber

RF measurements, such as power and SAR distributions, are very sensitive and are affected by several factors, such as the presence of large metallic objects and the movement of people nearby, as these can cause reflections and other unwanted artifacts. Moreover, as this measurement setup was built on a small space with constant presence of people, it was necessary to avoid interferences caused by the surroundings and, as such, precautions were taken. To hinder these complications, a measurement chamber was built by using commercial anechoic chamber panels that attenuate RF signals. These were used to surround the space where the RF measurements were performed. The measurement setup that is comprised of the antennas, phantom, and probe were placed in the middle of the chamber, at about half its height, by using cardboard and polystyrene foam, which are RF-transparent at the used frequencies. On the cardboard were drawn marking lines, represented in Figure 56, that represent the place where the phantom container had to be placed.

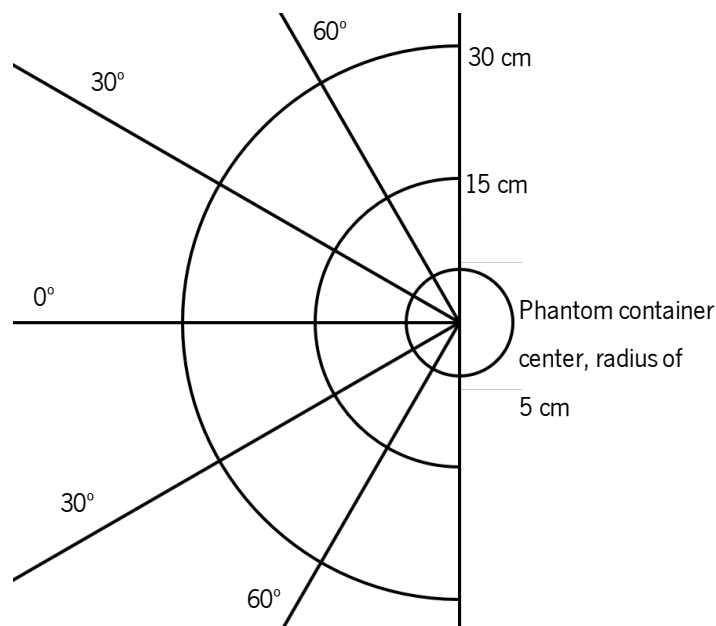


Figure 56 - Reference marks drawn on the cardboard.

Along with this, lines centered on it and separated by 30 degrees each and semicircles with a radius of 15 and 30 cm were also drawn. These markings were made to mark the position of the antennas at the desired angles to be studied and distanced of one and two wavelengths from the center of the phantom at 2 GHz. The developed chamber, shown in Figure 57, has got the following outer dimensions: 84 cm x 70 cm x 68 cm, which is enough to enclose the measurement setup.

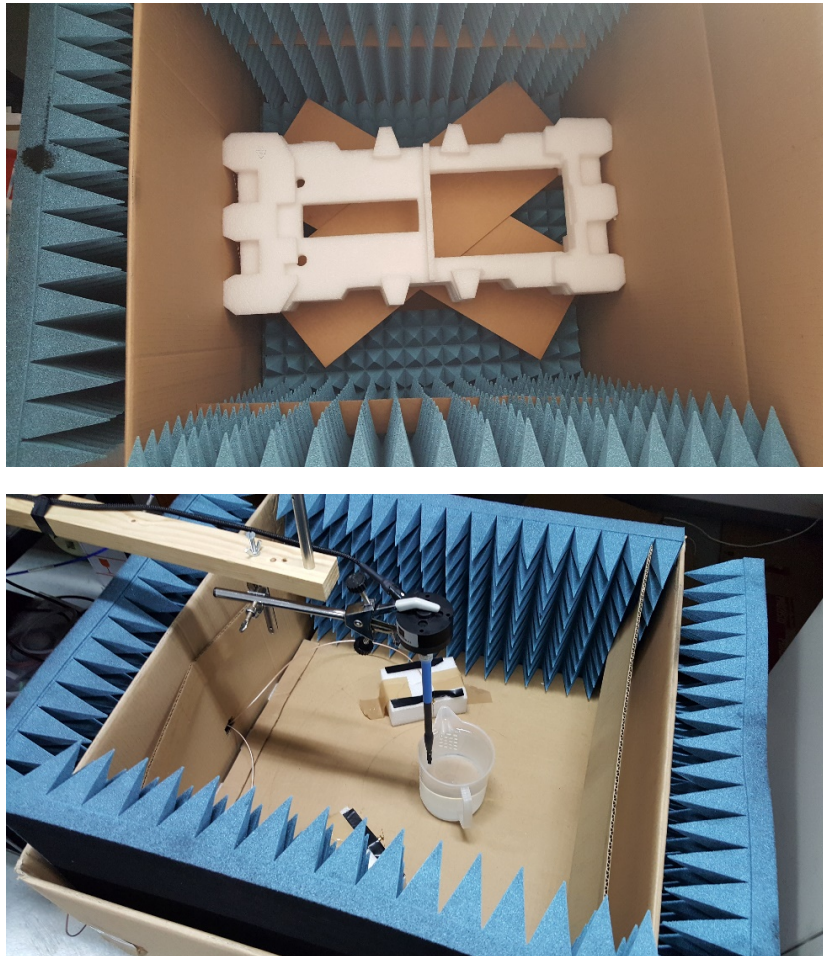


Figure 57 - Interior of the anechoic chamber with the supports on top, and an example of the installed measurement setup on the bottom, where two transmitting antennas are being used.

4.2.2 Probe position control

To place the probe in the measurement locations, two Standa 8MT177-100 [77] stepper motors were used. By mounting one on top of the other perpendicularly, they allow to make a two-dimensional sweeping surface with a resolution of up to 0.125 μm . The motors allow for high portability of the system, as each of them weighs just 1,5 kg each. Their range of movement is 10 cm, which is

sufficient for the desired positioning system, as it covers the measurement area, i.e. a cylinder with 10 cm in diameter, while also allowing for high resolution measurements to be performed.

To control these motors, it was necessary to use the 8SMC1-USBhF motor controller from Standa. This controller allows the stepper motors to be manipulated through a LabView script which was created using the development kit provided by the manufacturer.

When installing the stepper motor for probe placement in the measurement setup, it was important to consider that these are composed mostly out of metal, which is not advisable to be kept in close proximity to the antennas, as reflections of radiated RF signals could occur, which would interfere with the measurements. Consequently, they had to be deviated from the measurement area. As such, a piece of wood (which is almost transparent to RF) with a length of 90 cm was used to elongate the reach of the motorized positioners. This configuration of the stepper motors along with the wood rod, presented in Figure 58, allows for the SAR and S21 distribution measurements to be performed in a plane with minimal reflections.

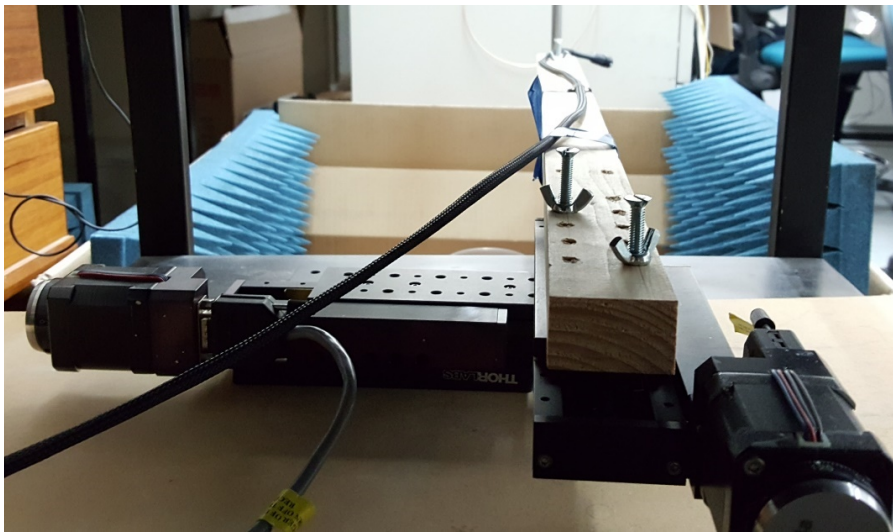


Figure 58 - Configuration of the two stepper motors, to position the probe, along with the wood rod to increase the range of the system.

4.2.3 Calibration issues

During the experimental measurement stage of this work, error sources associated with the experimental setup were identified, and will be described in the following paragraphs.

The positioning system, as well as the measurement chamber, are not physically secured onto a place nor to each other. Ideally, an automatic position calibration would be used, however, due to the

setup limitations such as having several moving parts and not having a vertical position motor to align the transmitting and receiving probes in the same plane, such solution was not possible to develop. Therefore, before each measurement it is necessary to manually place the probe on the initial position of the measurement while resorting to the manufacturer's positioning software at the same time, which can introduce errors in the measurement.

To obtain SAR measurements with a precise absolute value, the probe is calibrated by the manufacturer for the desired frequencies. In the case of the probe used in the system presented in this work, it was calibrated for the 900 MHz band (± 100 MHz). Having been used to measure SAR levels at 2 GHz, the absolute measured values will not be accurate. Nevertheless, the probe can be used to obtain relative SAR levels between two measurements at the same frequency, i.e. it can be used to determine SAR exposure variations. For absolute measurements, the probe needs to be recalibrated by the manufacturer for the frequency of interest, i.e. 2 GHz.

To simulate the SAR and power distributions on a human head, it was necessary to use a phantom that mimics its dielectric properties. The developed phantom, however, is composed of reagents that evaporate over time, which modifies its dielectric properties. To maintain them, it is necessary to regularly measure those properties and adjust them by adding small parts of the same reagents, which can lead to small variations of these properties and, consequently, of the measured values.

4.2.4 Complete characterization system

The complete characterization system is shown in Figure 59, where its components are identified. An interface was developed where few inputs are required. In case of a circular measurement area, a diameter and step size are required as an input for the software to calculate the points in which to place the probe. In case of a square area, its length and step size are required. Additionally, phases and time interval are required. The time interval, defines the amount of time that the probe will be stopped at a specific location, for probe oscillation stabilization. The frequency must also be defined when the S21 parameters will be measured, while for the SAR measurements, it is defined on the VNA. When two antennas are used, it is also necessary to input the phase difference or list of phase differences at which the measurements will be done.

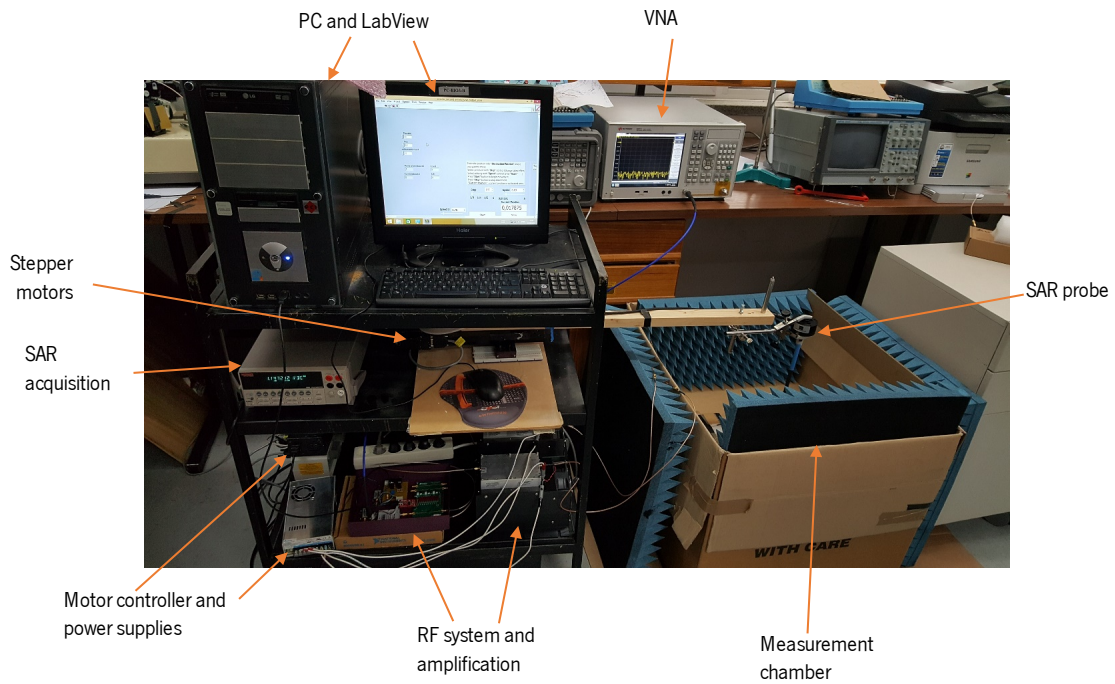


Figure 59 – Complete power and SAR distribution measurement setup.

4.3 Measurement

In the following sections, a description of the measurement protocol will be made. Additionally, the developed control software's architecture will be detailed. Finally, differences between the single transmitter and the dual transmitter scenarios will be highlighted.

4.3.1 Measurement protocol

As previously explained, the developed system maps the power and SAR levels inside a human head phantom. However, as some parts of the system can't be automated, the following procedure must be followed in order to perform the experimental measurements:

1. Make the 2GHz human-head phantom;
2. Calibrate the VNA and save state;
3. Install measurement probe and wireless signal generator;
4. Place the phantom's container, antennas and center the measurement probe;
5. Input the measurement parameters and start measurement;
6. Save the generated file.

To develop the phantom, it is necessary to measure its dielectric properties through the dielectric measurement kit. A new one can be made for each measurement, or small adjustments can be made on an existing one by adding a small volume of a given ingredient to compensate for dielectric properties change over time.

Afterwards, as the VNA was used to verify the dielectric properties of the phantom during the previous step, it is necessary to calibrate it for the power or SAR distribution measurement. To measure the S21 parameters, it is necessary to configure the frequency start and stop, both to the desired frequency, in this case 2 GHz, and perform the calibration of the VNA on the input (RF management system) and output (probe), to be later used by the developed LabView software. If the frequency is not modified and the same coaxial cables are used between the VNA and the system's input and output between different measurements, the state can be recalled from the previously saved one, allowing to save some time.

Depending on the measurement, it is necessary to install the corresponding probe and configure the wireless signal generator. For both types of measurements, power mapping and SAR, it is necessary to connect the VNA to the input of the system. However, for the power mapping measurement, it is necessary to install the developed antenna and connect it to the VNA, while for the SAR measurement, it is necessary to install the SAR probe and connect it to its acquisition system. The phase shifter is connected for either types of measurements and with one or two antennas. However, when the measurement is done with only one antenna, a termination is used on its output. Lastly, depending on the power levels desired, an RF power amplifier can be connected on each output.

With the measurement setup installed, it is necessary to center the container with the human head phantom on the cardboard with the markings, along with the transmitting RF antennas. Afterwards, the probe must be centered by moving the motors and verifying its position through the manufacturer's software. The SAR or power mapping is now performed with the measurement system, by resorting to the developed software, which is explained in the next section.

4.3.2 Control and readout software

As a starting point for the measurement system, a stepper control program provided by the manufacturer was used. However, it only allowed to move one motor to a single position. As two motors and a list of positions for the probe to be placed at were required for a two-dimensional sweep to be

performed, a LabView script was developed. The movement is controlled by moving a motor to the desired position on one axis, and only once it reaches its destination the same is done for the other motor. This, along with the positions to be measured that are defined by the user, allows for the movement to be done to every point of the measurement region, in a zig-zag configuration to avoid long movements and reducing the measurement time. Moreover, two distinct types of measurement were developed, allowing it to be done on a square area or a circular one. In both cases, an array with the coordinates to be measured is generated. For the case of the circular area, it is generated a square array where the positions that are further from the center than the desired radius are eliminated.

With the program that moves the stepper motors to the preplanned positions to be measured, it was necessary to perform the measurement. This can either be done by using the VNA or the SAR acquisition system and, as a result, either the S21 parameters at the desired frequency or electric field strength and SAR are measured. For the first scenario, the VNA had to be interfaced with the LabView software in order for the latter to access the S21 measurements. This was achieved resorting to LabView VI's and Standard Commands for Programmable Instruments. For SAR, it was necessary to interface the LabView program with the SAR acquisition system's measurement program, for LabView to access the measured values.

Lastly, a text file with the measured points' coordinates as well as the respective values is generated, which is saved with a user defined name, to later process and examine the results. This software does not impose any limitation in the frequency to be evaluated. For measurements on other frequencies it is only necessary to configure the VNA, save that configuration, and if necessary, replace the S21 probe with one that is compatible at that frequency, along with the respective phantom.

For the case of a single transmission antenna, two scripts were developed, one for power and one for SAR distributions, as either the VNA or the SAR measurement equipment were required to be used. For the two antennas scenario, similar programs as the ones used for the one antenna scenario were used. However, in addition, it was also necessary to control the phase shifter, for which a method was implemented. The phase differences to be measured are defined by the user before the measurement starts. Then, for each position of the probe, the respective measurement is performed for each phase difference. The phase control was done by interfacing the phase shifter software provided by the manufacturer with the previous programs, to perform the SAR and power measurements. On a side note, an offset correction between each of the signal paths was implemented, as a phase

difference is generated as between these. This happens because after the splitter one of the signals goes through the previously described attenuators, while the other goes through the phase-shifter.

The developed program's flowchart is presented in Figure 60. For this automated measurement system, four distinct LabView programs for four distinct types of measurement, due to different components being used were developed: S21 measurement with one antenna, SAR and electric field measurement with one antenna, S21 measurement with two antennas and varying phase, SAR and electric field measurement with two antennas with varying phase.

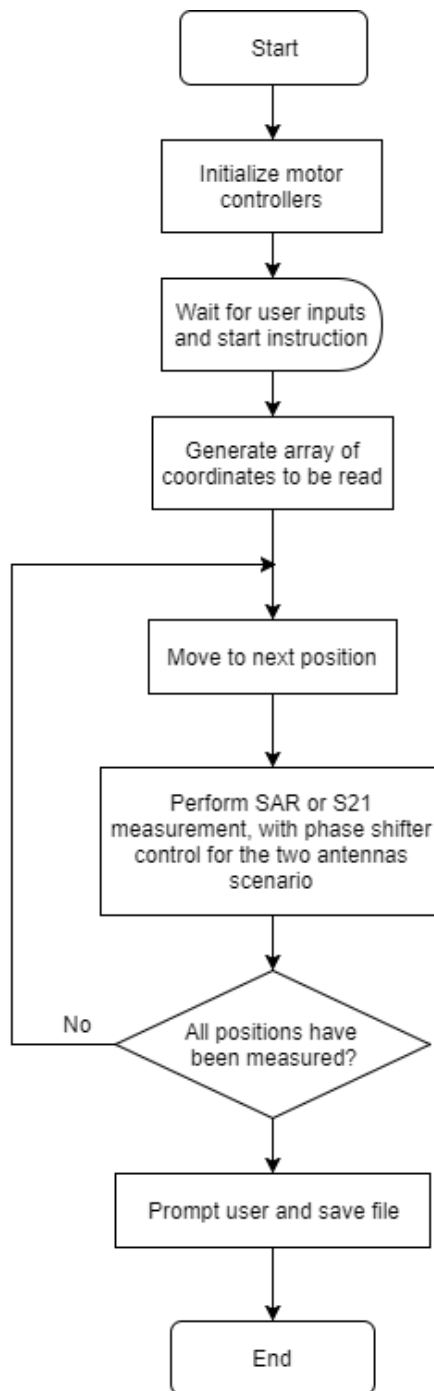


Figure 60 - Measurement system program flowchart.

The interface for this software is shown in Figure 61, which is correspondent to the S21 measurement with two antennas. In this case, it is necessary to input the frequency at which the measurement will be made, the phase differences to be measured in degrees, the diameter of the circle to be measured in millimeters, and the resolution in millimeters. If a pause is necessary in each

measurement for probe stabilization, an optional field was added in which it is possible to define how long that pause is in milliseconds. For the case where one antenna is used, the interface does not have the phase difference input, and for the case where the SAR is measured, the frequency input is also not present, as these are not necessary. After inputting these parameters, it is then necessary to press the “Start” button to perform the measurement. Finally, when the measurement is complete, the user is prompted to save the measurement file.

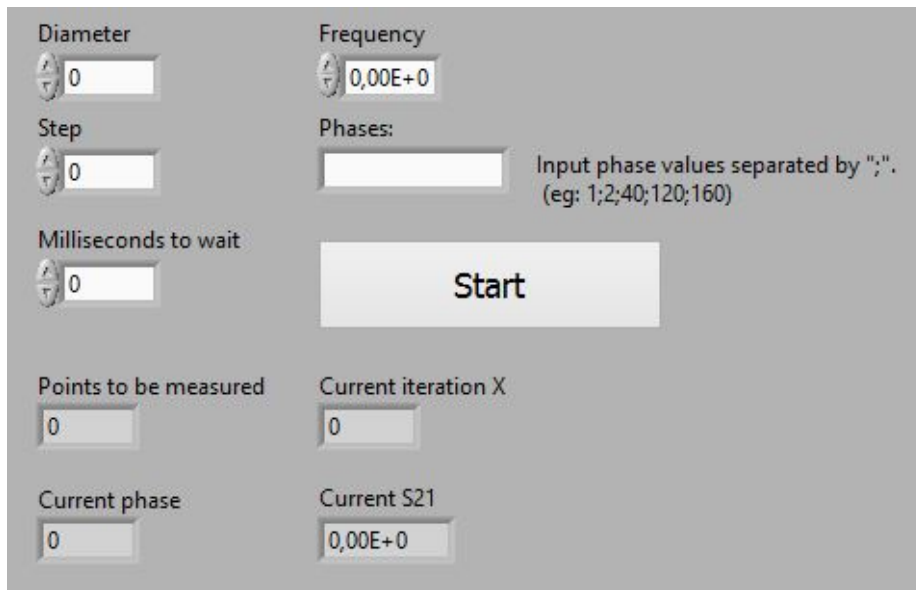


Figure 61 - LabView interface, with the user inputs and current measurement information.

4.4 Measurement setup evaluation

After developing the measurement setups, it was necessary to determine if they produced reliable results. For this, it was necessary to make the measurements to obtain a power and SAR distribution inside a human head phantom and compare them with simulated data. For this, an Ansys HFSS model replicating the experimental setup was created, as well as a Matlab post processing software to translate the output data from both simulations and measurements into images that can be more easily compared.

4.4.1 Post processing software

In both cases, it was necessary to compare the obtained results to visually compare them. The data files generated from the previously described measurement setup and simulations were used, for which a script to process the results was developed in Matlab. This script used the coordinates of the points measured to locate their correspondent values. Those values were then used to develop an image of the SAR and S21 distributions.

4.4.2 WPT measurement validation

The determination of the system's power mapping reliability was done by resorting to HFSS, where the experimental scenario was replicated. The simulated model was comprised of a cylinder of phantom with the dielectric properties of the human head at 2 GHz (the plastic container was considered RF transparent), and one emitting half-wavelength dipole, while for the situation where two antennas were used, two half-wavelength dipoles were modeled. Additionally, a receiving dipole was used to mimic the developed power distribution probe. The simulated model is presented in Figure 62.

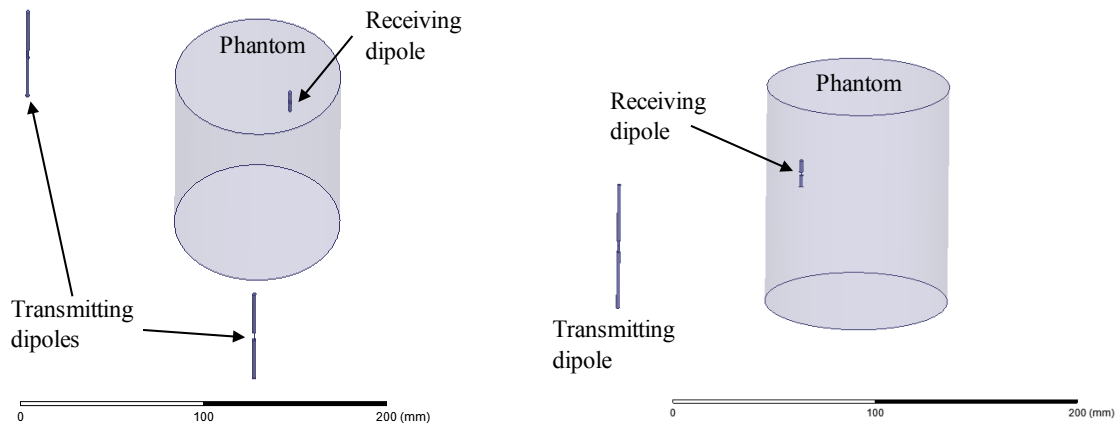


Figure 62 - Models used for the simulations. On the left is represented the case where two antennas were used, at an angle of 60° from the normal and on the right the case where one antenna was used.

The measurements were performed with the previously described setup, without the power amplifiers. To allow for matching experimental and simulation data, both were made within a circular area with a diameter of 90 mm and with a resolution of 2.5 mm for both the one and two transmitting

antenna scenarios. The results obtained, shown in Figure 63, correspond to the distribution at half the cylinder height, as the dipoles in both simulation and measurements were placed at that height.

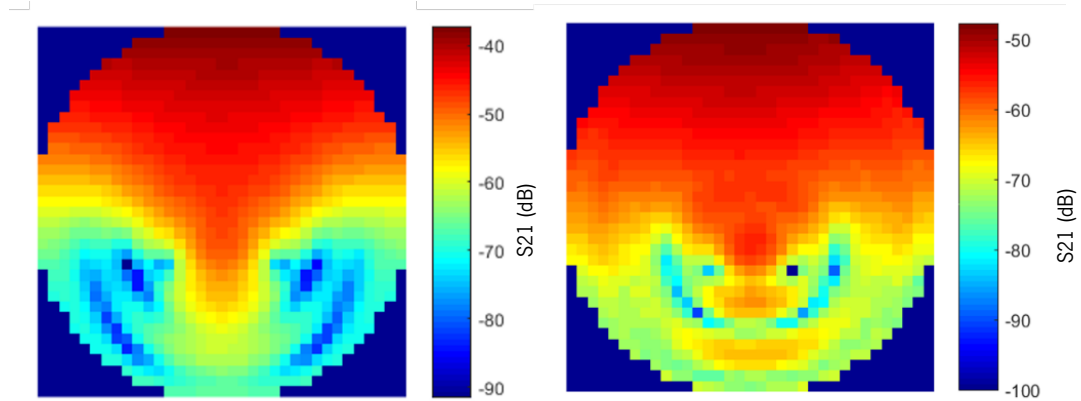


Figure 63 - Simulation (on the left) and measurement (on the right) of the power distribution inside the phantom for one antenna.

These results were obtained by simulating S_{21} parameters in HFSS and by measuring them with the VNA on the experimental setup. It is possible to verify that both simulations and measurements result in approximately the same results, where the measured values have a higher transmission loss, which is correspondent to the attenuation caused by the wireless signal generation system used, i.e. attenuators, splitter and cables.

For the case of the two antennas with variable phase, the results are shown in Figure 64. In the first case, for a phase difference of 0 degrees, the measured results are compared to the simulated ones and, again, agreement is verified in the shape of power distribution, although power levels are different due to the same reason as in the single-antenna scenario. For the second case, for a phase difference of 60 degrees, experimental results were compared to the simulated Poynting vector, which is a direct calculation of the power distribution inside of a volume or on a surface. Again, an excellent agreement is verified between the results, as power distributions match. It is therefore possible to conclude that the power mapping system produces reliable results and can be used for its goal.

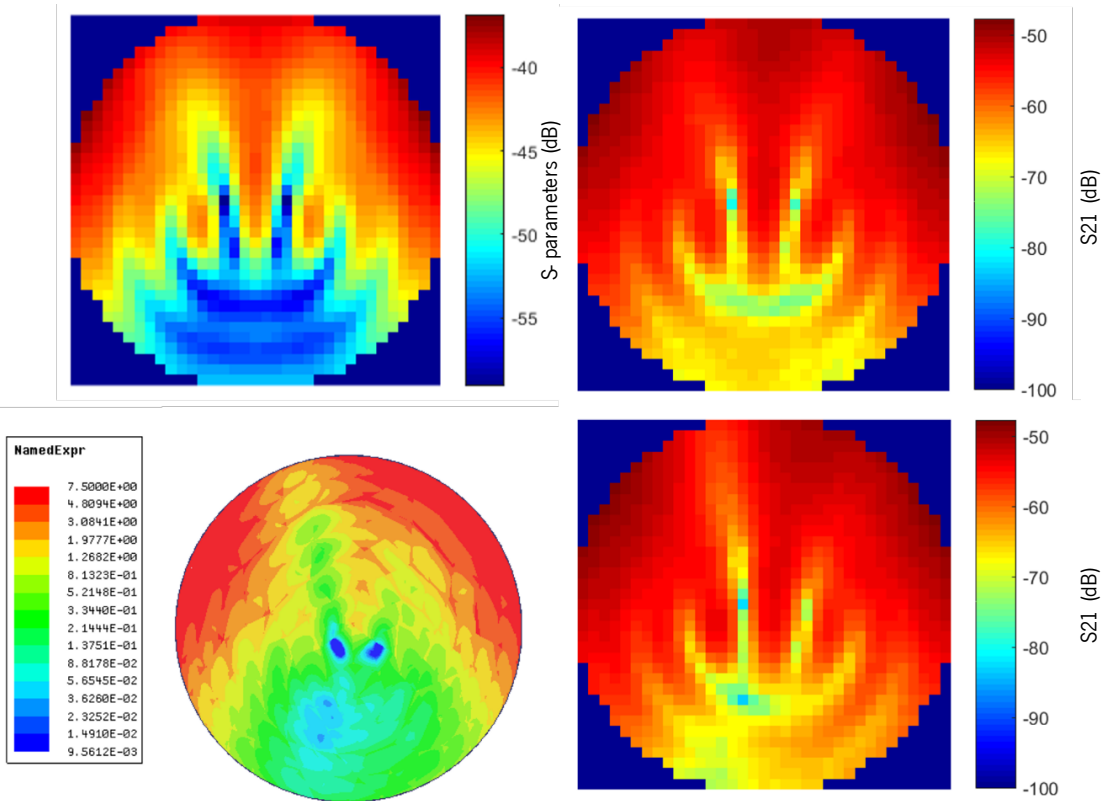


Figure 64 - Simulations (on the left) and measurements (on the right) of the power distribution inside the phantom for two antennas. On top with a 0 degree phase difference and on the bottom with a 60 degree phase difference.

4.4.3 SAR measurement validation

The SAR measurement system also had to be validated, for which the same HFSS model as the one in the previous validation was used, except for the receiving dipole antenna, which was not required since HFSS calculates SAR from field distributions inside of volumes. In the experimental setup, the receiving dipole antenna was also removed, as to measure SAR levels the electric-field probe is required. Both measurements and simulations were performed in the same 90 mm diameter surface and with 2.5 mm of resolution. The local SAR results of the simulation and measurements in the one transmitting antenna scenario are shown in Figure 65.

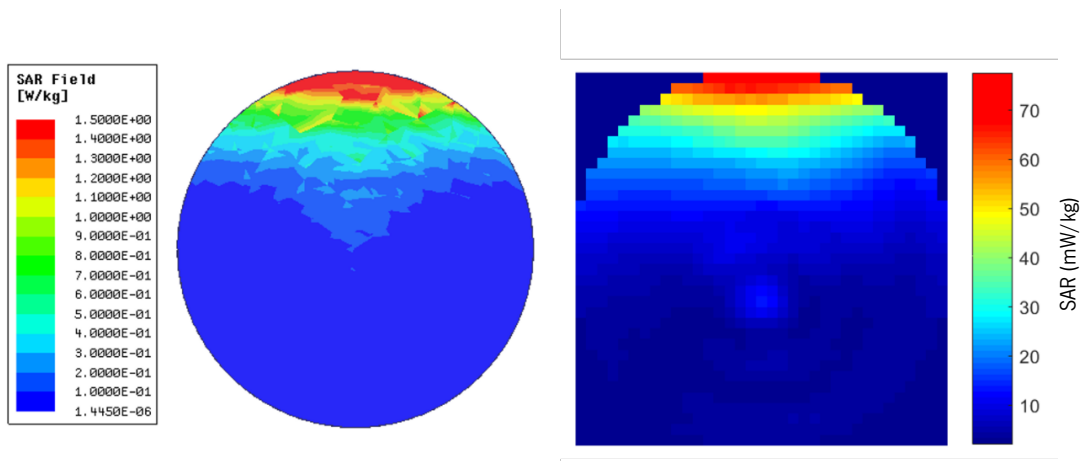


Figure 65 - Simulation (on the left) and measurement (on the right) of the local SAR levels for one antenna.

For the case of one antenna, the same SAR distribution can be observed in both simulations and measurements. The two antennas with variable phase scenario, shown in Figure 66, also produced the similar results, where the same SAR distribution was accomplished.

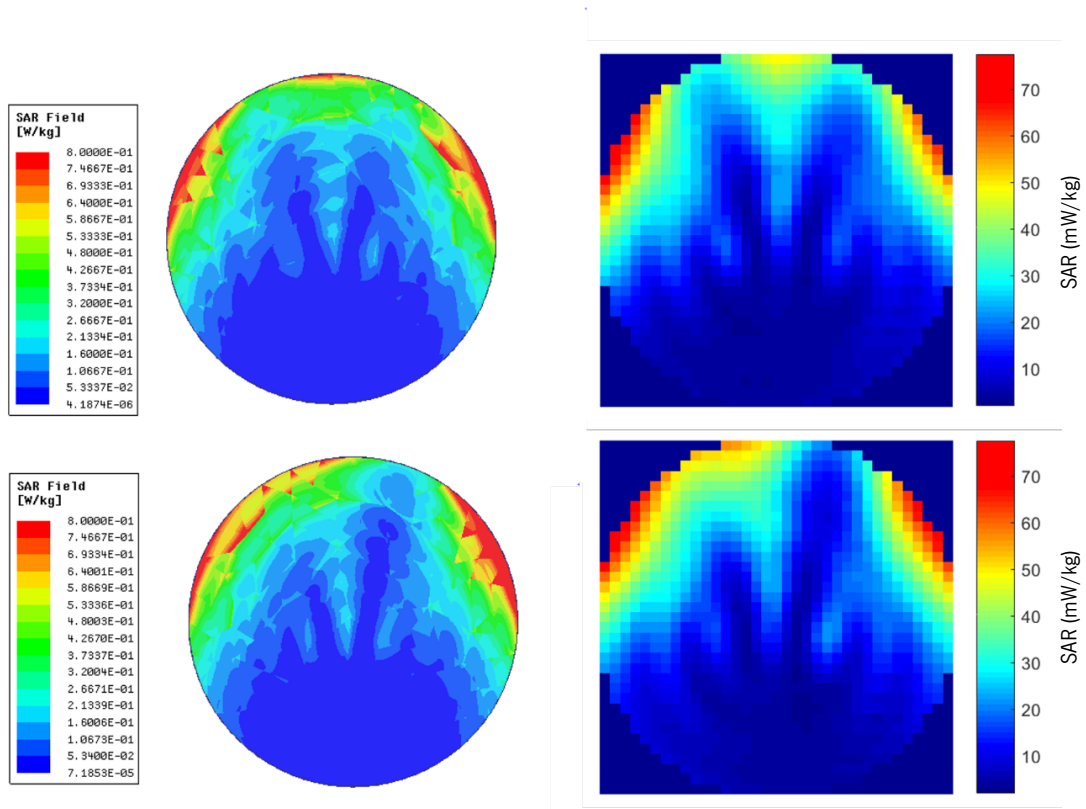


Figure 66 - Simulations (on the left) and measurements (on the right) of the local SAR levels for two antennas. On top with a 0 degree phase difference and on the bottom with a 60 degree phase difference.

In this case, the two antennas were powered with half the power used in the case of one antenna. This configuration was used to study the performance when using a multi-antenna system. In both scenarios, even though measured SAR distributions agreed with the simulated data, the absolute values were not the same. Such can be explained by the fact that the electric field probe was not calibrated for this experimental frequency (2 GHz), as previously explained. Nevertheless, relative measurements were performed and satisfying results were obtained. Additionally, the probe can be calibrated in the future, making it possible to obtain absolute measurements.

5 MEASUREMENTS AND RESULTS

In the previous chapters, the developed base station with a WPT and wireless communication system have been thoroughly described. Moreover, a SAR and power distribution measurement setup was built, which was validated through simulations and experimental results. In this chapter, the performance of these systems will be evaluated.

5.1 Wireless communication

To determine if this system could produce the necessary modulation and demodulation for communicating with the implant's chip, the system was modified, and a setup was implemented to measure the signal's characteristics. Lastly, a wireless link was established between the modulation and demodulation blocks to determine their performance.

5.1.1 Measurement setup

This system must establish a bidirectional link, however, the chip with whom this link had to be established was unavailable for testing, since it was under development on a parallel work. Hence, the modulation and demodulation blocks were tested separately.

To determine if the modulated signal could be generated, a low frequency OOK modulation was implemented. This allowed to determine whether the switch could generate that modulation, and if the carrier signal's frequency was 1 GHz. The generated signal was input in the E4404B spectrum analyzer from Agilent, which allowed to determine these parameters.

To assess the demodulation block's performance, two antennas were used to transmit and receive the modulated signal at the same time. The ones used were respectively a horn and a monopole, placed at approximately 1.5 m of distance. This modification bypassed the antenna's switch and the receiving antenna was directly connected to the power detector and baseband module. Through these tests, it is possible to verify the system's ability to implement a wireless link.

5.1.2 Measurements

A diagram representing the modulation block and the measurements carried out to test it are presented in Figure 67 and Figure 68, respectively. The full spectrum of the modulated signal couldn't be observed on the spectrum analyzer due to its lower frequency limit of 9 kHz. As a result of this, a low frequency modulation (1 Hz) was generated so that the spectrum of the modulation could be analyzed with the naked eye. It is possible to verify that the desired modulation can be generated by the implemented block, with a carrier wave at 1 GHz.

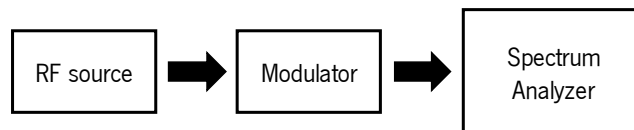


Figure 67 –Modulator block's test configuration.

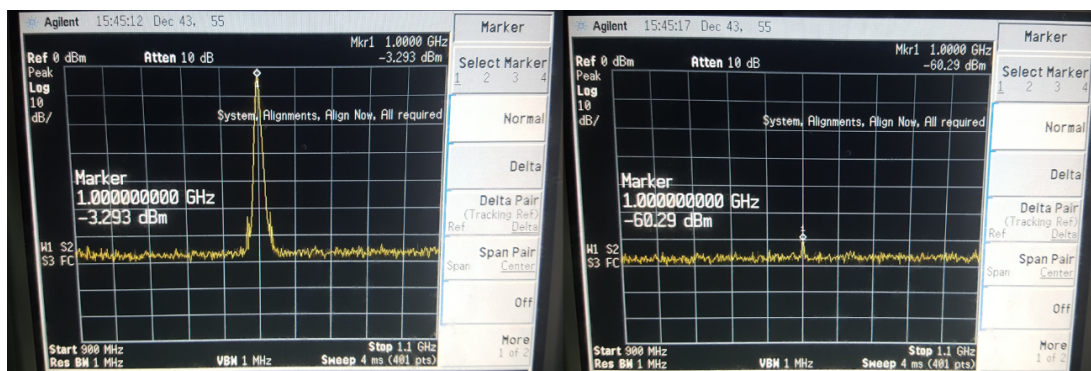


Figure 68 - Generated carrier signal, turned on (left), and turned off (right), on the output of the modulation block.

The following block to be tested was the demodulation block, whose configuration is presented in Figure 69. To do this, the microcontroller generated a square wave, which was used to modulate the signal. Not only did this allow to test the demodulation block, but also both blocks' frequency range. Both generated and received waves are shown in Figure 70.

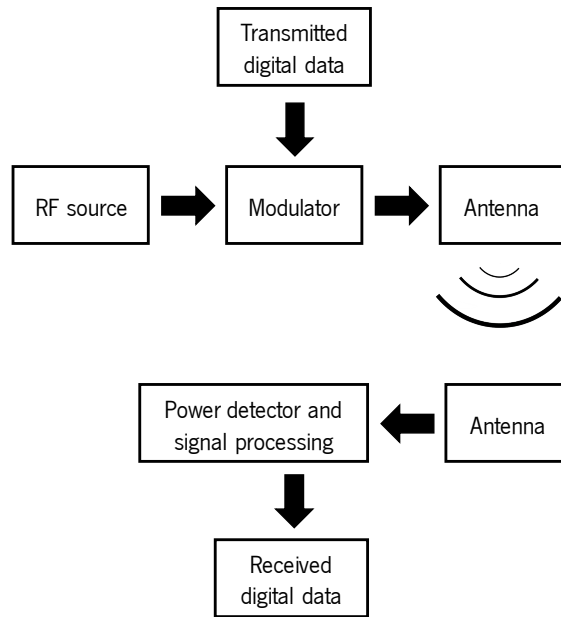


Figure 69 –Modulating and demodulating blocks' test configuration.

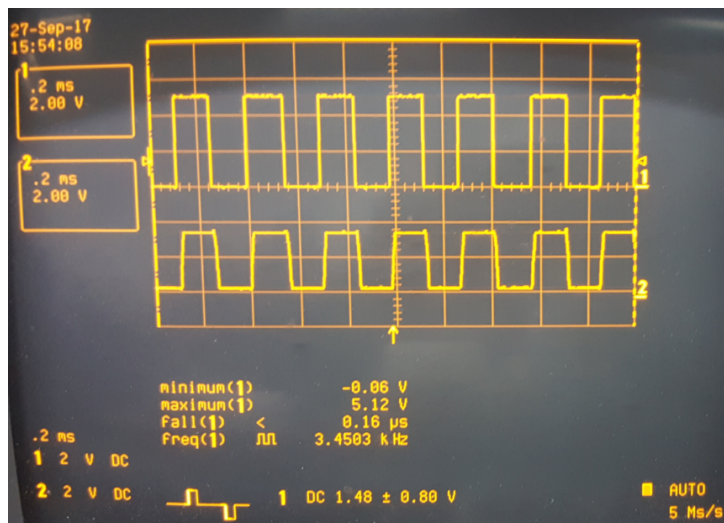


Figure 70 - Generated and received square wave before the modulation on top and after the demodulation on the bottom.

With both blocks' tests completed, and as an example, the “turn on” command to start the current sources in the chip was sent on a loop at the required frequency to establish the data transfer with the 621 Hz clock of the chip. It can be verified in Figure 71 that the command is successfully wirelessly sent and detected by each block of the base station, allowing for the bidirectional link to be established.

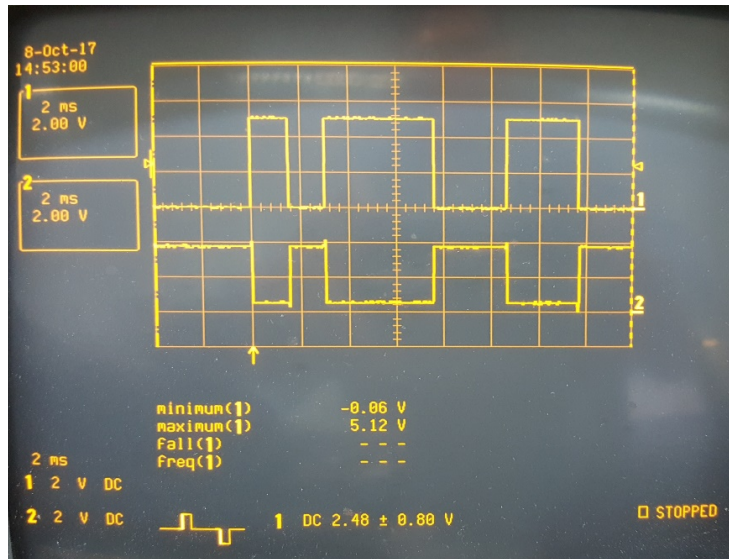


Figure 71 - Sent (top) and received (bottom) "turn on" command, before the modulation and after the demodulation.

5.1.3 Discussion and conclusions

The developed system, as proven by the results, allows for the generation of the required modulation. Although the isolation of the signal when a binary ZERO is sent is not perfect, it will not be detected by the receiver as it has got a very low power level. The demodulation block, as well as the baseband module, allow for the detection and recovery of the transmitted digital data.

From the performance of the analyzed blocks, it is possible to conclude that the developed system allows for the implementation of the desired wireless bidirectional communication with the chip. Moreover, it allows for future improvements and modifications, as it is a flexible system that can be easily modified to generate the same modulation with another carrier wave and with higher data transfer rates.

5.2 Wireless Power Transfer

The WPT system developed was tested in two parts. In the first one, the tracking algorithm's performance was evaluated, where the feedback and power amplifiers were not used. On the second one, the system's ability of wirelessly lighting up an LED was tested.

5.2.1 Measurement setup

To test the tracking algorithm, it was chosen to avoid the influence of the wireless feedback. Alternatively, the feedback link was implemented by connecting the receiving antenna to the power detector with a coaxial cable, as shown in Figure 72. Moreover, as the objective wasn't to transfer high amounts of power, the power amplifiers were not used. To monitor and analyze the tracking algorithm's performance, the transferred power level and the phase were sent through the serial port on each iteration. These values were read during 9000 iterations and had got a resolution of 1.4 degrees for the phase and 0.3 dBm for the power level.

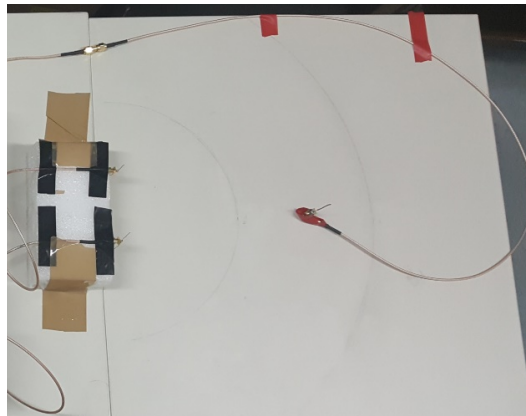


Figure 72 - Algorithm test setup, with a coaxial cable feedback.

5.2.2 Tracking algorithm validation

To validate the tracking algorithm, three different tests were made. The first one was done without moving the antenna, the second one with it moving at a fixed distance from the array, and the last one mimicked the movement around the housing's bounds. The first measurement, shown in Figure 73, was done to analyze the stability of the algorithm when the rodent is not moving. In this case, the antenna was stopped during the entire measurement, and a power variation of 0.6 dBm between the maximum and minimum values was achieved.

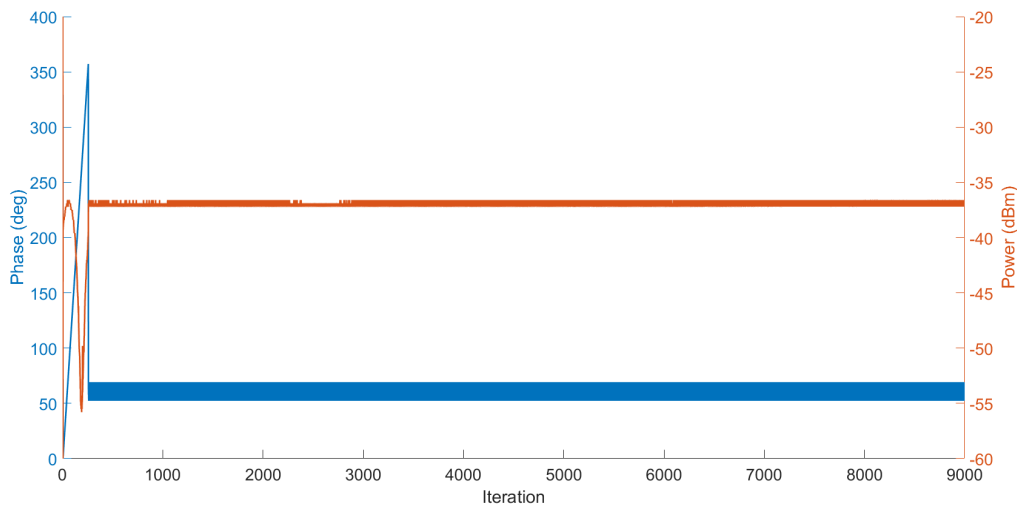


Figure 73 - Power level (orange) and phase variation (blue) during the tracking with the receiving antenna stopped.

The ideal stability for this system would result in a power variation of 0 dBm. However, due to the position feedback implemented, this is impossible to achieve as the power transfer on the adjacent positions of the rodent must be evaluated. Nonetheless, the power variation that results from this behavior can be diminished, but a consequence of this would be a reduction of the algorithm's capability to track the rodent, as less verifications to power level around the selected phase would be performed. The phase variation obtained is just the result of the algorithm evaluation around the position of the receiving antenna, which is correspondent to its minimum limits that originate from the step size. From the obtained power transfer results, it is possible to conclude that the variation of 0.6 dBm is close to the desired minimum, doesn't have a high impact on the amount of power transferred, and is adequate for this system. Lastly, it is possible to conclude that any power transfer change in the following tests will not be caused by algorithm instability.

The next step was to test the algorithm's ability to track and maintain the same power level when the movement was done at 30 cm from the antenna array. This test's results, shown in Figure 74, were obtained by placing the antenna directly in front of the array (center) and moving it in the following sequence: clockwise, counterclockwise, clockwise, and finally back to the initial position. In this experiment, the power varied 5.7 dBm considering the maximum and minimum values.

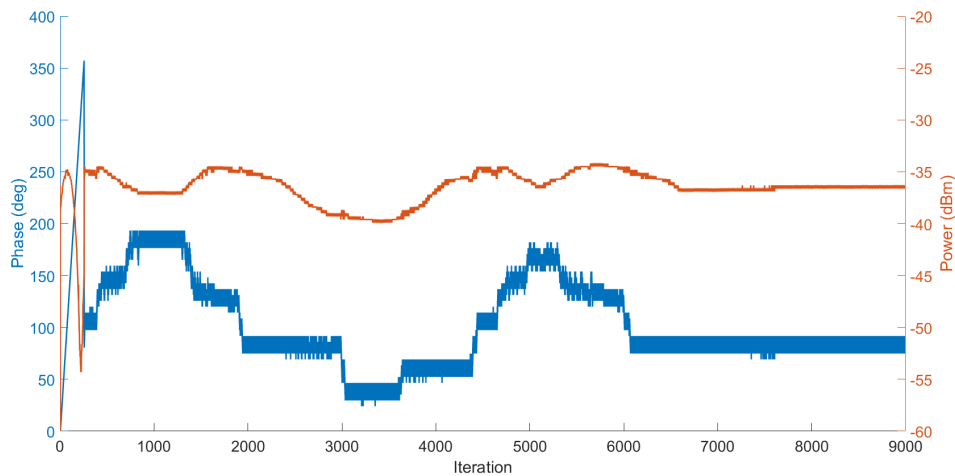


Figure 74 - Power level (orange) and phase variation (blue) during the movement at a constant distance.

Changing the angle at which the receiving antenna is placed allowed to assess the algorithm's capability of tracking and still transferring power. By analyzing the results, it is possible to conclude that the phase change is correspondent to the angular movement of the antenna throughout the experiment. The amount of power transferred presented a variation of 5.7 dBm, in which it must be considered that the movement was done by hand, the surroundings were not stable during the experiment, and that the orientation of the antenna is not constant due to the manual placement. By taking these factors into account, it is possible to conclude that the system was able to track the rodent.

Another test was done to verify if the algorithm could perform the tracking when not only the angle, but also the distance to the transmitting array changed. In this case, this test was done by simulating the movement around the cage. The initial position was 15 cm in front of the array (position A), and in a clockwise movement, the receiving antenna went through the corners of the defined area ($29 \times 47 \text{ cm}^2$), in alphabetic order, and ending in the initial position. These points, as well as the obtained measurements are shown in Figure 75 and Figure 76, respectively.

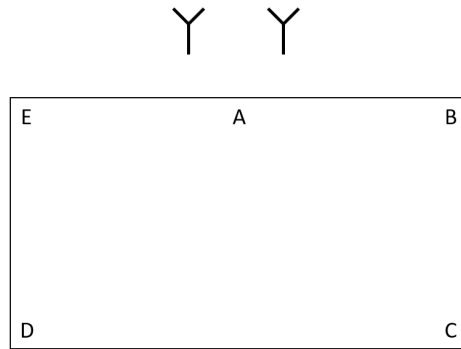


Figure 75 - Illustration of the corners of the defined area

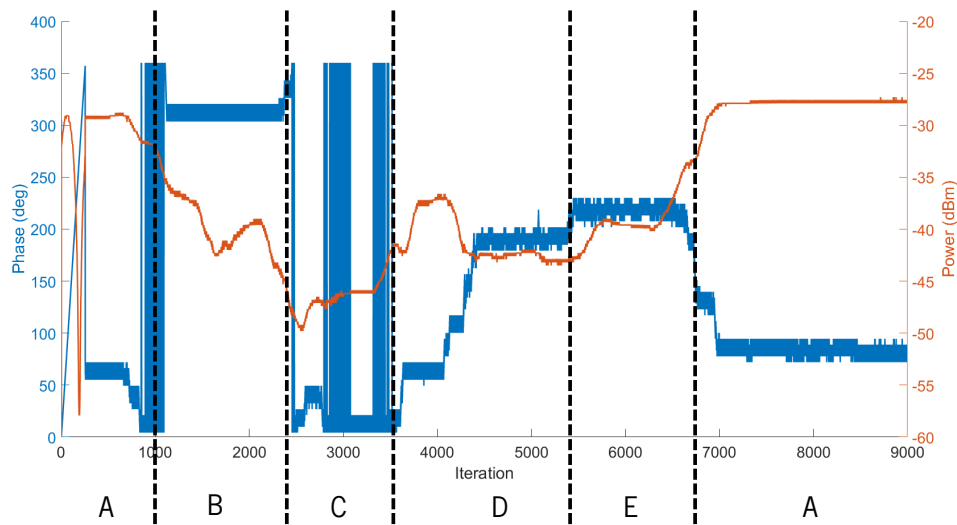


Figure 76 - Power level (orange) and phase variation (blue) during the tracking with the receiving antenna moving around the defined area.

Although the power transferred has got a high fluctuation which is caused by the free space path loss, due to the irregular distance of powering, the phase change over the iterations corresponds to the positions used in this test. The first movement from A to B corresponds to a small counterclockwise movement and a slight increase of distance, which results in a reduction of both phase value and transferred power. From B to C, a small clockwise movement with a distance increase takes place, which results in a transferred power reduction and increase in phase value. From C to D, a large clockwise movement across the area results in a large increase in phase, and in an increased power transfer in the middle of the path. From D to E, a slight shortening of distance and clockwise movement results in a slight increase of both transferred power and phase value. The final movement back to the initial position reestablishes the phase and transferred power to approximately the same

initial values. From this test, it is possible to conclude that the proposed algorithm is capable of tracking and transferring power within the defined area.

5.2.3 “Real” scenario validation

With the tracking algorithm tested, it was necessary to evaluate the power transfer link. For this part of the test, the receiving antenna had got an RF-DC board connected to it. An LED was used as the load and as a visual representation of how much power was being received by the board. To power it, it is necessary to have an input of at least 6 dBm. In this case, it was necessary to transfer high amounts of power, for which both power amplifiers were used along with two horn antennas. The coaxial feedback was replaced by the emitting and receiving feedback antennas, reestablishing the wireless feedback link. The test setup is shown in Figure 77.

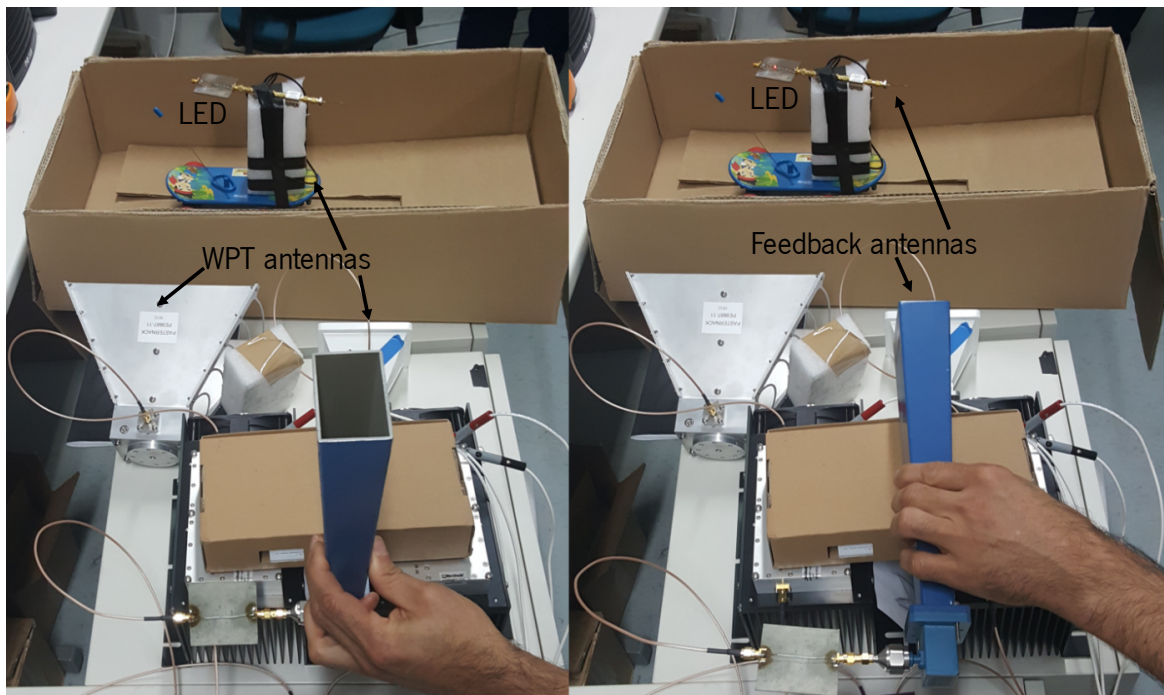


Figure 77 - WPT system setup, with the feedback horn turned away and the LED turned off on the left and the system fully working with the LED lit up on the right.

As it can be seen, the WPT system successfully lit up the led and tracked the receiver's position. To test the feedback loop and its usefulness, the feedback antenna was then turned away from the receiving one. Consequently, the feedback loop was broken, and its absence impeded the tracking system from working properly and tracking the device, resulting in the LED turning off.

5.2.4 Discussion and conclusions

From the previous tests, it is possible to conclude that the algorithm is adequate for this system to track the rodent. The algorithm provides a high stability with low power variation (0.6 dBm) when the receiving antenna is stopped. This value not only is influenced by the algorithm's behavior, but also by the power detector's linearity over its power range. As the power variation obtained in the stability test and the phase shifter's resolution is not being used to its fullest, it is possible to deduce that this algorithm allows for the system to be improved by implementing a more directive array.

The recombination in amplitude of both transmitted signals is maximum when their phase difference is null. To control the beam direction, or more specifically the direction where the recombination of the transmitted signals occurs, the excitation phase was controlled by the phase shifter. As described in [73], the first maximum of the array factor occurs when:

$$\Psi = kd \cos \theta + \beta = 0 \quad (9)$$

where d is the distance between the elements and $k = \frac{2\pi}{\lambda}$. When it is desired to direct the maximum radiation to the normal of the axis of the array ($\theta = 90^\circ$), the excitation phase $\beta = 0$. Similarly, to direct the beam toward $\theta = 0^\circ$ the excitation phase becomes $\beta = -kd$, and towards $\theta = 180^\circ$ the excitation phase becomes $\beta = kd$. Therefore, by moving the receiving the antenna clockwise around the array (increasing theta), the phase value is increased, and when moving it counterclockwise (reducing theta), it is decreased.

This variation can be verified on both moving tests, by the series of clockwise and counterclockwise movements. When the receiving antenna moved clockwise, the phase value was increased, and when the movement was counterclockwise, the phase value decreased. These tests also allowed to verify the algorithm's tracking capability when the receiver is moving, by analyzing that phase change. The achieved power levels' stability at a constant distance reveals that the algorithm is adequate for powering moving targets. When analyzing the power level variation in both scenarios, it must be considered that these tests were done by moving the antenna by hand. This results on imperfect movements, different orientations, and surroundings throughout the experiment, which contribute to the power change.

To conclude, live powering tests were made where the LED was successfully lit up. By visually and qualitatively analyzing the brightness of the LED, it was possible to determine that the input power level of the RF to DC converter was over 7 dBm. Considering that half of that power was used to

generate and transmit the wireless feedback signal, the power that was wirelessly transferred corresponded to at least 10 dBm. This doesn't consider the power losses caused by the receiving coaxial cable and splitter, meaning that the received power is over that value.

Comparing to the calculations made in the first chapter, when a battery of 51.8 mWh is fully depleted, it takes about 5 hours and 10 minutes to fully recharge it. This not only avoids the replacement of batteries and the problems associated with it, but also allows to increase the amount of discharges done per day while also extending the device's lifetime.

5.3 SAR

The developed SAR measurement system was validated at a frequency that generates relative SAR dosage values. In this section, as the calibration of the probe was done for 900 MHz, it will be used to evaluate absolute SAR levels.

5.3.1 Measurement setup

In this case, to measure and obtain absolute dosage levels, an RF signal at 900 MHz was radiated at a power level of 2 W. The same setup as the validation for one antenna in the section 4.4.2 was used, in which one half-wavelength dipole was built and placed at one wavelength (≈ 33 cm) from the center of the phantom. The dipole's center was placed at a height of 80 mm, while the probe was placed at 50mm, both in relation to the base of the phantom's container, as represented in Figure 78.

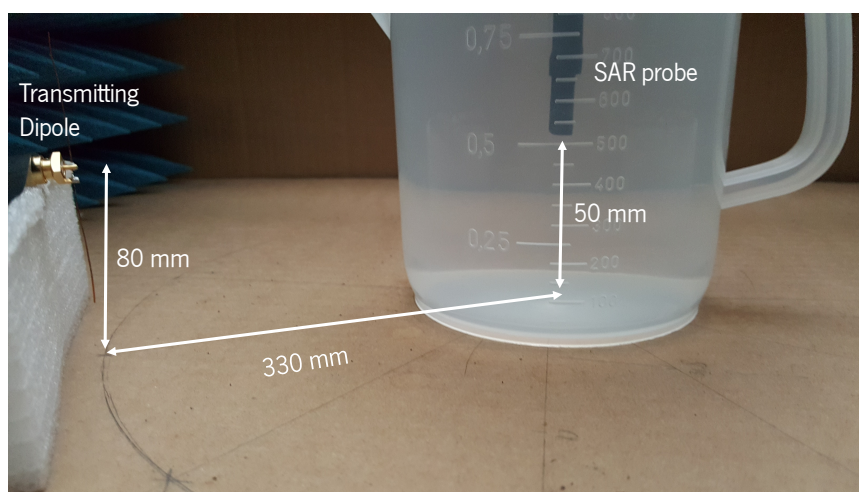


Figure 78 -900 MHz SAR measurement setup.

For this evaluation, the used phantom was prepared and characterized, and then used for the experiment. It had got a permittivity of 42.6 and a conductivity of 0.6 S/m. Lastly, the measured values were verified with an HFSS simulation, where these conditions were replicated, allowing for a direct comparison of the results.

5.3.2 SAR measured results

The results of the simulations and the measurements are presented in Figure 79, where the antenna radiated from the top of the images. In the previous chapter, the measured SAR distribution corresponded to the measured. Likewise, in this case, the SAR distribution pattern is the same as predicted in the simulation. Moreover, the values obtained are also correspondent in both cases. The hotspot in the center, has got a maximum local SAR value of around 350 mW/kg, which is also verified in the experiment's results. In addition to this, the hotspots on top and bottom of it also have similar values, which are around 140 mW/kg and 190 mW/kg, respectively. The distribution on the surface of the phantom is not correspondent to the simulation, as the probe's dimensions did not allow it to reach the edge of the phantom.

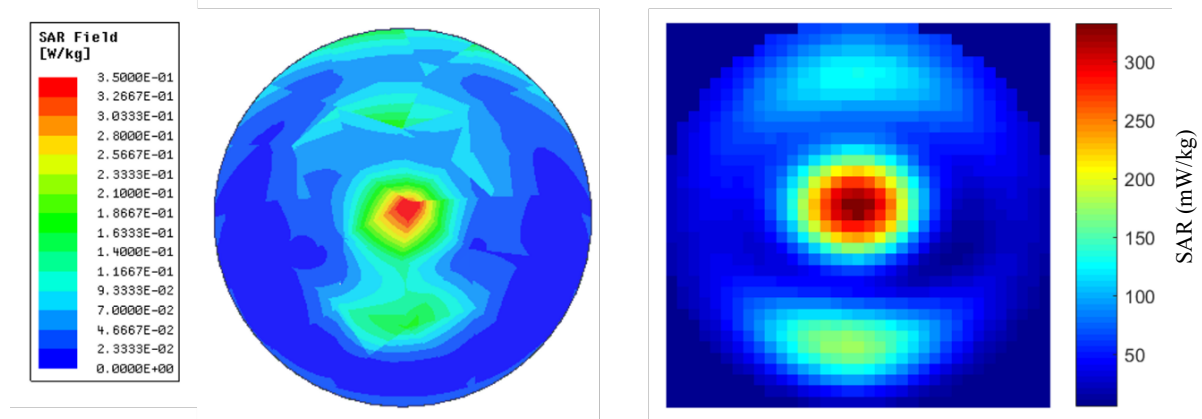


Figure 79 - Results of the simulations and measurements of SAR distribution for 900 MHz.

5.3.3 Discussion and conclusions

From the validation done in the previous chapter, along with the results obtained in this one, it is possible to conclude that a SAR measurement system was successfully implemented. It provides reliable results for the relative distribution of SAR levels, and when it is used to measure at the frequency for which the probe was calibrated, it also provides absolute values that agree with simulated

ones. These absolute values can currently be measured for 900 MHz, however, it is also possible to measure them for other frequencies. For this, it is only required to calibrate the probe at the desired frequency or frequency range. As the calibration is read from a text file provided by the manufacturer, this system can measure SAR at any frequency without the need to modify any physical part of it, as long as the calibration file is available for that frequency.

6 CONCLUSIONS AND FUTURE WORK

6.1 Conclusions

Biomedical devices are of paramount importance for the treatment of drug resistant diseases. The emphasis on the well-being and quality of life of patients leads to the development and exploration of innovative devices and methods for the treatment of such medical conditions. This ultimately implies that the performance of those devices on monitoring or treating those diseases must be assessed. However, several complications are associated with such tests. At first, these must be done on rodents, which imposes several device restrictions and experimental limitations. These include size and weight restrictions, which along with the quest for wire removal, severely restrict those experiments. These constraints are also extended for the device's implantation on humans, as the desired and perpetual urge for miniaturization and wire removal is also present. However, by accomplishing such goals, several issues arise. These are lack of power, which in turn leads to a lower device lifetime, and the necessity to remove the wiring, which aggravates the powering problem and removes a possible communication link.

The agglomerate of these factors demands for a solution to be developed. As such, the objective of this dissertation's work was the development of a base station that includes both wireless powering and wireless communication for an implantable device to be tested in rodents. The objective of this base station is to allow for the device miniaturization by reducing or completely removing the battery and at the same time allowing for wire removal, by establishing a powering and communication platform. Such system allows for extending the device's lifetime, for remote monitoring, to reducing the human interaction with the rodents, and for the accomplishment of long experiments. For both powering and communication links, it was opted to use RF. In the case of the communication, RF was used as it allows for a more flexible system and to increase the communication distance relatively to other wireless methods. Similarly, for the case of the power link, it allows for a higher device miniaturization and long-distance powering, due to its propagation capabilities. The combination of both parts culminates in a complete base station that allows for testing and monitoring the device's performance on rodents. With it, these experiments can be accomplished without the hassle of complicated logistics, battery and general device maintenance such as broken wiring. Moreover, as this system was planned to be used with rodents as test subjects, it tackled the previous issues, while regarding for their welfare

and housing conditions which are of paramount importance for most studies performed on these animal models.

The wireless communication link was planned, designed, and built by taking an in-house developed RFCMOS chip into account. This chip will be used to control the implant, and it requires a specific modulation and protocol to communicate with. Therefore, the developed modulation and demodulation blocks were assembled to conceive the complete wireless communication system and allow for the transmission and receiving of OOK modulated data at 1 GHz. This can be done within a distance of 1.5 m, while other common wireless systems such as WiFi routers are operating in the vicinity. The range of communication can be extended by making use of the installed optional amplifiers in the system. The communication link is managed by a microcontroller, for which an interface was developed, allowing for an easy control of the developed implantable thermal neuromodulator. Finally, this system can be readily modified to produce a modulation and protocol with different characteristics so that it can easily adapt to any chip modifications. As this is a modular system, it is possible to further customize it by replacing any component in case it is necessary, allowing this system to be used for other applications.

The WPT system was projected to transfer power by using RF at 2 GHz. To increase the amount of power transferred to a device implanted on a freely moving rodent while reducing power transferred to other directions, it was needed to habilitate this system with a power directing capability. For this, it was used beamforming, as it allows to generate and direct a RF beam by changing the phased array excitation phase. The used antenna array was comprised of two elements, as it allows to implement the desired system, without immensely increasing the cost and the volume of the system. To use this system with a freely moving rodent, it was necessary to track its position, for which a wireless feedback at 4 GHz that indicated a relative value of power delivered to the implant was implemented. Through this, a tracking algorithm at 1 kHz was implemented, which used that feedback to control the beam direction. This resulted in a powering system that allowed to track the rodent at a theoretical speed of up to 3.41 m/s, and could continuously transfer up to 10 mW. This allows to fully recharge a 51.8 mWh battery over a period of around 5 hours while it is implanted on a freely moving rodent. Like the communication system, this system can be easily readjusted for different power requirements. This can be done by replacing the RF source for one with a different power output, changing the power amplifiers, and altering the beamforming array's antennas.

Implantable medical devices are often implanted at a certain depth. Nonetheless, it is still necessary to power them, for which it was necessary to measure power and SAR distributions. As it is indispensable to recharge those devices, it is also necessary to maintain the wellbeing of the rodents. Moreover, wireless powering must be extended to human applications for which the same requisites are needed. To evaluate both powering and SAR dosage, a measurement setup was built. Software was developed for it, where it interfaced the SAR and power acquisition systems, controlled the positioning system, and phase shifter, for the case where phase control is needed. The used motors allow for a measurement area of $10 \times 10 \text{ cm}^2$, with a resolution of up to $0.125 \text{ }\mu\text{m}$. Lastly, these experiments also required the development of a human head phantom and a data processing script. The results obtained of both power and SAR distribution measurements are reliable, as determined with the performed HFSS simulations for the same problem.

6.2 Future work

In this section, a few aspects that may be improved will be highlighted. For the wireless communication system, when no further updates or modifications are necessary to communicate with a certain device, more specific RF components could be used, where the desired goal would be the reduction of the system's cost and volume. As a mean of achieving this, for example, instead of a VCO with a wide operating frequency range, a single frequency one could be used, and the same can be applied for the remaining components. Along with this, it is possible to reduce the size of the system even further by using smaller components. Although the power consumption is not problematic, by using less power-hungry components, it still can be reduced. Lastly and most importantly, it is still necessary to establish the bidirectional link with the developed chip. This wasn't accomplished yet, due to its late delivery and still ongoing characterization.

The WPT system can be improved by modifying some of its characteristics. For applications with higher power draw, it is necessary to increase the amount of power transferred. To achieve it, an RF source with a higher power output can be used, which consequently increases the power received by the device. Another form of doing this is by using amplifiers with a higher power output. On the other hand, if a power reduction is required, both elements' power output can be reduced. Increasing the power transfer efficiency is desired in every application. Some ways of accomplishing it are possible. Firstly, the used antennas can be replaced by more directive ones, increasing the gain of

the array. Along with this, it is also possible to further increase the system efficiency by replacing the power amplifiers with ones with that aren't as power hungry. To further increase the power transfer efficiency and more accurately track the rodent, an implementation of an antenna array with more elements would have to be used. This could generate a narrower beam, with a higher gain, increasing the power transferred by the system. In an application where the test subjects can move in various directions, such as monkeys, the beam direction must also be changed vertically. To obtain such degree of freedom, the implementation of an antenna array with more elements in a non-linear arrangement is needed. This not only allows for increasing the gain of the antenna array, but also for the tracking to be done not only horizontally but also vertically. This is achieved by modifying the excitation phases of an array such as the one shown in Figure 80.

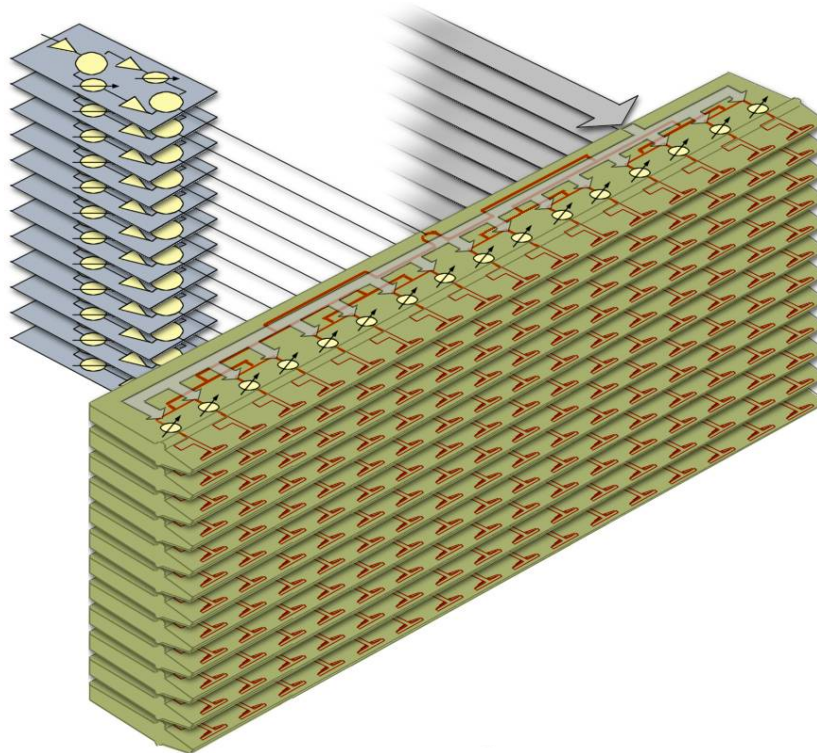


Figure 80 - Example of a planar phased array antenna [78].

For the power and SAR mapping setup, an improvement would be increasing the area of measurement. This can be done by replacing the motors used by ones with a longer range. In addition to this, to perform these mappings on a volume, another motor could be added, which would allow for the inclusion of vertical measurement positions. A calibration method is desired to reduce the hassle and duration of pre-measurement set-ups. With the addition of one extra motor and extension of the

measurement area, that calibration becomes possible by including a reference position and detection system such as a laser.

Further options for the area measurements would also be important, allowing for the mapping of irregular areas. This would allow the system to, for example, measure around devices placed inside the phantom, by modifying the way that the area to be measured is calculated and defined in the algorithm.

In the case where a measurement with more than two antennas is needed, the implemented software can be used. However, as several phase differences must be controlled, it is necessary to modify it by adding an input for each of the phases to be measured or each combination of phases. Along with the input modification of the LabView software, it would also have to be modified to control each of the phase shifters individually during the experiment. It is therefore also necessary to consider the phase difference that is generated on each path to the antennas and correct each of them with a respective offset, as was done with the two-antenna scenario. Due to the low speed of phase control through the program and limited number of USB ports, to control more than one phase shifter at the same time it is recommended to use a microcontroller and its SPI module.

REFERENCES

- [1] ResearchLLP, "Implantable Medical Devices Market Analysis and Trends - Product, Material - Forecast to 2025."
- [2] D. Fitzpatrick, *Implantable Electronic Medical Devices*, 1st ed. Academic Press, 2014.
- [3] E. C. Bryda, "The Mighty Mouse: the impact of rodents on advances in biomedical research.," *Mo. Med.*, vol. 110, no. 3, pp. 207–11, 2013.
- [4] M. Lee, D. Kim, H.-S. Shin, H.-G. Sung, and J. H. Choi, "High-density EEG Recordings of the Freely Moving Mice using Polyimide-based Microelectrode," *J. Vis. Exp.*, no. 47, pp. 2–5, Jan. 2011.
- [5] B. Lee, M. Kiani, and M. Ghovanloo, "A Smart Wirelessly Powered Homecage for Long-Term High-Throughput Behavioral Experiments," *IEEE Sens. J.*, vol. 15, no. 9, pp. 4905–4916, Sep. 2015.
- [6] Y. Choi, S. Park, Y. Chung, R. K. Gore, A. W. English, and R. V. Bellamkonda, "PDMS microchannel scaffolds for neural interfaces with the peripheral nervous system," in *2014 IEEE 27th International Conference on Micro Electro Mechanical Systems (MEMS)*, 2014, pp. 873–876.
- [7] S. Okada, H. Igata, T. Sakaguchi, T. Sasaki, and Y. Ikegaya, "A new device for the simultaneous recording of cerebral, cardiac, and muscular electrical activity in freely moving rodents," *J. Pharmacol. Sci.*, vol. 132, no. 1, pp. 105–108, Sep. 2016.
- [8] P. Cong, W. H. Ko, and D. J. Young, "Wireless Batteryless Implantable Blood Pressure Monitoring Microsystem for Small Laboratory Animals," *IEEE Sens. J.*, vol. 10, no. 2, pp. 243–254, Feb. 2010.
- [9] H. Bhamra, J.-W. Tsai, Y.-W. Huang, Q. Yuan, and P. Irazoqui, "21.3 A sub-mm 3 wireless implantable intraocular pressure monitor microsystem," in *2017 IEEE International Solid-State Circuits Conference (ISSCC)*, 2017, vol. 60, pp. 356–357.
- [10] E. Y. Chow, A. L. Chlebowski, and P. P. Irazoqui, "A miniature-implantable RF-wireless active glaucoma intraocular pressure monitor," *IEEE Trans. Biomed. Circuits Syst.*, vol. 4, no. 6 PART 1, pp. 340–349, 2010.
- [11] MultiChannel Systems, "Wireless2100-System Manual."
- [12] D. Fan *et al.*, "A Wireless Multi-Channel Recording System for Freely Behaving Mice and Rats," *PLoS One*, vol. 6, no. 7, p. e22033, Jul. 2011.
- [13] EmKa Technologies, "easyTEL implants for rodents." [Online]. Available: <http://www.emka.fr/product/implants-for-rodents/>. [Accessed: 01-Nov-2017].
- [14] E. G. Kilinc, C. Dehollain, and F. Maloberti, "Implantable Monitoring System for Rodents," Springer International Publishing Switzerland, 2016, pp. 13–23.
- [15] K. L. Montgomery *et al.*, "Wirelessly powered, fully internal optogenetics for brain, spinal and peripheral circuits in mice," *Nat. Methods*, vol. 12, no. 10, pp. 969–974, 2015.
- [16] P. Gould and A. Krahn, "in Response to Device Advisories," *Info*, vol. 295, no. 16, pp. 1907–1911, 2006.
- [17] Tianjia Sun, Xiang Xie, and Zhihua Wang, *Wireless Power Transfer for Medical Microsystems - Tianjia Sun, Xiang Xie, Zhihua Wang*. Springer, 2013.
- [18] T. Campi, S. Cruciani, V. De Santis, and M. Feliziani, "EMF Safety and Thermal Aspects in a Pacemaker Equipped With a Wireless Power Transfer System Working at Low Frequency," *IEEE Trans. Microw. Theory Tech.*, vol. 64, no. 2, pp. 1–8, 2016.
- [19] T. Campi, S. Cruciani, F. Palandrani, V. De Santis, A. Hirata, and M. Feliziani, "Wireless power transfer charging system for AIMDs and pacemakers," *IEEE Trans. Microw. Theory Tech.*, vol. 64, no. 2, pp. 633–642, 2016.
- [20] Medtronic, "Deep brain stimulation," 2016. [Online]. Available: <http://www.medtronic.com/us-en/healthcare-professionals/therapies-procedures/neurological/deep-brain-stimulation/indications-safety-warnings/brief-statement-movement-disorders.html>. [Accessed: 20-Jul-2011].
- [21] J. Kim, D. H. Kim, J. Choi, K. H. Kim, and Y. J. Park, "Free-positioning wireless charging system for small electronic devices

References

- using a bowl-shaped transmitting coil," *IEEE Trans. Microw. Theory Tech.*, vol. 63, no. 3, pp. 791–800, 2015.
- [22] F. Gadler *et al.*, "Economic impact of longer battery life of cardiac resynchronization therapy defibrillators in Sweden," *Clin. Outcomes Res.*, vol. Volume 8, pp. 657–666, Oct. 2016.
- [23] G. Boriani *et al.*, "Battery drain in daily practice and medium-term projections on longevity of cardioverterdefibrillators: An analysis from a remote monitoring database," *Europace*, vol. 18, no. 9, pp. 1366–1373, 2016.
- [24] V. B. Gore and D. H. Gawali, "Wireless power transfer technology for medical applications," in *2016 Conference on Advances in Signal Processing (CASP)*, 2016, pp. 455–460.
- [25] Q. Wang, "Determination of cardiac contractility in awake unsedated mice with a fluid-filled catheter," *AJP Hear. Circ. Physiol.*, vol. 286, no. 2, p. 806H–814, Feb. 2004.
- [26] I. A. S. Olsson and K. Dahlborn, "Improving housing conditions for laboratory mice: a review of 'environmental enrichment,'" *Lab. Anim.*, vol. 36, no. 3, pp. 243–270, Jul. 2002.
- [27] Committee for the Update of the Guide for the Care and Use of Laboratory Animals, *Guide for the Care and Use of Laboratory Animals*, 8th ed., vol. 46, no. 3. 2011.
- [28] E. G. Kilinc, G. Conus, C. Weber, B. Kawkabani, F. Maloberti, and C. Dehollain, "A system for wireless power transfer of micro-systems in-vivo implantable in freely moving animals," *IEEE Sens. J.*, vol. 14, no. 2, pp. 522–531, 2014.
- [29] B. Rezaei, X. Huang, J. R. Yee, and S. Ostadabbas, "Long-term non-contact tracking of caged rodents," *ICASSP, IEEE Int. Conf. Acoust. Speech Signal Process. - Proc.*, pp. 1952–1956, 2017.
- [30] Q. Xu, H. Wang, Z. Gao, Z.-H. Mao, J. He, and M. Sun, "A Novel Mat-Based System for Position-Varying Wireless Power Transfer to Biomedical Implants," *IEEE Trans. Magn.*, vol. 49, no. 8, pp. 4774–4779, Aug. 2013.
- [31] H. Mei, K. A. Thackston, R. A. Bercich, J. G. R. Jefferys, and P. P. Irazoqui, "Cavity resonator wireless power transfer system for freely moving animal experiments," *IEEE Trans. Biomed. Eng.*, vol. 64, no. 4, pp. 775–785, 2017.
- [32] C. Kwok, R. F. Jr. Cleveland, and D. L. Means, "Evaluating Compliance with FCC Guidelines for Human Exposure to Radiofrequency Electromagnetic Fields Supplement C," *Fed. Commun. Comm. Off. Eng. Technol.*, vol. 65, p. 36, 1997.
- [33] V. Silva, "Neuromodulador implantável com alimentação e comunicação sem fios em tecnologia RFCMOS 180 nm," University of Minho, 2017.
- [34] Futurlec, "ISM band FSK transmitter module RFM02," 2006.
- [35] Nordic Semiconductors, "nRF24L01+ Single Chip 2.4GHz Transceiver," 2008.
- [36] B. Bozorgzadeh, D. P. Covey, C. D. Howard, P. a Garris, and P. Mohseni, "A Neurochemical Pattern Generator SoC With Switched-Electrode Management for Single-Chip Electrical Stimulation and 9.3 μ W, 78 pA rms , 400 V/s FSCV Sensing," *IEEE J. Solid-State Circuits*, vol. 49, no. 4, pp. 881–895, Apr. 2014.
- [37] Samsung, "Wireless Charging Pad," 2017. [Online]. Available: <https://www.samsung.com/us/mobile/mobile-accessories/phones/wireless-charging-pad-black-sapphire-ep-pg920ibugus/>. [Accessed: 01-Nov-2017].
- [38] M. Kesler, "Highly Resonant Wireless Power Transfer: Safe, Efficient, and over Distance," *WiTricity Corp*, pp. 1–13, 2013.
- [39] J. Shin *et al.*, "Design and Implementation of Shaped Magnetic-Resonance-Based Wireless Power Transfer System for Roadway-Powered Moving Electric Vehicles," *IEEE Trans. Ind. Electron.*, vol. 61, no. 3, pp. 1179–1192, Mar. 2014.
- [40] C.-J. Ahn, T. Kamio, H. Fujisaka, and K. Haeiwa, "Prototype of 5 . 8 GHz Wireless Power Transmission System for Electric Vehicle System," *2nd Int. Conf. Environ. Sci. Technol.*, vol. 6, pp. 128–131, 2011.
- [41] X Development LLC, "Project Loon." [Online]. Available: <https://x.company/loon/>. [Accessed: 01-Nov-2017].
- [42] C. J. Ahn, "An applicable 5.8 GHz wireless power transmission system with rough beamforming to Project Loon," *ICT Express*, vol. 2, no. 2, pp. 87–90, 2016.
- [43] M. H. Capstick *et al.*, "A Radio Frequency Radiation Exposure System for Rodents Based on Reverberation Chambers," *IEEE*

-
- Trans. Electromagn. Compat.*, vol. 59, no. 4, pp. 1041–1052, Aug. 2017.
- [44] K. Eom *et al.*, “A wireless power transmission system for implantable devices in freely moving rodents,” *Med. Biol. Eng. Comput.*, vol. 52, no. 8, pp. 639–651, 2014.
- [45] B. M. Badr, R. Somogyi-Gsizmazia, K. R. Delaney, and N. Dechev, “Wireless Power Transfer for Telemetric Devices With Variable Orientation, for Small Rodent Behavior Monitoring,” *IEEE Sens. J.*, vol. 15, no. 4, pp. 2144–2156, Apr. 2015.
- [46] R. E. Millard and R. K. Shepherd, “A fully implantable stimulator for use in small laboratory animals,” *J. Neurosci. Methods*, vol. 166, no. 2, pp. 168–177, Nov. 2007.
- [47] R. Galvez, C. Weiss, S. Cua, and J. Disterhoft, “A novel method for precisely timed stimulation of mouse whiskers in a freely moving preparation: Application for delivery of the conditioned stimulus in trace eyeblink conditioning,” *J. Neurosci. Methods*, vol. 177, no. 2, pp. 434–439, Mar. 2009.
- [48] J. S. Ho *et al.*, “Self-tracking energy transfer for neural stimulation in untethered mice,” *Phys. Rev. Appl.*, vol. 4, no. 2, pp. 1–6, 2015.
- [49] J. Bito, S. Jeong, and M. M. Tentzeris, “A Novel Heuristic Passive and Active Matching Circuit Design Method for Wireless Power Transfer to Moving Objects,” *IEEE Trans. Microw. Theory Tech.*, vol. 65, no. 4, pp. 1094–1102, Apr. 2017.
- [50] A. S. Y. Poon, S. O’Driscoll, and T. H. Meng, “Optimal Frequency for Wireless Power Transmission Into Dispersive Tissue,” *IEEE Trans. Antennas Propag.*, vol. 58, no. 5, pp. 1739–1750, May 2010.
- [51] E. Y. Chow, S. Chakraborty, W. J. Chappell, and P. P. Irazoqui, “Mixed-signal integrated circuits for self-contained sub-cubic millimeter biomedical implants,” in *2010 IEEE International Solid-State Circuits Conference - (ISSCC)*, 2010, vol. 53, pp. 236–237.
- [52] E. Katz, *Implantable Bioelectronics*. 2014.
- [53] H. Dinis, J. Fernandes, V. Silva, I. Colmiais, and P. M. Mendes, “Thermal modeling of an implantable brain focal cooling device,” *ENBENG 2017 - 5th Port. Meet. Bioeng. Proc.*, 2017.
- [54] IndexSAR, “Cost-effective SAR-testing standards compliant system for SAR testing of wireless devices.”
- [55] The Microwave Vision Group, “RF Safety SAR & HAC test benches,” *Satimo*, pp. 1–25, 2008.
- [56] Aprel, “Standard ALSAS 10 Universal SAR & HAC (software),” no. 613, pp. 1–19, 2008.
- [57] SPEAG, “DASY6 Systems.” [Online]. Available: <https://www.speag.com/products/dasy6/overview/>. [Accessed: 01-Nov-2017].
- [58] C. K. Hung, “A Study of Electromagnetic Radiation and Specific Absorption Rate of Mobile Phones with Fractional Human Head Models,” City University of Hong Kong, 2008.
- [59] S. Gabriel, R. W. Lau, and C. Gabriel, “The dielectric properties of biological tissues: II. Measurements in the frequency range 10 Hz to 20 GHz,” *Phys. Med. Biol.*, vol. 41, no. 11, pp. 2251–2269, 1996.
- [60] C. Gabriel, S. Gabriel, and E. Corthout, “The dielectric properties of biological tissues: I. Literature survey,” *Phys. Med. Biol.*, vol. 41, no. 11, p. 2231, 1996.
- [61] S. Gabriel, R. W. Lau, and C. Gabriel, “The dielectric properties of biological tissues .3. Parametric models for the dielectric spectrum of tissues,” *Phys. Med. Biol.*, vol. 41, no. 11, pp. 2271–2293, 1996.
- [62] M. Lazebnik, E. L. Madsen, G. R. Frank, and S. C. Hagness, “Tissue-mimicking phantom materials for narrowband and ultrawideband microwave applications,” *Phys. Med. Biol.*, vol. 50, no. 18, pp. 4245–4258, Sep. 2005.
- [63] T. Yilmaz, R. Foster, and Y. Hao, “Broadband Tissue Mimicking Phantoms and a Patch Resonator for Evaluating Noninvasive Monitoring of Blood Glucose Levels,” *IEEE Trans. Antennas Propag.*, vol. 62, no. 6, pp. 3064–3075, Jun. 2014.
- [64] A. T. Mobashsher and A. M. Abbosh, “Three-Dimensional Human Head Phantom With Realistic Electrical Properties and Anatomy,” *IEEE Antennas Wirel. Propag. Lett.*, vol. 13, pp. 1401–1404, 2014.
- [65] A. Danideh and R. A. Sadeghzadeh, “Cpw-fed slot antenna for mimo system applications,” *Indian J. Sci. Technol.*, vol. 6, no. 1,

References

- pp. 3872–3875, 2013.
- [66] V. Valérie and B. Fabrice, “BIOLOGICAL TISSUES EQUIVALENT LIQUIDS IN THE FREQUENCY RANGE 900- 3000 MHz,” *Symp. A Q. J. Mod. Foreign Lit.*, vol. 0, no. 1, pp. 1–4, 1800.
- [67] L. Jofre, M. S. Hawley, A. Broquetas, E. De Los Reyes, M. Ferrando, and A. R. Elias-Fusté, “Medical Imaging with a Microwave Tomographic Scanner,” *IEEE Trans. Biomed. Eng.*, vol. 37, no. 3, pp. 303–312, 1990.
- [68] Y. Gimm, “General Method Of Formulating The Human Tissue,” *Emc’04*, 2004.
- [69] Wi-Charge, “The challenge of true mobility: untethered power.” [Online]. Available: <https://www.wi-charge.com/technology/>. [Accessed: 01-Nov-2017].
- [70] Ossia, “Cota®: Real Wireless Power.” .
- [71] AirFuel, “AirFuel RF.” [Online]. Available: <http://www.airfuel.org/what-is-airfuel/airfuel-rf/>. [Accessed: 01-Nov-2017].
- [72] M. Xia and S. Aïssa, “On the Efficiency of Far-Field Wireless Power Transfer,” *IEEE Trans. Signal Process.*, vol. 63, no. 11, pp. 2835–2847, 2015.
- [73] C. A. Balanis, *Antenna theory - analysis and design*, 3rd ed. Wiley-Interscience.
- [74] R. Hansen, *Phased Array Antennas*. Wiley-Interscience, 1998.
- [75] R. M. Lewis, V. J. Torczon, and M. W. Trosset, “Direct Search Methods: Then and Now,” *J. Comput. Appl. Math.*, vol. 124, pp. 191–207, 2000.
- [76] Staubli, “TX60 industrial robot.”
- [77] Standa, “8MT177-100 - Motorized Stage.” [Online]. Available: http://www.standa.it/products/catalog/motorised_positioners?item=242. [Accessed: 20-Jul-2011].
- [78] C. Wolff, “Phased Array Antenna.” [Online]. Available: <http://www.radartutorial.eu/06.antennas/Phased Array Antenna.en.html>.

Appendix I. CHARACTERISTICS OF THE SYSTEMS' COMPONENTS

Coaxial High Power Amplifier

ZHL-10W-2G+

50Ω 10W 800 to 2000 MHz

Features

- High power, 10 Watt
- Low Current consumption, 4A typ.
- High IP3, +50 dBm typ.
- Usable over 700 to 2200 MHz
- No damage with an open or short output load under full CW output power

Applications

- Cellular
- PCN
- GSM
- ISM
- Lab Test



Model No.	ZHL-10W-2G+	ZHL-10W-2GX+ ²
Case Style	BT1204	
Connectors	SMA	

+RoHS Compliant
The +Suffix identifies RoHS Compliance. See our web site for RoHS Compliance methodologies and qualifications

Electrical Specifications

Parameter	ZHL-10W-2G+			ZHL-10W-2GX+ ²			Units
	Min.	Typ.	Max.	Min.	Typ.	Max.	
Frequency Range	800		2000	800		2000	MHz
Gain	40	43	49	40	43	49	dB
Gain Flatness			±2.0			±2.0	dB
Output Power at 1dB compression	+39	+40		+39	+40		dBm
Saturated Output Power at 3dB compression	+40	+41		+40	+41		dBm
Noise Figure		7.0			7.0		dB
Output third order intercept point		+50			+50		dBm
Input VSWR		1.3			1.3		:1
Output VSWR		1.3			1.3		:1
DC Supply Voltage		24	28		24	28	V
Supply Current ¹			5.0			5.0	A

¹ Power Supply should be capable of delivering 6A at start up.

² Heat sink and fan not included. Alternative heat sinking and heat removal must be provided by the user to limit maximum base-plate temperature to 75°C, in order to ensure proper performance. For reference, this requires thermal resistance of user's external heat sink to be 0.08°C/W max.

Figure 81 - MiniCircuits ZHL-10W-2G+ High Power Amplifier characteristics.

PE44820

Document Category: Product Specification

UltraCMOS® RF Digital Phase Shifter 8-bit, 1.7–2.2 GHz



Features

- 8-bit full-range phase shifter of 358.6°; 180°, 90°, 45°, 22.5°, 11.2°, 5.6°, 2.8° and 1.4° bits
- Low RMS phase and amplitude error
 - RMS phase error of 1.0°
 - RMS amplitude error of 0.1 dB
- High linearity of +60 dBm IIP3
- Extended narrow band frequency operation of 1.1–3.0 GHz
- +105 °C operating temperature
- Packaging – 32-lead 5 × 5 × 0.85 mm QFN

Applications

- Base station transceivers
- Weather and military radar
- Active antenna arrays

Figure 1 • PE44820 Functional Diagram

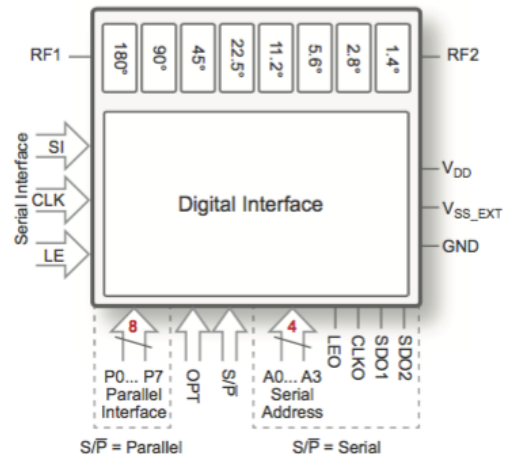


Figure 82 – Peregrine Semiconductor PE44820 Digital Phase Shifter characteristics.

SMA Fixed Attenuator

50Ω 1W 3dB DC to 6000 MHz

VAT-3+



CASE STYLE: FF704

Connectors	Model
SMA	VAT-3+

+RoHS Compliant
The +Suffix identifies RoHS Compliance. See our web site for RoHS Compliance methodologies and qualifications

Maximum Ratings

Operating Temperature -45°C to 100°C
Storage Temperature -55°C to 100°C
Permanent damage may occur if any of these limits are exceeded.

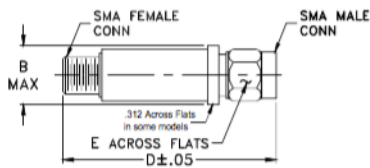
Features

- wideband coverage, DC to 6000 MHz
- 1 watt rating
- rugged unibody construction
- off-the-shelf availability
- very low cost

Applications

- impedance matching
- signal level adjustment

Outline Drawing



Outline Dimensions (inch/mm)

B	D	E	wt
.410	1.43	.312	grams
10.41	36.32	7.92	10.0

Electrical Specifications

FREQ. RANGE (MHz)	ATTENUATION * (dB)				VSWR (:1)			MAX. INPUT POWER (W)	
	Flatness **				DC-3 GHz	3-5 GHz	5-6 GHz		
	DC-3 GHz	3-5 GHz	5-6 GHz	DC-6 GHz					
f ₁ - f ₂	Nom.	Typ.	Typ.	Typ.	Typ.	Max.	Typ.	Max.	Typ.
DC-6000	3±0.3	0.20	0.15	0.15	0.45	1.05 1.20	1.15 1.40	1.40	1.0

* Attenuation varies by 0.3 dB max. over temperature.
** Flatness= variation over band divided by 2.

Typical Performance Data

Frequency (MHz)	Attenuation (dB)	VSWR (:1)
0.03	3.02	1.00
50.00	3.00	1.00
100.00	3.00	1.01
500.00	3.05	1.03
1000.00	3.10	1.05
2000.00	3.19	1.05
3000.00	3.31	1.03
4000.00	3.43	1.10
5000.00	3.58	1.24
6000.00	3.81	1.39

Figure 83 – MiniCircuits VAT-3+ SMA fixed attenuator characteristics.

DC Pass Power Splitter/Combiner

2 Way-0° 50Ω 800 to 2700 MHz

ZAPD-2-272+



CASE STYLE: F53

Connectors	Model
N-TYPE	ZAPD-2-272-N+
SMA	ZAPD-2-272-S+

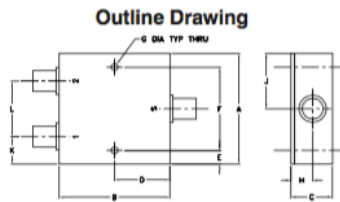
Maximum Ratings

Operating Temperature	-55°C to 90°C
Storage Temperature	-55°C to 100°C
Power Input (as splitter)	10W max.
Internal Dissipation	0.125W max.
DC Current	80mA (40mA for each port)

Permanent damage may occur if any of these limits are exceeded.

Coaxial Connections

SUM. PORT	S
PORT 1	1
PORT 2	2



Features

- wideband, 800-2700 MHz
- low insertion loss, 0.3 dB typ.
- good isolation, 25 dB typ.
- good amplitude unbalance, 0.05 dB typ. and phase unbalance, 0.7 deg. typ.

Applications

- LMDS • UHF
- VSAT • PCS
- GPS • cellular

+RoHS Compliant
The +Suffix identifies RoHS Compliance. See our web site for RoHS Compliance methodologies and qualifications

Electrical Specifications at 25°C

Parameter	Frequency (MHz)	Min.	Typ.	Max.	Unit
Frequency Range		800		2700	MHz
Insertion Loss Above 3.0 dB	800-2700	—	0.3	0.5	dB
Isolation	800-2700	18	22	—	dB
Phase Unbalance	800-2700	—	1.1	3.0	Degree
Amplitude Unbalance	800-2700	—	0.05	0.3	dB
VSWR (Port S)	800-2700	—	1.3	1.5	:1
VSWR (Port 1-2)	800-2700	—	1.2	1.3	:1

Figure 84 - MiniCircuits ZAPD-2-272+ SMA Power Splitter/Combiner characteristics.

Coaxial Voltage Controlled Oscillator

Wide Band 1900 to 3700 MHz

ZX95-3800A+



CASE STYLE: GB956

Connectors	Model
SMA	ZX95-3800A-S+

Features

- low phase noise
- low pulling
- low pushing
- protected by US patent 6,790,049

Applications

- r & d
- lab
- instrumentation
- wireless communications
- point-to-point systems

+RoHS Compliant
The +Suffix identifies RoHS Compliance. See our web site for RoHS Compliance methodologies and qualifications

Electrical Specifications

MODEL NO.	FREQ. (MHz)		POWER OUTPUT (dBm)	PHASE NOISE dBc/Hz SSB at offset frequencies, kHz				TUNING					NON HARMONIC SPURIOUS (dBc)	HARMONICS (dBc)		PULLING pk-pk @12 dB (MHz)	PUSHING (MHz/V)	DC OPERATING POWER	
	Min.	Max.		Typ.	1	10	100	1000	VOLTAGE RANGE (V)	SENSITIVITY (MHz/V)	PORT CAP (pF)	3 dB MODULATION BANDWIDTH (MHz)		Typ.	Typ.			Max.	Typ.
ZX95-3800A+	1900	3700	+5	-65	-89	-110	-130	0.5	20	60-150	50	70	-90	-22	-10	2	4.5	6	55

Maximum Ratings

Operating Temperature	-55°C to 85°C
Storage Temperature	-55°C to 100°C
Absolute Max. Supply Voltage (Vcc)	7V
Absolute Max. Tuning Voltage (Vtune)	21V
All specifications	50 ohm system

Permanent damage may occur if any of these limits are exceeded.



NOTE: When soldering the DC connections, caution must be used to avoid overheating the DC terminals. See Application Note AN-40-10.

Figure 85 - MiniCircuits ZX95-3800A+ Voltage Controlled Oscillator characteristics.

Coaxial Power Detector

50Ω, -60dBm to +5dBm, 10 to 8000 MHz

Maximum Ratings

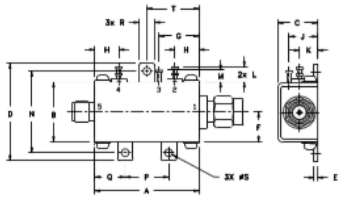
Operating Temperature	-40°C to 85°C
Storage Temperature	-55°C to 100°C
DC Power:	
Max. voltage	5.7V
Max. current	120mA
Internal Power Dissipation	0.73W
Input Power	+15dBm

Permanent damage may occur if any of these limits are exceeded.

Coaxial Connections

RF IN	1
DC OUT	5
Vcc (+5V)	2
TEMPERATURE SENSOR	4
GROUND	3

Outline Drawing



Features

- Low Noise (Output Ripple) for ZX47-60LN+, 20mVp-p Typ. @ 10MHz
- High Dynamic Range
- Wide Bandwidth
- Single Supply Voltage: +5V
- Stability Over Temperature
- Built-in Temperature Sensor
- Protected by US patent 6,790,049

Applications

- RF/IF Power Measurements
- Low Cost Power Monitoring System
- RF Leakage Monitors
- Fast feedback Levelling Circuits
- RF Power Control
- Receiver RF/IF Gain Control
- RSSI measurements

ZX47-60+ ZX47-60LN+



CASE STYLE: HN1173

Connectors	Model
SMA	ZX47-60-S+
SMA	ZX47-60LN-S+

+RoHS Compliant

The +Suffix identifies RoHS Compliance. See our web site for RoHS Compliance methodologies and qualifications

Electrical Specifications (T_{AMB} = 25°C)

FREQ. (MHz)	DYNAMIC RANGE AT ±1dB ERROR (dBm)		OUTPUT VOLT. RANGE (V)	SLOPE (mV/dB) (Note 1)	VSWR (±1)	PULSE RESPONSE TIME (nSec) Typ.		TEMP. SENSOR OUTPUT SLOPE (mV/°C) (Note 2)	DC OPERATING POWER					
	Min.	Max.				Typ.	Typ.		Typ.	Min.	Typ.	Max.	Typ.	
10	1000	-55 to 0												
1000	5000	-60 to -5												
5000	6000	-55 to +5	0.50 - 2.10	-25										
6000	8000	-50 to +5												

Figure 86 - MiniCircuits ZX47-60+ Power Detector characteristics.

Coaxial Voltage Controlled Oscillator

ZX95-2150VW+ ZX95-2150VW

Linear Tuning 970 to 2150 MHz

Features

- wide bandwidth
- 5V supply voltage
- low pushing
- protected by US patent 6,790,049

Applications

- r & d
- lab
- instrumentation
- test equipment



CASE STYLE: GB956

Connectors	Model	Price	Qty.
SMA	ZX95-2150VW-S+	\$54.95 ea.	(1-9)
SMA	ZX95-2150VW-S	\$54.95 ea.	(1-9)

+ RoHS compliant in accordance with EU Directive (2002/95/EC)

The +Suffix identifies RoHS Compliance. See our web site for RoHS Compliance methodologies and qualifications.

Electrical Specifications

MODEL NO.	FREQ. (MHz)		POWER OUTPUT (dBm)	PHASE NOISE dBc/Hz SSB at offset frequencies, kHz				TUNING					NON HARMONIC SPURIOUS (dBc)	HARMONICS (dBc)		PULLING pk-pk @ 12 dB (MHz)	PUSHING (MHz/V)	DC OPERATING POWER	
	Min.	Max.		Typ.	1	10	100	1000	VOLTAGE RANGE (V)	SENSI- TIVITY (MHz/V)	PORT CAP (pF)	3 dB MODULATION BANDWIDTH (MHz)		Typ.	Typ.			Max.	Typ.
ZX95-2150VW(+)	970	2150	+4	-74	-99	-120	-140	0.5	25	32-78	290	15	-90	-22	-	4	1.5	5	26

Maximum Ratings

Operating Temperature	-55°C to 85°C
Storage Temperature	-55°C to 100°C
Absolute Max. Supply Voltage (Vcc)	6V
Absolute Max. Tuning Voltage (Vtune)	28V
All specifications	50 ohm system

Permanent damage may occur if any of these limits are exceeded.

Figure 87 - MiniCircuits ZX95-2150VW+ Voltage Controlled Oscillator characteristics.

PMT Panel Mount Power Supply 24V 350W 1 Phase / PMT-24V350W1A□



PMT

Highlights & Features

- AC input range selectable by switch
- Full Aluminium casing for light weight and corrosion resistant handling
- Built-in automatic fan speed control circuit
- MTBF > 700,000 hrs. as per Telcordia SR-332
- Short Circuit / Overvoltage / Overload / Over Temperature Protections

Safety Standards



CB Certified for worldwide use

Model Number: PMT-24V350W1A□
Unit Weight: 0.82 kg (1.81 lb)
Dimensions (L x W x D): 215 x 115 x 50 mm
 (8.46 x 4.53 x 1.97 inch)

General Description

The PMT-24V350W1A□ offers a nominal output voltage of 24V with a wide operating temperature range from -10°C to +70°C and can withstand shock and vibration according to IEC 60068-2. In addition to features like overvoltage and overload protections, Delta's PMT series of panel mount power supplies is unlike many other brands in the same price level. The PMT series is designed for cost competitive markets without compromising the quality of the components and product specifications. The series of products has an expected life time of 10 years and will have no output power de-rating from 100Vac to 132Vac & 200Vac to 264Vac.

Model Information

PMT Panel Mount Power Supply

Model Number	Input Voltage Range	Rated Output Voltage	Rated Output Current
PMT-24V350W1A□	90-132Vac, 180-264Vac (Selectable by Switch)	24Vdc	14.6A

Figure 88 – Delta PMT-24V350W1A Panel Mount Power Supply characteristics.

SPDT RF SWITCH

50Ω DC-3000 MHz

Absorptive RF Switch with internal driver.
Single Supply Voltage

Product Features

- Low Insertion loss over entire frequency range
- Super High Isolation over entire frequency range
- High Input IP3, +55 dBm typ.
- Single positive supply voltage, +2.7V to +5V
- Unique design-simultaneous switch off of RF1&RF2
- Rigid unibody case

Typical Applications

- Lab
- Instrumentation
- Test equipment



ZX80-DR230+

CASE STYLE: HL1162

Connectors	Order P/N
SMA	ZX80-DR230-S+

+RoHS Compliant

The +Suffix identifies RoHS Compliance. See our web site for RoHS Compliance methodologies and qualifications

Figure 89 – MiniCircuits ZX80-DR230+ SPDT RF Switch characteristics.

Coaxial Low Noise Amplifier

ZX60-33LN+

50Ω

50 to 3000 MHz

Features

- wide bandwidth, 50 to 3000 MHz
- low noise figure 1.1 dB typ.
- output power, up to 17.5 dBm typ.
- protected by US patent 6,790,049

Applications

- front-end amplifier
- cellular
- GPS
- bluetooth
- lab
- instrumentation
- test equipment



Case Style: GC957
Connectors Model
SMA ZX60-33LN-S+

+RoHS Compliant
The +Suffix identifies RoHS Compliance. See our web site for RoHS Compliance methodologies and qualifications

Electrical Specifications at 25°C

Parameter	Condition(MHz)	Min	Typ.	Max.	Units
Frequency	—	50	—	3000	MHz
Noise Figure (Note 1)		—	1.1	1.9	dB
Gain	100	—	21.9	—	dB
	1000	—	18.8	—	
	2000	13	14.5	—	
	3000	—	11.9	—	
Gain Flatness		—	—	—	dB
Output Power at 1dB compression		14.5	16.5	—	dBm
Output third order intercept point		—	+32	—	dBm
Input VSWR		—	2.0	—	:1
Output VSWR		—	1.6	—	:1
Active Directivity		—	—	—	dB
DC Supply Voltage		—	5	—	V
Supply Current		—	70	80	mA

Note 1: 2.3 dB max from 50 to 100 MHz

Figure 90 - MiniCircuits ZX60-33LN+ Low Noise Amplifier characteristics.

Coaxial Low Noise Amplifier

ZFL-1000LN+

50Ω 0.1 to 1000 MHz

Features

- low noise figure, 2.9 dB typ.
- wideband, 0.1 to 1000 MHz
- protected by US Patent 6,943,629

Applications

- VHF/UHF
- cellular
- small signal amplifier



Case Style: Y460

Connectors	Model
SMA	ZFL-1000LN+
BRACKET (OPTION "B")	

+RoHS Compliant

The +Suffix identifies RoHS Compliance. See our web site for RoHS Compliance methodologies and qualifications

Electrical Specifications

Parameter	Frequency (MHz)	Min.	Typ.	Max.	Units
Frequency Range		0.1		1000	MHz
Noise Figure	0.1-1000	—	2.9	—	dB
Gain	0.1-1000	20	—	—	dB
Gain Flatness	0.1-1000	—	—	±0.5	dB
Output Power at 1dB compression	0.1-1000	—	+3	—	dBm
Output third order intercept point	0.1-1000	—	+14	—	dBm
Input VSWR	0.1-1000	—	1.5	—	:1
Output VSWR	0.1-1000	—	2.0	—	:1
DC Supply Voltage		—	15	—	V
Supply Current		—	—	60	mA

Open load is not recommended, potentially can cause damage.
With no load derate max input power by 20 dB

Figure 91 - MiniCircuits ZFL-1000LN+ Low Noise Amplifier characteristics.

Coaxial Bandpass Filter

50Ω 800 to 1050 MHz

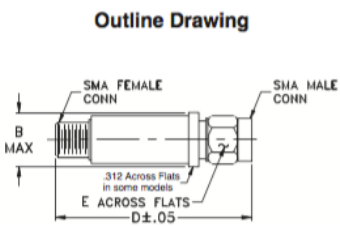
Maximum Ratings

Operating Temperature -55°C to 100°C

Storage Temperature -55°C to 100°C

RF Power Input* 7W at 25°C

*Passband rating, derate linearly to 3W at 100°C ambient. Permanent damage may occur if any of these limits are exceeded.



Features

- Good Rejection, 30dB up to 18GHz
- Low insertion loss
- Excellent power handling, 7W
- Temperature stable LTCC internal structure
- Rugged stainless steel unibody
- Protected by US Patent 6,943,646

Application

- Harmonic rejection
- Transmitters/receivers
- Lab use
- Test instrumentation

VBFZ-925+



CASE STYLE: FF1145

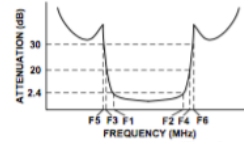
Connectors	Model
SMA	VBFZ-925-S+

+RoHS Compliant
The +Suffix identifies RoHS Compliance. See our web site for RoHS Compliance methodologies and qualifications

Bandpass Filter Electrical Specifications (T_{AMB} = 25°C)

CENTER FREQ. (MHz)	PASSBAND (MHz) (Loss < 2.4dB)	STOPBANDS (MHz)				VSWR (:1)		
		(Loss > 20dB)		(Loss 30dB Typ)		Passband		Stopband
Fc	F1 - F2	F3	F4	F5	F6	Typ.	Max.	Typ.
925	800 - 1050	530	1550	500	1620 - 18000	1.6	2.3	20

Typical Frequency Response



Functional Schematic

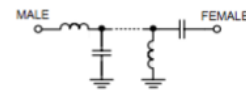


Figure 92 - MiniCircuits VBFZ-925+ Bandpass Filter characteristics.